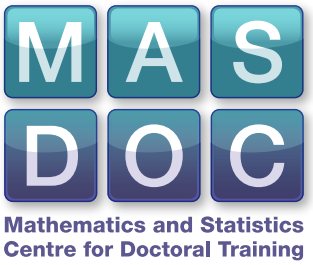

Atomistic-to-continuum coupling

by

Huan Wu

Thesis

Submitted for the degree of

Doctor of Philosophy

Mathematics Institute

The University of Warwick

September 2017

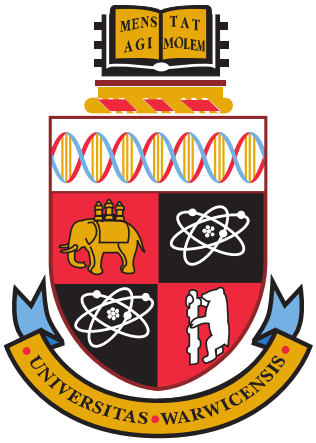

Contents

Acknowledgments

It has been eight years for me at the University of Warwick, including my undergraduate study. The Warwick Mathematics Institute has become a second home to me. I immensely appreciate the supporting and encouraging environment that WMI has provided during my time here.

Most importantly, I would like to address a special thanks to my First Supervisor Professor Christoph Ortner and Second Supervisor Professor Andreas Dedner, who have generously put their experience and wisdom at my disposal. In particular, I would like to express my enormous gratitude to Professor Christoph Ortner who I have worked closely for four years and has inspired me beyond academics with his incredible intelligence and work ethic.

I would also like to thank Professor Charlie Elliott, who was my undergraduate tutor and continued his support during my postgraduate study.

The Mathematics and Statics Centre for Doctoral Training has provided excellent research environment and I would like to thank the staff of this centre. My funding body Engineering and Physical Sciences Research Council has provided financial support to me.

I should also mention my MASDOC colleagues: Faizan, Simon, Ben, Jere, Jorge, Graham, David, Ollie, Matt, Jack, John, Jake, Jamie and Luke, who not only shared their wisdom but also contributed to many happy memories during my life at Warwick. I would also like to thank my friends Becky, Fei, Anna and Orange who accompanied me through difficulties.

Last but not least I would like to thank my parents Lifang Guo and Bin Wu. I would never have achieved anything without their tremendous love and support.

Declarations

I declare that this thesis is the result of my own work, except where otherwise stated. I declare that any part of this thesis has not previously been submitted for a degree or any other qualification at this University or any other institution. I declare that Chapter 3 has been accepted by ESAIM: Mathematical Modelling and Numerical Analysis (ESAIM: M2AN) and published on `https://arxiv.org/abs/1607.05936` with title "Analysis of patch-test consistent atomistic-to-continuum coupling with higher-order finite elements". I declare that Chapter 4 has been published on `http://arxiv.org/abs/1709.05977` with title "Coupling Atomistic, Elasticity and Boundary Element Models".

Abstract

The present thesis is on error analysis of atomistic-to-continuum (A/C) coupling models for crystal defects, which is a class of multi-scale coupling models that combine atomistic interactions around the defect cores and continuum elasticity models at far-fields.

This thesis consists of two parts. The first part presents a sharp error analysis of an A/C model in 2D with high-order finite element methods, whereas in the past the analysis for employing FEM has been restricted to first-order. The second part discusses a new A/C coupling scheme employing a boundary element method to improve the description of the far-field.

In the first part we formulate a "patch test consistent" atomistic-to-continuum coupling (a/c) scheme that employs a second-order (potentially higher-order) finite element method in the material bulk. We prove a sharp error estimate in the energy-norm, which demonstrates that this scheme is (quasi-)optimal amongst energy-based sharp-interface a/c schemes that employ the Cauchy–Born continuum model. Our analysis also shows that employing a continuum discretization with order greater than two does not yield qualitative improvements to the rate of convergence.

In the second part we formulate a new A/C coupling scheme that employs a boundary element method to obtain an improved far-field boundary condition. We establish sharp error bounds in a 2D model problem for a point defect embedded in a homogeneous crystal. The error analysis shows that it is possible to entirely bypass the FEM region while maintaining an optimal convergence rate.

The thesis is accompanied by an introduction to atomistic-to-continuum coupling and literature review on various coupling methods and the general framework for error analysis.

Chapter 1

Introduction

Material science has become increasingly prominent over the past several decades, in part due to advances in molecular modeling and new engineering tools. The study of nanoscale systems opens up opportunities in a wide range of applications, including medical diagnostic, material reinforcement, chemical sensing, material design and so on. Once the physical models for materials are established, computational methods are developed. Despite the rapid development of computing powers, simulations on full microscopic scale are still too costly. This is due to the fact that many materials display different properties at different length and time scales. For example, the strengthening properties of steel exist at different material length scales, ranging from quantum scale with atomic lattice uncertainties, to submicroscale with thermodynamics uncertainties, to microscale inclusions, to ultimately macroscale of the formation of a ship (see Figure 1.1). Single-scale models are not sufficient for this type of systems.

Multiscale coupling is a class of modeling methods that describe microscopic configurations of regions of interest, and approximate using coarser models (such as continuum mechanics) far away from the "core areas". In principle these methods can reduce computational costs while maintaining the accuracy of the atomistic models.

At the defect core, the material displays atomistic behaviours that cannot be modeled by macroscopic systems. But outside the defect core, the elastic fields are often modeled by continuum mechanics. The resulted techniques are called atomistic-to-continuum coupling (a/c) methods. They are a prototypical atomistic-level multi-scale scheme. Using finite element schemes on a coarse mesh in the continuum region further improves computational efficiency.

Early ideas of a/c coupling occurred in several works from 1950s to 1970s, such as [26] and [50] using continuum linear elasticity to describe far-field behaviour. Later on the methodology of employing finite elements to discretize the continuum model was introduced in [37], [19] and [27]. The introduction of variational framework and the Cauchy–Born model by [38] was a key step for the development of a/c coupling. Since then the term "quasicontinuum" is widely used. It is now widely understood that the treatment of interface region is crucial for constructions of a/c coupling methods. Various

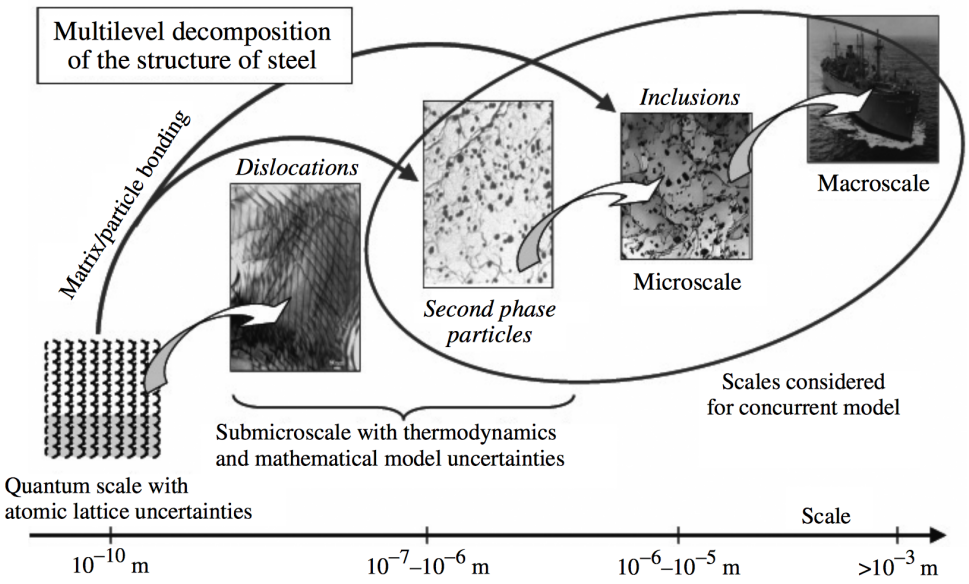

Figure 1.1: Multiscale properties of steel. This illustration is taken from [31]

methods have been proposed: the quasi-non-local coupling [49], blending schemes [55], force-based a/c coupling [36], and the ghost force correction method [48]. In Chapter 2, we briefly introduce the concepts of blending type methods and ghost forces. Throughout this thesis we focus on quasi-non-local (QNL) coupling and the error analysis resulting from both the coupling method and the use of different numerical schemes for describing bulk elasticity.

In terms of numerical simulations, it is important to quantify the accuracy of the simulation to determine how good the models and numerical schemes are. The continuum regions of a/c coupling methods are usually computed on coarse meshes in order to reduce cost. On the other hand, it is crucial to ensure that the numerical schemes do not add significant inaccuracy to the simulation. So it is necessary to balance these two aspects to obtain optimal computational parameters. Thus our goal is to determine the "optimal error" that can be obtained from numerical simulations with a given computational cost. This involves both analysis of the pure modelling error of non-linear coupled systems and error estimation and optimization of finite element schemes and other optimal approximation parameters.

Chapter 2

Background

2.1 Interatomic potentials

In this section, we introduce interatomic potentials for crystals. Let Z be an index set. The (deformed) atom configuration is represented by $y : Z \to \mathbb{R}^d$, $d = 1, 2, 3$. Then the distance between two atom positions is written as $R_{ij} := |y(i) - y(j)|$.

2.1.1 Pair potentials

Pair potentials are the simplest interatomic potentials. For a configuration $y : Z \to \mathbb{R}^d$, $d = 1, 2, 3$, the potential energy is written as

$$E(y) = \sum_{i,j \in Z, i \neq j} \phi(|y(i) - y(j)|),$$

where $\phi : [0, \infty) \to \mathbb{R} \cup \{+\infty\}$ is a pair potential. The Lennard-Jones potential ([25]) is an example which is widely used in molecular simulations. It is given by

$$\phi_{LJ}(r) := r^{-12} - 2r^{-6}.$$

2.1.2 The embedded atom method (EAM)

Phenomenological observations of metallic systems indicate the presence of significant many-atom interactions which pair potential models fail to describe. Table 1 in [11] shows that Ni, Cu, Pd, Ag, Pt and Au all display many-body effects. Consequently there is a need for more complex models that capture the fact that, in general, bond interactions are not independent from each other.

In [10] the embedded atom method was proposed, in which the total energy is obtained by embedding an atom into the local electron density provided by the rest of the atoms in the system, in addition to an electrostatic interaction. The general formulation of the total energy E is

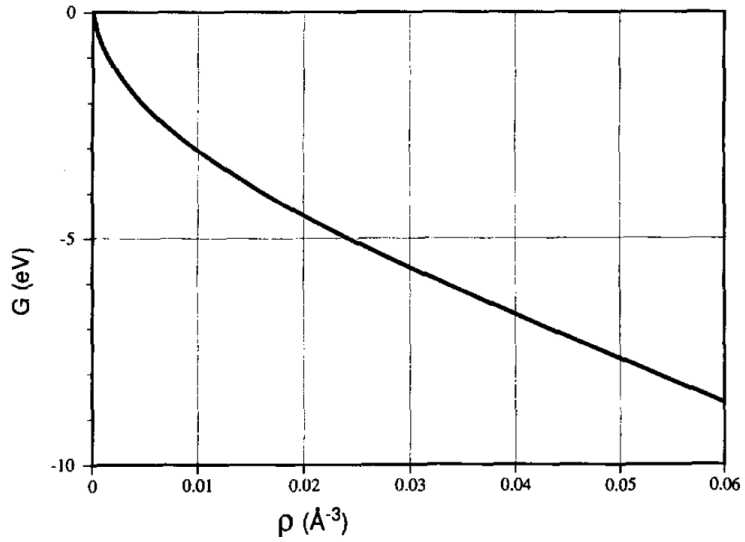

Figure 2.1: Embedding energy of Ni as a function of the density of background electron gas. This figure is copied from [11].

$$E(y) = \sum_{i \in Z} E_i^{\mathrm{EAM}}(y), \tag{2.1.1}$$

with

$$E_i^{\mathrm{EAM}}(y) := G\left(\sum_{j \in Z, j \neq i} \rho_j(R_{ij})\right) + \sum_{j \in Z, i \neq j} \phi(R_{ij}),$$

where G is the embedding energy, ρ_j is the atomistic electron density, the summation $\sum_{j \in Z, j \neq i} \rho_j(R_{ij})$ represents the spherically averaged electron density and ϕ is the electrostatic two-atom interaction. The embedding energy G is defined by the interaction of the atom with the background electron gas. Figure 2.1 is an example of an embedding energy. The background density ρ is determined by evaluating at its nucleus the superposition of atomic-density tails from the other atoms. Figure 2.2 is an example of pair interaction.

As we can see from the formulation, EAM is inherently more complex than pair-bond models.

2.1.3 General site energies

All interatomic potential energies can be written in the form of site energies, namely, for an atom position map $y : Z \to \mathbb{R}^d$,

$$E(y) = \sum_{\ell \in Z} E_\ell(y),$$

where $E_\ell(y)$ are the site energies.

For the sake of analysis, we need the following assumptions on E_ℓ:

1. **Invariance under isometries:** let $y_0 \in \mathbb{R}^d$ and $M \in \mathrm{SO}(d)$, then $E_\ell(My + y_0) =$

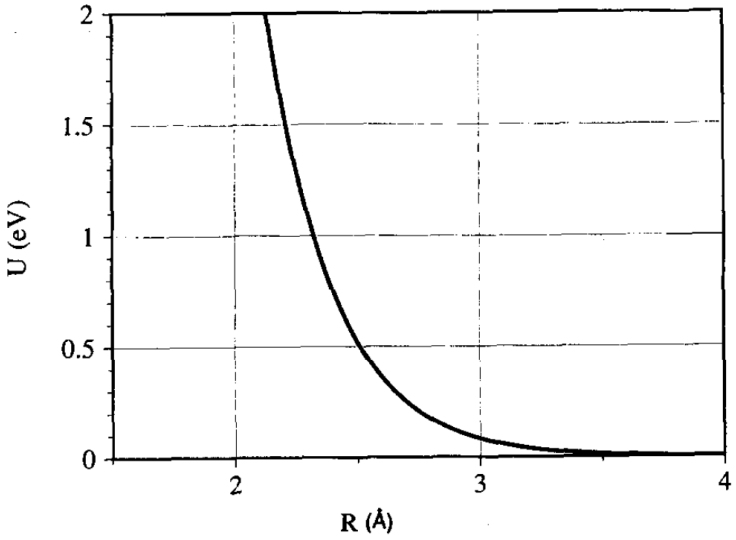

Figure 2.2: Pair interaction of Ni as a function of separation. This figure is copied from [11].

$E_\ell(y)$.

2. **Permutation invariance:** for all permutations p of Z, and $y_p(\ell) := y(p(\ell))$, we have $E_{p(\ell)}(y) = E_\ell(y_p)$.

3. **Smoothness:** E_ℓ is a "smooth" function of y for the "required range" of configurations y. Normally, we require that E_ℓ is smooth at all configurations y for which $y_\ell \neq y_n$ for all $\ell, n \in Z$.

4. **Locality:** there exists $r_{\text{cut}} > 0$ such that E_ℓ is only a function of $|y_\ell - y_k| < r_{\text{cut}}$.

2.2 Crystals and defects

2.2.1 Lattices

In the present work, we are concerned with crystalline solids, described in the form of Bravais lattices.

Definition 2.2.1. *A Bravais lattice is defined by* $\mathsf{A}\mathbb{Z}^d$ *with* $d = 1, 2, 3$*, where* $\mathsf{A} \in \mathbb{R}^{d\times d}$ *is non-singular.* For example, in Chapter 2, we discuss a triangular lattice in 2D with

$$\mathsf{A} = \begin{pmatrix} 1 & \cos(\pi/3) \\ 0 & \sin(\pi/3) \end{pmatrix}.$$

2.2.2 Point defects

In reality, atoms in solids are not arranged in perfect lattices. One of the reasons causing this is the occurrence of defects. Figure 2.3 illustrates several example of defects.

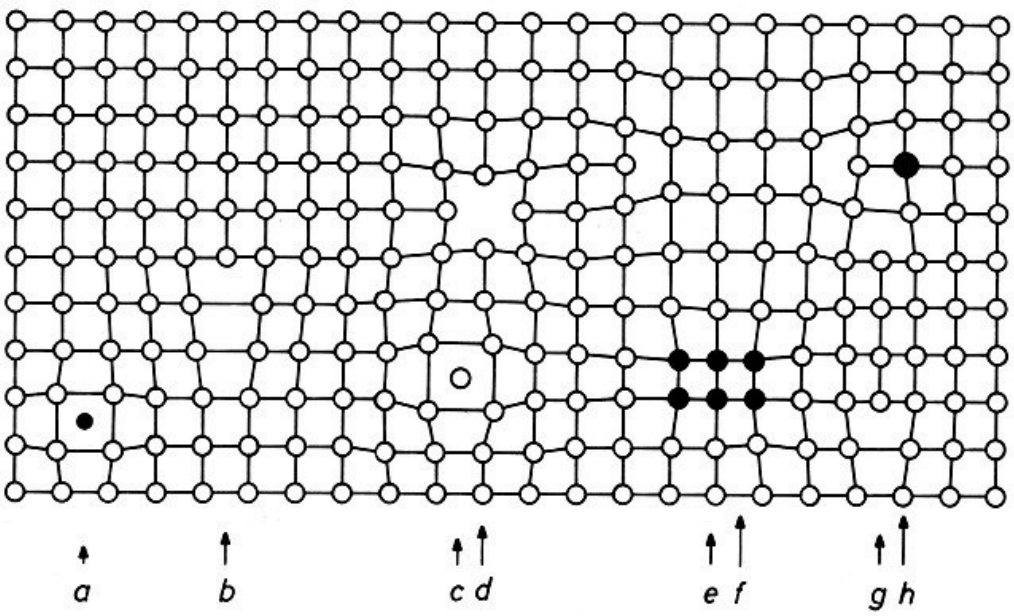

Figure 2.3: a) Interstitial impurity atom, b) Edge dislocation, c) Self interstitial atom, d) Vacancy, e) Precipitate of impurity atoms, f) Vacancy type dislocation loop, g) Interstitial type dislocation loop, h) Substitutional impurity atom. This illustration is drawn by Helmut Föll and is taken from `https://www.tf.uni-kiel.de/matwis/amat/def_en/overview_main.html`

In the present work, we focus on point defects. Examples include impurities, interstitials and vacancies (a, c and d in Figure 2.3 respectively).

To simulate point defect configurations, we first set up a reference configuration $\Lambda \subset \mathbb{R}^d$ that coincides with a Bravais lattice far away from the defect core.

Definition 2.2.2. *[18] A discrete set Λ is a point defect reference configuration if there exists a Bravais lattice Λ^{hom} and a radius R_{core} such that $\Lambda \setminus B_{R_{\text{core}}} = \Lambda^{\text{hom}} \setminus B_{R_{\text{core}}}$ and $\Lambda \cap B_{R_{\text{core}}}$ is finite.*

2.2.3 Dislocations

Dislocations have been intensively studied since they are the carriers of plastic deformation. Generally speaking there are two types of dislocations:

1. *Edge dislocations*: produced by a half-plane inserted or removed from the lattice, see b) and g) in Figure 2.3 and A in Figure 2.4.

2. *Screw dislocations*: created by slip parallel to the dislocation line, see B in Figure 2.4.

Much (possibly all) of the theory we develop in this thesis can be extended to dislocations using the techniques employed in [52] and [18]. For the sake of simplicity, and to focus on

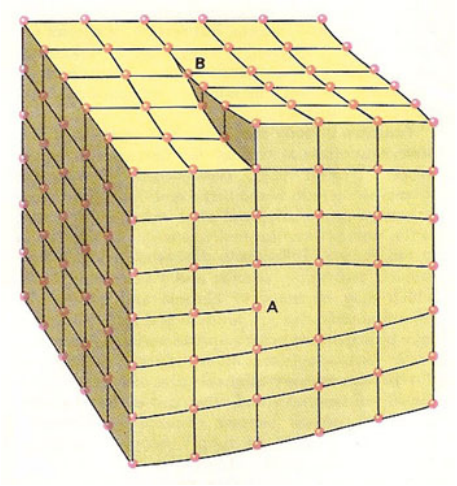

Figure 2.4: Section of a crystal lattice including an edge dislocation (A) and a screw dislocation (B). This illustration is drawn by David Darling and is taken from `http://www.daviddarling.info/encyclopedia/D/dislocation.html`.

numerical discretization aspects rather than atomistic mechanics aspects, later chapters of this thesis will be restricted to point defect only.

2.3 Atomistic-to-continuum models

The first key step in a/c multi-scale modelling is to approximate the atomistic model by a continuum elasticity model. In this way we can reduce the computational costs while maintaining significant accuracy. One of the mostly widely used continuum models is the Cauchy–Born model, which will be used throughout this thesis.

2.3.1 The Cauchy–Born model

The Cauchy–Born model introduced by [6] and [4] has been widely employed as the continuum model in a/c coupling. The Cauchy–Born potential is an elastic potential derived from the atomistic energy by averaging the energy per unit volume. It is a useful tool for macroscopic models since the elastic response is derived from the interatomic potential without the need for fitting parameters. Various a/c coupling methods have been developed based on the Cauchy–Born model.

For a homogeneous configuration $\Lambda = \mathsf{A}\mathbb{Z}^d$, The physical position of a defective lattice is described by a deformation map $y : \Lambda \to \mathbb{R}^d$. Define the displacement map $u : \Lambda \to \mathbb{R}^d$ as $u := y - x$. Let us consider an atomistic energy with interaction range $R_{\rm nn}$. Long-range interactions (i.e. interaction range greater than $R_{\rm nn}$) can be treated using the same approach. The atomistic energy is then given by

$$\mathcal{E}^{\rm hom}(u) = \sum_{\ell \in \Lambda} V(Du(\ell)),$$

where

$$Du(\ell) = \Big(u(\ell) - u(k)\Big)_{|\ell-k|<R_{\rm nn},\ell\neq k}.$$

Formally we can rescale space and energy by $\Lambda \rightsquigarrow \epsilon\Lambda$, $x \rightsquigarrow \epsilon x$, $u \rightsquigarrow \epsilon u$, and $V \rightsquigarrow \epsilon^d V$ for $\epsilon > 0$. The scaled energy is written as

$$\mathcal{E}_\epsilon^{\rm hom}(u) = \sum_{\ell\in\epsilon\Lambda} \epsilon^d V(D_\epsilon u(\ell)),$$

where

$$D_\epsilon u(\ell) := \left(\frac{u(\ell) - u(k)}{\epsilon}\right)_{|\ell-k|<\epsilon R_{\rm nn},\ell\neq k}.$$

Letting $\epsilon \to 0$ gives the Cauchy–Born energy [24]

$$\mathcal{E}_\epsilon^{\rm hom} \to \mathcal{E}^{\rm c} := \int_{\mathbb{R}^d} W(\nabla\tilde{u})dx,$$

where

$$W(\mathsf{F}) := V(\mathsf{F}\xi)_{\xi\in\Lambda\setminus 0,|\xi|<R_{\rm nn}}, \quad \mathsf{F}\in\mathbb{R}^{d\times d},$$

$\tilde{u}$ is some continuous interpolant of u. In later sections we will discuss the formulation of the Cauchy–Born strain energy function $W : \mathbb{R}^{d\times d} \to \mathbb{R}$ for specific models.

2.3.2 Quasicontinuum coupling

To incorporate atomistic models around defects with elastic continuum models at far-field, quasicontinuum (QC) coupling has been proposed in [38]. The original QC coupling is rather intuitive. Formally, the fully atomistic energy in terms of each atom is written as

$$\mathcal{E}^{\rm a} = \sum_{\ell\in\Lambda} E_\ell^{\rm a}.$$

Outside the defect bulk, the energy can be approximated by a continuum model with appropriate elasticity strain derived from the atomistic interactions. Formally, the (local) continuum energy at each atom ℓ is written as

$$E_\ell^{\rm c} = \int_{\omega_\ell} W(\nabla u)$$

where ω_ℓ are non-overlapping regions containing one atom only. Throughout this thesis we employ the Cauchy–Born potential as the elasticity strain energy. Such atoms are called *local* because the energy is irrelevant to the atoms outside the element. See §2.4, §3.1 for specific examples of $E^{\rm a}$ and $\mathcal{E}^{\rm c}$ in 1D and 2D respectively. The quasicountinuum coupling energy is then given by

$$\mathcal{E}^{\rm ac} = \sum_{\ell\in\mathcal{A}} E_\ell^{\rm a} + \sum_{\ell\in\mathcal{C}} E_\ell^{\rm c}, \tag{2.3.1}$$

where $\mathcal{A}$ and $\mathcal{C}$ represent the sets of non-local and local atoms respectively and $\mathcal{A}\cup\mathcal{C} = \Lambda$.

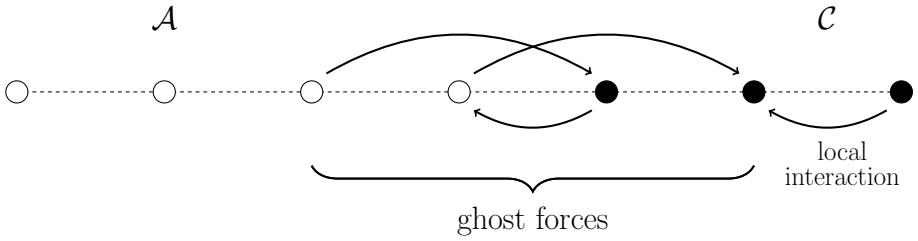

Figure 2.5: Ghost forces from a QC model on a homogenenous lattice in 1D. We assume next-nearest-neighbour interaction in the atomistic region $\mathcal{A}$, whereas the Cauchy–Born energy in the continuum region is local.

However, as demonstrated in [49], the QC energy formulation above results in non-zero forces around the interface atoms, which are *ghost forces*. This is formally explained as follows.

Let u be a homogeneous displacement on a lattice $\Lambda \subset \mathbb{R}^d$, i.e. $u(x) := \mathsf{F} \cdot x$, where $\mathsf{F} \in \mathbb{R}^{d\times d}$. The ghost force on each atom $\ell \in \Lambda$ is defined by

$$G_\ell(u) := \frac{\partial \mathcal{E}^{\rm ac}}{\partial u(\ell)}.$$

It is clear that for homogeneous displacement ghost forces should be zero at all atoms because it is in fact a perfect crystal without defects. But the QC coupling defined in (2.3.1) exhibits non-zero ghost forces. See Figure 2.5 for an illustration. One can remove these ghost forces by using "correction forces", which unfortunately are nonconservative (see [48]).

2.3.3 Quasi-nonlocal-continuum(QNL) coupling

In order to develop a conservative coupling of atomistic and continuum methods, [49] introduced quasi-nonlocal atoms around the interface region such that no ghost-force is exhibited. The concept is that between the nonlocal and local regions quasi-nonlocal atoms are added, which experience interactions with only nearest-neighbour atoms as well as all nonlocal atoms within the cut-off range. Consequently they act like local atoms on the local side, and nonlocal atoms on the nonlocal side. Formally, the total energy of quasi-nonlocal coupling is given by

$$\mathcal{E}^{\rm qnl} = \sum_{\ell\in\mathcal{A}} E_\ell^{\rm a} + \sum_{\ell\in\mathcal{I}} E_\ell^{Q} + \sum_{\ell\in\mathcal{C}} E_\ell^{\rm c},$$

where $\mathcal{A}, \mathcal{I}$ and $\mathcal{C}$ represent the atomistic, interface and continuum atoms respectively. The idea is to choose E_ℓ^Q in such a way that $G_\ell(\mathsf{F}\cdot x) = 0$ for all $\mathsf{F} \in \mathbb{R}^{d\times d}$. This idea allows the construction of various ghost-force free methods. See §2.4 for an example in 1D and §3 for an example in 2D.

2.3.4 Energy blending method (B-QCE)

There have been other quasicontinuum coupling methods developed in order to either reduce or remove ghost forces. [55] proposed an energy blending method which does not remove but reduce the ghost forces. Formally, with a blending function $\beta : \Lambda \to [0, 1]$, the energy function is defined by

$$\mathcal{E}^{\text{bqce}} = \sum_{\ell \in \Lambda} \{(1 - \beta(\ell))E^{\text{a}}_\ell + \beta(\ell)E^{\text{c}}_\ell\},$$

where E^{a}_ℓ is the atomistic site energy and E^{c}_ℓ is the corresponding Cauchy–Born site energy.

The advantage of B-QCE is stability [28]. Yet again the gost-forces are not eliminated completely.

2.3.5 Force-based coupling (QCF)

A popular alternative to the QC method has been an a/c approximation based on coupling forces, see [9]. The key concept is to compute the force on each atom from either the atomistic or the continuum model. Let $\mathcal{A}$ be the set of atomistic sites and $\mathcal{C}$ be the set of continuum sites, then the force on each atom ℓ is defined by

$$\mathcal{F}^{\text{qcf}}_\ell(u) := \begin{cases} \frac{\partial \mathcal{E}^{\text{a}}(u)}{\partial u_\ell}, & \text{for } \ell \in \mathcal{A}, \\ \frac{\partial \mathcal{E}^{\text{c}}(u)}{\partial u_\ell}, & \text{for } \ell \in \mathcal{C}, \end{cases}$$

Then we solve the non-linear system

$$\mathcal{F}^{\text{qcf}}_\ell(u) = f_\ell, \quad \text{for all } \ell \in \Lambda,$$

where f_ℓ is the external force acting on each atom ℓ.

As discussed in [33], the non-symmetric and indefinite structure of the QCF method presents a challenge to the efficiency of solving the QCF equations.

2.3.6 Force-based blending (B-QCF)

In [32] a blended version of QCF is constructed, which is stable with respect to the discrete $W^{-1,2}$-seminorm. The blended force is given by

$$\mathcal{F}^{\text{bqcf}}_\ell(u) := \beta(\ell)\mathcal{F}^{\text{a}}_\ell(u) + (1 - \beta(\ell))\mathcal{F}^{\text{c}}_\ell(u).$$

The consistency of the B-QCF method is well-established since there is no interface coupling error. In terms of stability, it can be shown that by choosing a sufficiently large blending region, then up to a controllable error, B-QCF is stable in the discrete $W^{-1,2}$-seminorm.

2.4 General framework for analyzing A/C coupling models: an example in 1D

In [33] a general framework is provided for a/c coupling models using examples in 1D with static defects. Briefly, the potential energy of a defective system is approximated by a coupled energy that consists of atomistic potentials around the defect core, a continuum elasticity approximation outside the defect core and a modified energy term around the interface (e.g. the quasi-nonlocal term in the previous section). We then seek the existence and stability of the minimizer of this coupled energy and estimate the error against the "true" displacement (i.e. the atomistic solution) to quantify the accuracy of the model. The key components of the error analysis are consistency and stability estimates. Then using the inverse function theorem gives existence and uniqueness results, as well as an error estimate.

In this section we use an 1D quasi-nonlocal model with next nearest-neighbour interaction to demonstrate the general idea. We only formally outline the structure of the analysis and refer to the literature and later chapters for details.

2.4.1 Atomistic model

Let us consider an infinite atomistic chain, denoted by $\mathbb{Z}$. A displacement of the chain is represented by a map $u : \mathbb{Z} \to \mathbb{R}$. The reference lattice is denoted by $A\mathbb{Z}$ with $A > 0$. Thus the deformation of the atomistic chain is given by $y(\ell) := Al + u(\ell)$. We assume that $y(\ell) - y(\ell - 1) > 0$, that is, no atom jumps over another, and thus $u(\ell) - u(\ell - 1) > -A$.

We consider a Lennard-Jones potential that describes first and second neighbour interactions:

$$\phi(r) = r^{-12} - 2r^{-6}.$$

This potential ϕ satisfies the following properties

(i) $\phi \in C^\infty((0, +\infty); \mathbb{R})$,

(ii) there exists $r_* > 0$ such that ϕ is convex in $(0, r_*)$ and concave in $(r_*, +\infty)$, and

(iii) $\phi^{(n)}(r) \to 0$ rapidly as $r \nearrow \infty$, for $n = 0, ..., 4$.

The atomistic energy of a next-nearest-neighbour model for displacement u is then written as

$$\mathcal{E}^{\mathrm{a}}(u) = \sum_{\ell \in \mathbb{Z}} \{\phi_1(u'_\ell) + \phi_2(u'_\ell + u'_{\ell+1})\},$$

where $\phi_i(s) := \phi(iA + s)$ and $u'_\ell := u(\ell) - u(\ell - 1)$.

For simplicity and clarity of analysis, we will consider problems with antisymmetric forces and corresponding antisymmetric displacements. Let us define the space of antisymmetric displacements as

$$\mathcal{U} := \{u : \mathbb{Z}_+ \to \mathbb{R} \,|\, u' \in \ell^2 \text{ and } u(0) = 0\}.$$

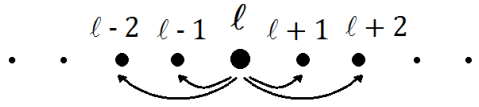

Figure 2.6: Interactions in a 1D next-nearest neighbour model.

Throughout we assume the displacement map $u|_{\mathbb{Z}_+}$ belongs to $\mathcal{U}$ and identify $u(-\ell) := -u(\ell)$ for all $\ell \in \mathbb{Z}_-$. So we can write the atomistic energy in this antisymmetric setting in the form

$$\mathcal{E}^{\rm a}_+(u) := \frac{1}{2}\Phi^{\rm a}_0(u) + \sum_{\ell=1}^{\infty} \Phi^{\rm a}_\ell(u), \tag{2.4.1}$$

where the *atomistic site energy* is

$$\Phi^{\rm a}_\ell(u) := \frac{1}{2}[\phi_1(u'_\ell) + \phi_1(u'_{\ell+1}) + \phi_2(u'_{\ell-1} + u'_\ell) + \phi_2(u'_{\ell+1} + u'_{\ell+2})].$$

Then we have the identity $\mathcal{E}^{\rm a}(u) = 2\mathcal{E}^{\rm a}_+(u)$. For simplicity we drop the subscript from $\mathcal{E}_+$ since we only consider antisymmetric problems. We will use this representation of the atomistic energy because it is the form in which more realistic interatomic potentials are normally given: see Figure 2.6.

For simplicity we consider only dead load external forces throughout this section. Let $f : \mathbb{Z} \to \mathbb{R}$ with $f(\ell) \to 0$ as $|l| \to \infty$. Then we seek a solution of

$$u^{\rm a} \in \arg\min\{\mathcal{E}^{\rm a}(u) - \langle f, u\rangle_{\mathbb{Z}_+}\}. \tag{2.4.2}$$

If $u^{\rm a}$ is a solution to (2.4.2), it naturally satisfies the Euler–Lagrange equation:

$$\frac{d}{dt}\left[\mathcal{E}^{\rm a}(u+tv) - \langle f, u+tv\rangle_{\mathbb{Z}}\right]\Big|_{t=0} = 0 \quad \text{for all } v \in \mathcal{U}$$

which is normally written as

$$\langle \delta\mathcal{E}^{\rm a}(u^{\rm a}), v\rangle = \langle f, v\rangle_{\mathbb{Z}_+} \quad \text{for all } v \in \mathcal{U}. \tag{2.4.3}$$

2.4.2 Cauchy–Born continuum model

To approximate the atomistic energy, we consider the continuum elasticity model with an energy functional of the form

$$\mathcal{E}^{\rm c}(u) = \int_{\mathbb{R}_+} W(|\nabla u|)dx,$$

where $W : (0,\infty) \to \mathbb{R}$ is a suitable strain energy function and $u \in \mathcal{U}$ is identified with its linear interpolant in this case. For the continuum model, we use the Cauchy–Born strain

energy density function

$$W(F) := \phi_1(F) + \phi_2(2F).$$

We shall remark that the atomistic and continuum energies are only formally defined, but see [43] for justification. However the first and second variations are well-defined as stated. And only those are needed for the analysis.

Let us consider a finite element Cauchy–Born model on an infinite atomistic chain. We take the atomistic chain as the set of nodes and consider $u : \mathbb{R}_+ \to \mathbb{R}$ as the continuous piecewise linear interpolation of the discrete displacement mapping $u : \mathbb{Z}_+ \to \mathbb{R}$. Then the Cauchy-Born model is rewritten as

$$\mathcal{E}^{\mathrm{c}}(u) = \sum_{\ell=1}^{\infty} \Phi_\ell^{\mathrm{c}}(u), \tag{2.4.4}$$

where the *Cauchy–Born site energy* is

$$\Phi_\ell^{\mathrm{c}}(u) := \tfrac{1}{2} W(u'_\ell) + \tfrac{1}{2} W(u'_{\ell+1}).$$

For this discretized Cauchy-Born model, we seek

$$u^{\mathrm{c}} \in \arg\min\{\mathcal{E}^{\mathrm{c}}(u) - \langle f, u\rangle_{\mathbb{Z}_+}\},$$

which solves the Euler-Lagrange equation

$$\langle \delta\mathcal{E}^{\mathrm{c}}(u^{\mathrm{c}}), v\rangle = \langle f, v\rangle_{\mathbb{Z}_+} \quad \text{for all } v \in \mathcal{U},$$

where

$$\begin{aligned}\langle \delta\mathcal{E}^{\mathrm{c}}(u^{\mathrm{c}}), v\rangle &= \sum_{\ell\in\mathbb{Z}_+} W'(u'_\ell) v'_\ell \\ &= \sum_{\ell\in\mathbb{Z}_+} \{\phi_1'(u'_\ell) v'_\ell + \phi_2'(2u'_\ell)(2v'_\ell)\}.\end{aligned}$$

2.4.3 QNL a/c coupling method in 1D

The first method of this kind was formulated by Shimokawa [49]. In this section, for simplicity, we consider the construction valid only for 1D pair interactions, employing an approximation of bonds rather than site energies. Following [46] we approximate

$$\phi_2(u'_\ell + u'_{\ell+1}) \approx \frac{1}{2}\phi_2(2u'_\ell) + \frac{1}{2}\phi_2(2u'_{\ell+1}).$$

The total energy using QNL coupling is therefore expressed as

$$\mathcal{E}^{\mathrm{qnl}}(u) := \mathcal{E}^{\mathrm{a}}(u) + \sum_{\ell=K+1}^{\infty} [\frac{1}{2}\{\phi_2(2u'_\ell) + \phi_2(2u'_{\ell+1})\}] - \phi_2(u'_\ell + u'_{\ell+1}),$$

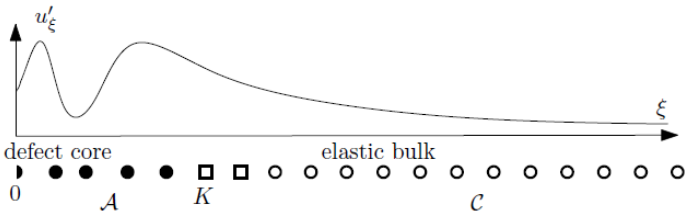

Figure 2.7: Illustration of the constuction of the QNL method, where $\mathcal{A}$ is the atomistic region, $\{K, K+1\}$ is the interface region and $\mathcal{C}$ is the continuum region

where K is the site where we start approximating atomistic interaction by continuum models. We can also rewrite $\mathcal{E}^{\rm qnl}$ as a decomposition into the atomistic region, the interface region and the continuum region:

$$\mathcal{E}^{\rm qnl}(u) = \sum_{\ell=0}^{K-1} \Phi^{\rm a}_\ell(u) + \sum_{\ell=K}^{K+1} \Phi^{\rm qnl}_\ell(u) + \sum_{\ell=K+2}^{\infty} \Phi^{\rm c}_\ell(u), \tag{2.4.5}$$

where $\Phi^{\rm a}_\ell(u)$ is defined in (2.4.1), $\Phi^{\rm c}_\ell(u)$ is defined in (2.4.4) and

$$\Phi^{\rm qnl}_\ell(u) := \frac{1}{2}\{\phi_1(u'_\ell) + \phi_2(u'_{\ell-1} + u'_\ell) + W(u'_{\ell+1})\},$$

At the reference state, the first variations of both sides are equal

$$\phi'_2(0)(v'_\ell + v'_{\ell+1}) = \frac{1}{2}\phi'_2(0)(2v'_\ell) + \frac{1}{2}\phi'_2(0)(2v'_{\ell+1}),$$

which shows that there are no ghost forces: $\delta\mathcal{E}^{\rm qnl}(0) = 0$ as opposed to other coupling methods such as QCE and B-QCE, which is one of the advantages of QNL method.

In (2.4.5), the interface atoms $\{K, K+1\}$ are called 'quasi-non-local' because their interaction with the atomistic region, i.e. the term $\phi_2(u'_{K-1} + u'_K)$, is non-local but their interaction with the continuum region, i.e. the term $W(u'_{K+1})$, is local. See Figure 2.7.

We approximate the atomistic problem 2.4.2 by

$$u^{\rm qnl} \in \arg\min\{\mathcal{E}^{\rm qnl}(u) - \langle f, u\rangle_{\mathbb{Z}_+}\}. \tag{2.4.6}$$

2.4.4 Error Estimation

The general approach for obtaining an error estimate for $u^{\rm a} - u^{\rm qnl}$ uses stability and consistency results. In the case of modelling crystal defects, we have the following notion of stability and consistency:

$\mathcal{E}^h$, where h represents a particular approximate model, is *stable* on a displacement map u if there exists a constant $\gamma > 0$ such that

$$\langle \delta^2\mathcal{E}^h(u)v, v\rangle \geq \gamma\|v\|^2 \quad \text{for all } v \in \mathcal{U}.$$

A *consistency error estimate* $\eta(u)$ of $\mathcal{E}^h$ at u is often expressed as

$$\langle \delta\mathcal{E}^h(u) - \delta\mathcal{E}^{\rm a}(u), v\rangle \lesssim \eta(u)\|v\|,$$

where $\eta(u)$ is determined by discrete derivatives of u.

We note that $\delta^2\mathcal{E} : \mathcal{U} \to \mathcal{U}^*$. For example

$$\langle \delta^2\mathcal{E}^{\rm a}(u)v, v\rangle = \sum_{\ell\in\mathbb{Z}_+} \{\phi_1''(u_\ell')(v_\ell')^2 + \phi_2''(u_\ell' + u_{\ell+1}')(v_\ell' + v_{\ell+1}')^2\}.$$

The stability property comes from the positive-definiteness of the Hessian of the model, since a solution is a minimizer of the problem $\mathcal{E}^h(u) - \langle f, u\rangle_{\mathbb{Z}_+}$.

With stability and consistency estimates defined above, we can employ the inverse function theorem to obtain the desired error estimates.

Before discussing error estimates, we shall assume that $\mathcal{E}^{\rm a}$ and $\mathcal{E}^{\rm qnl}$ satisfy the following global bounds.

(A) There exist finite constants $M_a^{(j)}$ and $M_{\rm qnl}^{(j)}$ such that, if $\sum_{i=1}^j \frac{1}{p_i} = 1$, then $\delta^j\mathcal{E}^{\rm a}$ and $\delta^j\mathcal{E}^{\rm qnl}$ satisfy the bounds, for all $u \in \mathcal{U}$,

$$\langle \delta^j\mathcal{E}^{\rm a}u, \mathbf{v}\rangle \le M_a^{(j)} \prod_{i=1}^j \|v_i'\|_{\ell^{p_i}},$$

$$\langle \delta^j\mathcal{E}^{\rm qnl}u, \mathbf{v}\rangle \le M_{\rm qnl}^{(j)} \prod_{i=1}^j \|v_i'\|_{\ell^{p_i}}, \quad \text{for all } v_i \in \mathcal{U}.$$

We shall remark that realistically the interatomic potentials are singular as the distance between any two atoms tends to zero, which contradicts Assumption A. It is purely for the simplicity of analysis. Removing these global bounds does not change the main concept of the analysis but only adds complications to formulations and proofs.

Recalling the QNL and atomistic energy functionals defined in (2.4.5) and (2.4.1), we can compute the error in the first variation: for $u, v \in \mathcal{U}$,

$$\begin{aligned}\langle \delta\mathcal{E}^{\rm qnl}(u) - \delta\mathcal{E}^{\rm a}(u), v\rangle = \sum_{\ell\in K+2}^{\infty} &\big\{2\phi_2'(2u_\ell') - \phi_2'(u_\ell' + u_{\ell+1}') - \phi_2'(u_{\ell-1}' + u_\ell')\big\}v_\ell' \\ &+ \big\{\phi_2'(2u_{K+1}') - \phi_2'(u_{K+1}' + u_{K+2}')\big\}v_{K+1}'.\end{aligned}$$

Note that the right hand side above does not include any contribution from the atomistic

region. Using Taylor's expansion we can estimate

$$\begin{aligned}
&|2\phi_2'(2u_\ell') - \phi_2'(u_\ell' + u_{\ell+1}') - \phi_2'(u_{\ell-1}' + u_\ell')| \\
\approx&\big|\phi_2''(2u_\ell')\big\{4u_\ell' - (u_\ell' + u_{\ell+1}') - (u_{\ell-1}' + u_\ell')\big\} \\
&\quad + \tfrac{\phi_2'''(\theta)}{2}\big\{(2(u_\ell') - (u_\ell' + u_{\ell+1}'))^2 + (2(u_\ell') - (u_{\ell-1}' + u_\ell'))^2\big\}\big| \\
=&\big|\phi_2''(2u_\ell')\big\{ - u_{\ell+1}'''\big\} + \tfrac{\phi_2'''(\theta)}{2}\big\{(u_{\ell+1}'')^2 + (u_\ell'')^2\big\}\big| \\
\le& M_{\rm qnl}^2|u_{\ell+1}'''| + M_{\rm qnl}^3|(u_{\ell+1}'')^2 + (u_\ell'')^2|,
\end{aligned}$$

where $u_\ell'' := u_{\ell+1}' - u_\ell'$ and $u_\ell''' := u_\ell'' - u_{\ell-1}''$. Similarly we have

$$|\phi_2'(2u_{K+1}') - \phi_2'(u_{K+1}' + u_{K+2}')| \approx |\phi_2''(\theta)(2u_{K+1}' - u_{K+1}' - u_{K+2}')| \le M_{\rm qnl}^2|u_{K+1}''|.$$

Applying the Cauchy-Schwarz inequality gives the consistency estimate,

$$\langle \delta\mathcal{E}^{\rm qnl}(u) - \delta\mathcal{E}^{\rm a}(u), v\rangle \lesssim (\|u'''\|_{\ell^2(\mathcal{C})} + \|u''\|_{\ell^4(\mathcal{C})}^2 + |u_{K+1}''|)\|v'\|_{\ell^2}. \tag{2.4.7}$$

For stability, we shall first see that the reference state $u = 0$ is stable in the atomistic model if and only if it is stable in the Cauchy–Born model. At the reference state $u = 0$, a brief calculation shows that

$$\begin{aligned}
\langle \delta^2\mathcal{E}^{\rm c}(0)v, v\rangle &= \tfrac{1}{2}W''(0)|v_0'|^2 + W''(0)\sum_{\ell=1}^{\infty}|v_\ell'|^2 \\
&= \langle \delta^2\mathcal{E}^{\rm a}(0)v, v\rangle + \phi_2''(0)\sum_{\ell=1}^{\infty}|v_\ell''|^2,
\end{aligned}$$

where we used the fact that $W''(0) = \phi_1''(0) + 4\phi_2''(0)$ and the parallelogram identity

$$|v_\ell' + v_{\ell+1}'|^2 = 2|v_\ell'|^2 + 2|v_{\ell+1}'|^2 - |v_\ell''|^2. \tag{2.4.8}$$

For Lennard-Jones type potentials we have that $\phi_2''(0) < 0$, hence

$$\langle \delta^2\mathcal{E}^{\rm a}(0)v, v\rangle \ge \langle \delta^2\mathcal{E}^{\rm c}(0)v, v\rangle.$$

It can be checked [13] that

$$\inf_{\|v'\|_{\ell^2}=1}\langle \delta^2\mathcal{E}^{\rm c}(0)v, v\rangle \ge \inf_{\|v'\|_{\ell^2}=1}\langle \delta^2\mathcal{E}^{\rm a}(0)v, v\rangle.$$

Consequently we can state that the reference state $u = 0$ is stable in the atomistic model if and only if it is stable in the Cauchy–Born model.

Now we consider the stability of the QNL model. Using the parallelogram identity

(2.4.8) we have

$$\begin{aligned}\langle \delta^2 \mathcal{E}^{\mathrm{qnl}}(0)v, v\rangle &= \phi_1''(0)\sum_{\ell=1}^{\infty}|v_\ell'|^2 + \phi_2''(0)|2v_1'|^2 \\ &\quad + \phi_2''(0)\sum_{\ell=1}^{K}|v_\ell' + v_{\ell+1}'|^2 + \phi_2''(0)\sum_{\ell=K+1}^{\infty}\left(\tfrac{1}{2}|v_\ell'|^2 + \tfrac{1}{2}|v_{\ell+2}'|^2\right) \\ &= \langle \delta^2 \mathcal{E}^{\mathrm{c}}(0)v, v\rangle - \phi_2''(0)\sum_{\ell=1}^{K}|v_\ell''|^2.\end{aligned}$$

Similar to the Cauchy–Born case, the reference state $u = 0$ is stable in the QNL model if and only if the atomistic and Cauchy–Born Hessians are stable.

More generally, we can prove the following result:

Theorem 2.4.1. *([33, Theorem 7.8]) Suppose there exists an atomistic solution u^{a} to* (2.4.2) *that satisfies, for some $\gamma^{\mathrm{a}} > 0$,*

$$\langle \delta^2 \mathcal{E}^{\mathrm{a}}(u^{\mathrm{a}})v, v\rangle \geq \gamma^{\mathrm{a}}\|v'\|_{\ell^2}^2, \qquad \forall v \in \mathcal{U},$$

with discrete derivatives decaying as follows, for some $\alpha > 1/2$,

$$|(u^{\mathrm{a}})^{(j)}(x)| \lesssim x^{-\alpha+1-j}, \qquad j = 0, 1, 2, 3.$$

Then there exists $\gamma_0^{\mathrm{qnl}} > 0$ such that

$$\langle \delta^2 \mathcal{E}^{\mathrm{qnl}}(0)v, v\rangle \geq \gamma_0^{\mathrm{qnl}}\|v'\|_{\ell^2}^2, \qquad \forall v \in \mathcal{U}.$$

Then there exists $\gamma^{\mathrm{qnl}} > 0$ such that

$$\langle \delta^2 \mathcal{E}^{\mathrm{qnl}}(u^{\mathrm{a}})v, v\rangle \geq \gamma^{\mathrm{qnl}}\|v'\|_{\ell^2}^2, \qquad \forall v \in \mathcal{U}, \tag{2.4.9}$$

when K is sufficiently large.

Combining the consistency estimate (2.4.7) and the stability estimate (2.4.9), we can apply the inverse function theorem (see Theorem 3.4.1) to conclude that there exists a solution $u^{\mathrm{qnl}} \in \mathcal{U}$ to (2.4.6) such that

$$\langle \delta^2 \mathcal{E}^{\mathrm{qnl}}(u^{\mathrm{qnl}})v, v\rangle = 0,$$

and

$$\|(u^{\mathrm{a}})' - (u^{\mathrm{qnl}})'\|_{\ell^2} \lesssim \|(u^{\mathrm{a}})'''\|_{\ell^2(\mathcal{C})} + \|(u^{\mathrm{a}})''\|_{\ell^4(\mathcal{C})}^2 + |(u^{\mathrm{a}})''_{K+1}|.$$

2.4.5 Error estimates for other a/c coupling methods

In [33], error estimates for QCE and QCF methods in 1D are also discussed and summarized.

Recall that the QCE energy is defined in §2.3.4. Suppose $\beta(|x|) = 0$ for $|x| \leq K$ and $\beta(|x|) = 1$ for $|x| \geq L$, then the consistency error is reduced to be $(L-K)^{-\frac{3}{2}}$ (see [34] for detailed optimization). The stability is guaranteed up to an error controllable by the blend width $(L-K)$.

The QCF model introduced in §2.3.5 is proven not to be stable in the discrete $W^{-1,2}$-seminorm in [15]. However, it has been shown that it is stable in the discrete $W^{-1,\infty}$-seminorm ([14]). Hence tha error estimates are established in the discrete $W^{-1,\infty}$-seminorm.

Chapter 3

A/C coupling with high-order finite elements

The theory of high-order finite element methods (FEM) in partial differential equations, and applications in solid mechanics is well established; see [47] and references therein. However, most work on the rigorous error analysis of a/c coupling has been restricted to P1 finite element methods; the only exception we are aware of is [45], which focuses on blending-type methods.

In the present chapter we estimate the accuracy of a QNL method employing a P2 FEM in the continuum region against an exact solution obtained from a fully atomistic model. Since stability of QNL type couplings is a subtle issue [41] we will primarily analyse the consistency errors, taking into account the relative sizes of the fully resolved atomistic region and of the entire computational domain (Sections 6.1-6.6). We will then optimize these relative sizes as well as the mesh grading in the continuum region in order to minimize the total consistency error (Section 6.7). We will observe that, using P1-FEM in the continuum region, the error resulting from FEM approximations is the dominating contributor of the consistency estimates, which implies that increasing the order of the FEM can indeed improve the accuracy of the simulation. We will show that, using Pk-FEM with $k \geq 2$, the FEM approximation error is dominated by the interface error which comes purely from the coupling construction, and in particular demonstrate that the P2-FEM is sufficient to achieve the optimal convergence rate for the consistency error. Finally, *assuming* the stability of the G23 coupling (see assumption **(A2)** in § 3.2.2, and also [41] why this must be an assumption and cannot be proven), we prove a rigorous error estimate in §3.5.

Finally, we conduct numerical experiments on a 2D anti-plane model problem to test our analytical predictions. The numerical results display the predicted error convergence rates for the fully atomistic model, P1-FEM G23 model, and P2-FEM G23 model.

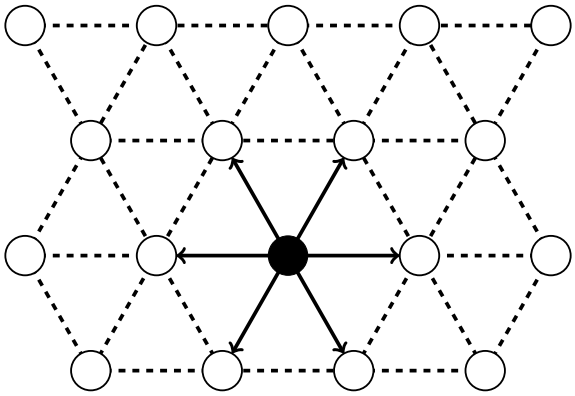

Figure 3.1: The lattice and its canonical triangulation.

3.1 Preliminaries

Our setup and notation follows [44]. As our model geometry we consider an infinite 2D triangular lattice,

$$\Lambda := \mathsf{A}\mathbb{Z}^2, \quad \text{with } \mathsf{A} = \begin{pmatrix} 1 & \cos(\pi/3) \\ 0 & \sin(\pi/3) \end{pmatrix}.$$

We define the six nearest-neighbour lattice directions by $a_1 := (1, 0)$, and $a_j := Q_6^{j-1} a_1, j \in \mathbb{Z}$, where Q_6 denotes the rotation through the angle $\pi/3$. We supply Λ with an *atomistic triangulation*, as shown in Figure 3.1, which will be convenient in both analysis and numerical simulations. We denote this triangulation by $\mathcal{T}$ and its elements by $T \in \mathcal{T}$. We also denote $\boldsymbol{a} := (a_j)_{j=1}^6$, and $\mathsf{F}\boldsymbol{a} := (\mathsf{F}a_j)_{j=1}^6$, for $\mathsf{F} \in \mathbb{R}^{m\times 2}$.

We identify a discrete displacement map $u : \Lambda \to \mathbb{R}^m$, $m = 1, 2, 3$, with its continuous piecewise affine interpolant, with weak derivative ∇u, which is also the pointwise derivative on each element $T \in \mathcal{T}$. For $m = 1, 2, 3$, the spaces of displacements are defined as

$$\begin{aligned} \mathcal{U}_0 &:= \big\{ u \,|\, \Lambda \to \mathbb{R}^m : \operatorname{supp}(\nabla u) \text{ is compact} \big\}, \quad \text{and} \\ \dot{\mathcal{U}}^{1,2} &:= \big\{ u \,|\, \Lambda \to \mathbb{R}^m : \nabla u \in L^2 \big\}. \end{aligned}$$

We equip $\dot{\mathcal{U}}^{1,2}$ with the H^1-seminorm, $\|u\|_{\mathcal{U}^{1,2}} := \|\nabla u\|_{L^2(\mathbb{R}^2)}$. From [40] we know that $\mathcal{U}_0$ is dense in $\dot{\mathcal{U}}^{1,2}$ in the sense that, if $u \in \dot{\mathcal{U}}^{1,2}$, then there exist $u_j \in \mathcal{U}_0$ such that $\nabla u_j \to \nabla u$ strongly in L^2.

A *homogeneous displacement* is a map $u_\mathsf{F} : \Lambda \to \mathbb{R}^m, u_\mathsf{F}(x) := \mathsf{F}x$, where $\mathsf{F} \in \mathbb{R}^{m\times 2}$.

For a map $u : \Lambda \to \mathbb{R}^m$, we define the finite difference operator

$$\begin{aligned} D_j u(x) &:= u(x + a_j) - u(x), \quad x \in \Lambda, j \in \{1, 2, ..., 6\}, \quad \text{and} \\ Du(x) &:= (D_j u(x))_{j=1}^6. \end{aligned} \tag{3.1.1}$$

Note that $Du_\mathsf{F}(x) = \mathsf{F}\boldsymbol{a}$.

3.1.1 2D many-body nearest neighbour interactions

We assume that the atomistic interaction is described by a nearest-neighbour many-body site energy potential $V \in C^r(\mathbb{R}^{m\times 6})$, $r \geq 5$, with $V(\mathbf{0}) = 0$. Furthermore, we assume that V satisfies the *point symmetry*

$$V((-g_{j+3})_{j=1}^6) = V(\boldsymbol{g}) \quad \forall \boldsymbol{g} \in \mathbb{R}^{m\times 6}.$$

The energy of a displacement $u \in \mathcal{U}_0$, given by

$$\mathcal{E}^{\mathrm{a}}(u) := \sum_{\ell\in\Lambda} V(Du(\ell)),$$

is well-defined since the infinite sum becomes finite. To formulate a variational problem in the energy space $\dot{\mathcal{U}}^{1,2}$, we need the following lemma to extend $\mathcal{E}^{\mathrm{a}}$ to $\dot{\mathcal{U}}^{1,2}$.

Lemma 3.1.1. *$\mathcal{E}^{\mathrm{a}} : (\mathcal{U}_0, \|\nabla\cdot\|_{L^2}) \to \mathbb{R}$ is continuous and has a unique continuous extension to $\dot{\mathcal{U}}^{1,2}$, which we still denote by $\mathcal{E}^{\mathrm{a}}$. Furthermore, the extended $\mathcal{E}^{\mathrm{a}} : (\dot{\mathcal{U}}^{1,2}, \|\nabla\cdot\|_{L^2}) \to \mathbb{R}$ is r-times continuously Fréchet differentiable.*

Proof. See Lemma 2.1 in [18]. □

For the sake of analysis we need the following global bounds on the potential V. For $\boldsymbol{g} \in \mathbb{R}^{m\times 6}$, define the first and second partial derivatives, for $i, j = 1, \ldots, 6$, by

$$\partial_j V(\boldsymbol{g}) := \frac{\partial V(\boldsymbol{g})}{\partial g_j} \in \mathbb{R}^m, \quad \text{and} \quad \partial_{i,j} V(\boldsymbol{g}) := \frac{\partial^2 V(\boldsymbol{g})}{\partial g_i \partial g_j} \in \mathbb{R}^{m\times m},$$

and similarly for the third derivatives $\partial_{i,j,k} V(\boldsymbol{g}) \in \mathbb{R}^{m\times m\times m}$. We assume that the second and third derivatives are bounded

$$M_2 := \sum_{i,j=1}^6 \sup_{\boldsymbol{g}\in\mathbb{R}^{m\times 6}} \sup_{\substack{h_1,h_2\in\mathbb{R}^2,\\ |h_1|=|h_2|=1}} \partial_{i,j} V(\boldsymbol{g})[h_1, h_2] < \infty, \quad \text{and} \tag{3.1.2}$$

$$M_3 := \sum_{i,j,k=1}^6 \sup_{\boldsymbol{g}\in\mathbb{R}^{m\times 6}} \sup_{\substack{h_1,h_2,h_3\in\mathbb{R}^2,\\ |h_1|=|h_2|=|h_3|=1}} \partial_{i,j,k} V(\boldsymbol{g})[h_1, h_2, h_3] < \infty. \tag{3.1.3}$$

With the above bounds it is easy to show that

$$\begin{aligned} \sum_{i=1}^6 |\partial_i V(\boldsymbol{g}) - \partial_i V(\boldsymbol{h})| &\leq M_2 \max_{j=1,\ldots,6} |g_j - h_j|, \\ \sum_{i,j=1}^6 |\partial_i\partial_j V(\boldsymbol{g}) - \partial_i\partial_j V(\boldsymbol{h})| &\leq M_3 \max_{k=1,\ldots,6} |g_k - h_k|, \quad \text{for } \boldsymbol{g}, \boldsymbol{h} \in \mathbb{R}^{m\times 6}. \end{aligned} \tag{3.1.4}$$

3.1.2 The variational problem

We add an external potential $f \in C^r(\dot{\mathcal{U}}^{1,2})$ with $\partial_{u(\ell)} f(u) = 0$ for all $|\ell| \geq R_f$, where R_f is some given radius, and $f(u+c) = f(u)$ for all constants c. For example, we can think of f modelling a substitutional impurity. See also [30, 39] for similar approaches.

We then seek the solution to

$$u^{\mathrm{a}} \in \arg\min \left\{ \mathcal{E}^{\mathrm{a}}(u) - f(u) \,|\, u \in \dot{\mathcal{U}}^{1,2} \right\}. \tag{3.1.5}$$

For $u, \varphi, \psi \in \dot{\mathcal{U}}^{1,2}$ we define the *first and second variations* of $\mathcal{E}^{\mathrm{a}}$ by

$$\begin{aligned} \langle \delta \mathcal{E}^{\mathrm{a}}(u), \varphi \rangle &:= \lim_{t \to 0} t^{-1} \left(\mathcal{E}^{\mathrm{a}}(u + t\varphi) - \mathcal{E}^{\mathrm{a}}(u) \right), \\ \langle \delta^2 \mathcal{E}^{\mathrm{a}}(u)\varphi, \psi \rangle &:= \lim_{t \to 0} t^{-1} \left(\langle \delta \mathcal{E}^{\mathrm{a}}(u + t\varphi), \psi \rangle - \langle \delta \mathcal{E}^{\mathrm{a}}(u), \psi \rangle \right). \end{aligned}$$

We use analogous definitions for all energy functionals introduced in later sections.

3.1.3 The Cauchy–Born Approximation

The Cauchy–Born strain energy function, corresponding to the interatomic potential V is

$$W(\mathsf{F}) := \frac{1}{\Omega_0} V(\mathsf{F}\boldsymbol{a}), \qquad \text{for } \mathsf{F} \in \mathbb{R}^{m \times 2},$$

where $\Omega_0 := \sqrt{3}/2$ is the volume of a unit cell of the lattice Λ. Thus $W(\mathsf{F})$ is the energy per volume of the homogeneous lattice $\mathsf{F}\Lambda$.

3.1.4 The G23 coupling method

Let $\mathcal{A} \subset \Lambda$ denote the set of all lattice sites for which we want to maintain full atomistic accuracy. We denote the set of interface lattice sites by

$$\mathcal{I} := \left\{ \ell \in \Lambda \setminus \mathcal{A} \,\middle|\, \ell + a_j \in \mathcal{A} \text{ for some } j \in \{1, \ldots, 6\} \right\}$$

and we denote the remaining lattice sites by $\mathcal{C} := \Lambda \setminus (\mathcal{A} \cup \mathcal{I})$. Let Ω_ℓ be the Voronoi cell associated with site ℓ. We define the atomistic, interface and continuum regions respectively by

$$\Omega^{\mathrm{a}} := \bigcup_{\ell \in \mathcal{A}} \Omega_\ell, \quad \Omega^{\mathrm{i}} := \bigcup_{\ell \in \mathcal{I}} \Omega_\ell, \quad \text{and} \quad \Omega^{\mathrm{c}} := \mathbb{R}^2 \setminus \bigcup_{\ell \in \mathcal{A} \cup \mathcal{I}} \Omega_\ell;$$

see Figure 3.2 for a visualisation.

A general form for the GRAC-type a/c coupling energy [16, 44] is

$$\mathcal{E}^{\mathrm{ac}}(u) = \sum_{\ell \in \mathcal{A}} V(Du(\ell)) + \sum_{\ell \in \mathcal{I}} V\left((\mathcal{R}_\ell D_j u(\ell))_{j=1}^6 \right) + \int_{\Omega^{\mathrm{c}}} W(\nabla u(x))\, \mathrm{d}x,$$

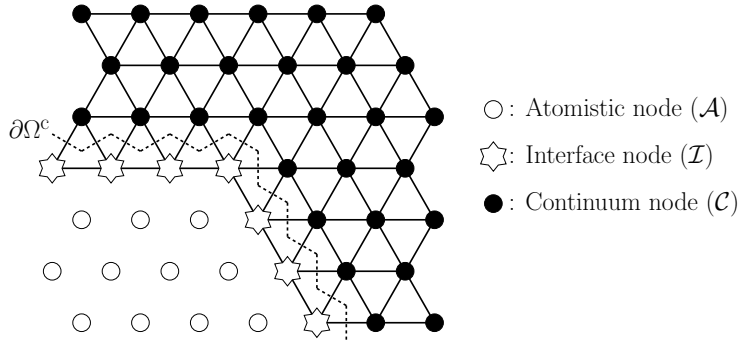

Figure 3.2: The domain decomposition with a layer of interface atoms.

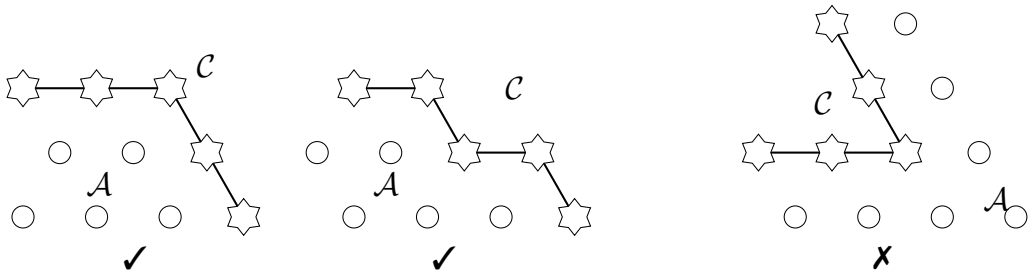

Figure 3.3: The first two configurations are allowed. The third configuration is not allowed as the interface atom at the corner has no nearest neighbour in the continuum region, and should instead be taken as an atomistic site.

where $\mathcal{R}_\ell D_j u(\ell) := \sum_{i=1}^6 C_{\ell,j,i} D_i u(\ell)$. For the sake of brevity of notation we will often write

$$V_\ell^i(Du(\ell)) := V\left((\mathcal{R}_\ell D_j u(\ell))_{j=1}^6\right).$$

The parameters $C_{\ell,j,i}$ are to be determined in order for the coupling scheme to satisfy the "patch tests":

$\mathcal{E}^{\rm ac}$ is *locally energy consistent* if, for all $\mathsf{F} \in \mathbb{R}^{m\times 2}$,

$$V_\ell^i(\mathsf{F}\boldsymbol{a}) = V(\mathsf{F}\boldsymbol{a}) \quad \forall \ell \in \mathcal{I}. \tag{3.1.6}$$

$\mathcal{E}^{\rm ac}$ is *force consistent* if, for all $\mathsf{F} \in \mathbb{R}^{m\times 2}$,

$$\delta\mathcal{E}^{\rm ac}(u_\mathsf{F}) = 0, \tag{3.1.7}$$

where $u_\mathsf{F} \in \dot{\mathcal{U}}^{1,2}$ and $u_\mathsf{F}(x) := \mathsf{F}x$ for all $x \in \mathbb{R}^2$.

$\mathcal{E}^{\rm ac}$ is *patch test consistent* if it satisfies both (3.1.6) and (3.1.7).

Following [44] we make the following standing assumption (see Figure 3.3 for examples).

(A0) *Each vertex $\ell \in \mathcal{I}$ has exactly two neighbours in $\mathcal{I}$, and at least one neighbour in $\mathcal{C}$.*

Under this assumption, the geometry reconstruction operator $\mathcal{R}_\ell$ is then defined

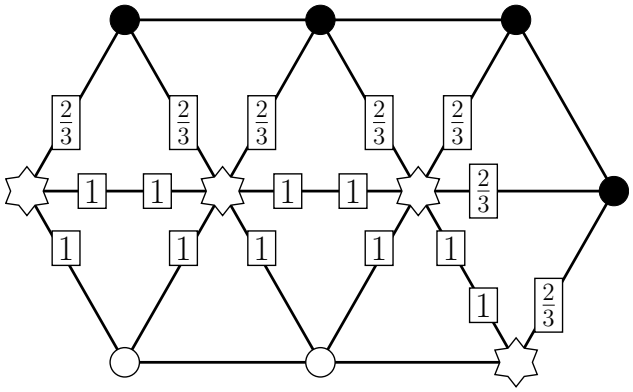

Figure 3.4: The geometry reconstruction coefficents $\lambda_{x,j}$ at the interface sites.

by

$$\begin{aligned} \mathcal{R}_\ell D_j u(\ell) &:= (1-\lambda_{\ell,j}) D_{j-1} u(\ell) + \lambda_{\ell,j} D_j u(\ell) + (1-\lambda_{\ell,j}) D_{j+1} u(\ell), \\ \lambda_{x,j} &:= \begin{cases} 2/3, & x + a_j \in \mathcal{C} \\ 1, & \text{otherwise} \end{cases}; \end{aligned} \tag{3.1.8}$$

see Figure 3.4. The resulting coupling method is called G23 and the corresponding energy functional $\mathcal{E}^{\mathrm{g23}}$:

$$\mathcal{E}^{\mathrm{g23}}(u) := \sum_{\ell \in \mathcal{A}} V(Du(\ell)) + \sum_{\ell \in \mathcal{I}} V\left((\mathcal{R}_\ell D_j u(\ell))_{j=1}^6\right) + \int_{\Omega^{\mathrm{c}}} W(\nabla u(x))\,\mathrm{d}x, \tag{3.1.9}$$

where $\mathcal{R}_\ell D_j u(\ell)$ is defined as (3.1.8). This choice of coefficients (and only this choice) leads to patch test consistency (3.1.6) and (3.1.7). We refer to [44] for a detailed proof.

For future reference we decompose the canonical triangulation $\mathcal{T}$ as follows:

$$\begin{aligned} \mathcal{T}_\mathcal{A} &:= \{T \in \mathcal{T} \,|\, T \cap (\mathcal{I} \cup \mathcal{C}) = \emptyset\}, \\ \mathcal{T}_\mathcal{C} &:= \{T \in \mathcal{T} \,|\, T \cap (\mathcal{I} \cup \mathcal{A}) = \emptyset\} \quad \text{and} \\ \mathcal{T}_\mathcal{I} &:= \mathcal{T} \setminus (\mathcal{T}_\mathcal{C} \cup \mathcal{T}_\mathcal{A}). \end{aligned} \tag{3.1.10}$$

3.1.5 Notation for a P2 finite element scheme

In the atomistic and interface regions, the interactions are represented by discrete displacement maps, which are identified with their linear interpolant. Here, we identify the displacement map with its P1 interpolant. No approximation error is committed.

On the other hand, in the continuum region where the interactions are approximated by the Cauchy–Born energy, we could increase the accuracy by using Pp-FEM with $p > 1$. In later sections we will review that the Cauchy–Born approximation yields a 2nd-order error, whereas employing the P1-FEM in the continuum region would reduce the accuracy to first order. In fact, we will show that, with optimized mesh grading, P2-FEM is sufficient to obtain a convergence rate that cannot be improved by other choices of continuum discretisations. High-order Pp-FEM with $p > 2$ will increase the computational

costs but yield the same error convergence rate (see § 3.2.5).

Let $K > 0$ denote the inner radius of the atomistic region,

$$K := \sup\big\{r > 0 \,|\, \mathcal{B}_r \cap \Lambda \subset \mathcal{A}\big\},$$

where $\mathcal{B}_r$ denotes the ball of radius r centred at 0. In order for the defect to be contained in the atomistic region we assume throughout that $K \geq R_f$.

Let Ω_h denote the entire bounded computational domain and $N > 0$ denote the inner radius of Ω_h, i.e.,

$$N := \sup\big\{r > 0 \,|\, \mathcal{B}_r \subset \Omega_h\big\}.$$

Let $\mathcal{T}_h$ be a finite element triangulation of Ω_h which satisfies that, for $T \in \mathcal{T}_h$, T is closed and

$$T \cap (\mathcal{A} \cup \mathcal{I}) \neq \emptyset \quad \Rightarrow \quad T \in \mathcal{T}.$$

In other words, $\mathcal{T}_h$ and $\mathcal{T}$ coincide in the atomistic and interface regions, whereas in the continuum region the mesh size may increase towards the domain boundary. Define the mesh size $h(x) := \mathrm{diam}(T)$ with $x \in T$. The optimal rate at which the mesh size h increases will be determined in later sections.

We note that the concrete construction of $\mathcal{T}_h$ will be based on the choice of the domain parameters K and N; hence, when emphasizing this dependence, we will write $\mathcal{T}_h(K, N)$. We assume throughout that the family $(\mathcal{T}_h(K, N))_{K,N}$ is *uniformly shape-regular*, i.e., there exists $c > 0$ such that,

$$\mathrm{diam}(T)^2 \leq c|T|, \quad \forall T \in \mathcal{T}_h(K, N), \forall K \leq N. \tag{3.1.11}$$

This assumption eliminates the possibility of extreme angles on elements, which would deteriorate the constants in finite element interpolation error estimates. For the most part we will again drop the parameters from the notation by writing $\mathcal{T}_h \equiv \mathcal{T}_h(K, N)$ but implicitly will always keep the dependence.

Similar to (3.1.10), we define the atomistic, interface and continuum elements as $\mathcal{T}_h^a, \mathcal{T}_h^i$ and $\mathcal{T}_h^c$, respectively. Note that $\mathcal{T}_h^a = \mathcal{T}_{\mathcal{A}}$ and $\mathcal{T}_h^i = \mathcal{T}_{\mathcal{I}}$. We also let $\mathcal{N}_h$ denote the number of degrees of freedom of $\mathcal{T}_h$.

We define the finite element space of admissible displacements as

$$\begin{aligned}\mathcal{U}_h := \big\{u \in C(\mathbb{R}^2; \mathbb{R}^m) \,|\, \mathrm{supp}(u) \subset \Omega_h, u|_T \in \mathbb{P}^1(T) \text{ for } T \subset \mathcal{T}_h^a \cup \mathcal{T}_h^i \text{ and} \\ u|_T \in \mathbb{P}^2(T) \text{ for } T \subset \mathcal{T}_h^c\big\}.\end{aligned} \tag{3.1.12}$$

In defining $\mathcal{U}_h$ we have made two approximations to the class of admissible displacements: (1) truncation to a finite computational domain and (2) finite element coarse-graining.

The computational scheme is to find

$$u_h^{\mathrm{g23}} \in \arg\min\big\{\mathcal{E}^{\mathrm{g23}}(u_h) - f(u_h) \,|\, u_h \in \mathcal{U}_h\big\}. \tag{3.1.13}$$

Remark 3.1.2. $\mathcal{U}_h$ is embedded in $\mathcal{U}_0$ via point evaluation. Through this identification, $f(u_h)$ is well-defined for all $u_h \in \mathcal{U}_h$.

We will make this identification *only* when we evaluate $f(u_h)$. The reason for this is a conflict when interpreting elements u_h as lattice functions due to the fact that we identify lattice functions with their continuous interpolants with respect to the canonical triangulation $\mathcal{T}$, which would be different from the function u_h itself. However, for the evaluation of $f(u_h)$ this issue does not arise. □

3.2 Summary of results

3.2.1 Regularity of u^{a}

The approximation error analysis in later sections requires estimates on the decay of the elastic fields away from the defect core. These results follow from a natural stability assumption:

(A1) The atomistic solution is strongly stable, that is, there exists $C_0 > 0$ such that

$$\langle \delta^2 \mathcal{E}^{\mathrm{a}}(u^{\mathrm{a}})\varphi, \varphi \rangle \geq C_0 \|\nabla \varphi\|_{L^2}^2, \quad \forall \varphi \in \dot{\mathcal{U}}^{1,2}, \tag{3.2.1}$$

where u^{a} is a solution to (3.1.5).

Corollary 3.2.1. *Suppose that* **(A1)** *is satisfied, then there exists a constant $C > 0$ such that, for $1 \leq j \leq r-2$,*

$$|D^j u^{\mathrm{a}}(\ell)| \leq C|\ell|^{-1-j}.$$

Proof. See Theorem 2.3 in [18]. □

3.2.2 Stability

In [41] it is shown that there is a "universal" instability in 2D interfaces for QNL-type a/c couplings: it is impossible to prove in full generality that $\delta^2 \mathcal{E}^{\mathrm{g23}}(u^{\mathrm{a}})$ is a positive definite operator, even if we assume (3.2.1). Indeed, this potential instability is universal to a wide class of generalized geometric reconstruction methods. However, it is rarely observed in practice. To circumvent this difficulty, we make the following standing assumption:

(A2) The *homogeneous lattice* is strongly stable under the G23 approximation, that is, there exists $C_0^{\mathrm{g23}} > 0$ which is independent of K such that, for K sufficiently large,

$$\langle \delta^2 \mathcal{E}^{\mathrm{g23}}(0)\varphi_h, \varphi_h \rangle \geq C_0^{\mathrm{g23}} \|\nabla \varphi_h\|_{L^2}^2, \quad \forall \varphi_h \in \mathcal{U}_h. \tag{3.2.2}$$

Since (3.2.2) does not depend on the solution it can be tested numerically. But a precise understanding under which conditions (3.2.2) is satisfied is still missing. In [41] a method of stabilizing 2D QNL-type schemes with flat interfaces is introduced, which could

replace this assumption, however we are not yet able to extend this stabilizing method for interfaces with corners, such as the configurations discussed in this thesis.

3.2.3 Main results

To state the main results it is convenient to employ a smooth interpolant to measure the regularity of lattice functions. In Lemma 3.5.1, we define such an interpolant $\tilde{u} \in C^{2,1}(\mathbb{R}^2)$ for $u \in \mathcal{U}_0$, for which there exists a universal constant $\tilde{C}$ such that, for all $q \in [1,\infty]$, $0 \le j \le 3$,

$$|D^j u(\ell)| \le \tilde{C}\|\nabla^j \tilde{u}\|_{L^1(\omega_\ell)} \quad \text{and} \quad \|\nabla^j \tilde{u}\|_{L^q(T)} \le \tilde{C}\|D^j u\|_{\ell^q(\Lambda\cap T)}$$

where $\omega_\ell := \ell + \mathsf{A}(-1,1)^2$.

3.2.3.1 Consistency error estimate

In (3.4.6) we define a quasi-best approximation operator $\Pi_h : \mathcal{U}_0 \to \mathcal{U}_h$, which truncates an atomistic displacement to enforce the homogeneous Dirichlet boundary condition, and then interpolates it onto the finite element mesh.

Our main result is the following consistency error estimate.

Theorem 3.2.2. *If u^{a} is a solution to* (3.1.5) *then we have, for all $\varphi_h \in \mathcal{U}_h$,*

$$\begin{aligned}\langle \delta\mathcal{E}^{\mathrm{g23}}(\Pi_h u^{\mathrm{a}}), \varphi_h\rangle \lesssim \Big(&\|\nabla^2\tilde{u}^{\mathrm{a}}\|_{L^2(\Omega^{\mathrm{i}})} + \|\nabla^3\tilde{u}^{\mathrm{a}}\|_{L^2(\Omega^{\mathrm{c}})} + \|\nabla^2\tilde{u}^{\mathrm{a}}\|^2_{L^4(\Omega^{\mathrm{c}})} \\ &+ \|h^2\nabla^3\tilde{u}^{\mathrm{a}}\|_{L^2(\Omega_h^{\mathrm{c}})} + \|\nabla\tilde{u}^{\mathrm{a}}\|_{L^2(\mathbb{R}^2\setminus\mathcal{B}_{N/2})} \\ &+ N^{-1}\|h^2\nabla^2\tilde{u}^{\mathrm{a}}\|_{L^2(\mathcal{B}_N\setminus B_{N/2})}\Big)\|\nabla\varphi_h\|_{L^2(\mathbb{R}^2\setminus\Omega^{\mathrm{a}})},\end{aligned} \tag{3.2.3}$$

where Ω_h^{c} corresponds to the continuum region of Ω_h, and $h(x) := \mathrm{diam}(T)$ with $x \in T \in \mathcal{T}_h$.

3.2.3.2 Optimizing the approximation parameters

Before we estimate the error $\|\nabla\tilde{u}^{\mathrm{a}} - \nabla u_h^{\mathrm{g23}}\|_{L^2}$, we optimize the approximation parameters in the computational scheme. This means that the radius K of the atomistic region, the radius N of the entire computational domain and the mesh size h should satisfy certain balancing relations. We only outline the result of this optimisation and refer to § 3.5.7 for the details.

Due to the decay estimates on $\tilde{u}^{\mathrm{a}}$ (cf. Corollary 3.2.1) the dominating terms in (3.2.3) turn out to be

$$\|\nabla^2\tilde{u}^{\mathrm{a}}\|_{L^2(\Omega^{\mathrm{i}})} \lesssim K^{-5/2} \qquad \text{and} \qquad \|\nabla\tilde{u}^{\mathrm{a}}\|_{L^2(\mathbb{R}^2\setminus\mathcal{B}_{N/2})} \lesssim N^{-1}. \tag{3.2.4}$$

	β	N	$\mathcal{N}_h$	consistency error
P2-FEM	$(1, \frac{3}{2})$	$K^{5/2}$	K^2	$K^{-5/2}$
P1-FEM	$(1, \frac{3}{2})$	K^2	K^2	K^{-2}

Table 3.1: Quasi-optimal relations between approximation parameters for P2-GR23 and, for comparision, for P1-GR23.

(We will see momentarily that the mesh size plays a minor role.) These two terms result from the nature of the coupling scheme and the far-field truncation error. In particular, both of these cannot be improved by the choice of discretisation of the Cauchy–Born model, e.g., order of the FEM. We also note that, if we had employed a P1-FEM, the only different terms in the analog of (3.2.3) are $\|h\nabla^2\tilde{u}^{\rm a}\|_{L^2(\Omega^{\rm c})}$ rather than $\|h^2\nabla^3\tilde{u}^{\rm a}\|_{L^2(\Omega^{\rm c})}$, and $N^{-1}\|h\nabla\tilde{u}^{\rm a}\|_{L^2(\mathcal{B}_N\setminus B_{N/2})}$ rather than $N^{-1}\|h^2\nabla^2\tilde{u}^{\rm a}\|_{L^2(\mathcal{B}_N\setminus B_{N/2})}$, hence the limiting factor would have been $\|h\nabla^2\tilde{u}^{\rm a}\|_{L^2(\Omega^{\rm c})} \lesssim K^{-4}$ (at best); cf. §3.5.7.

We can balance the two terms in (3.2.4) by choosing $N \approx K^{5/2}$. It then remains to determine a mesh-size so that the finite element error contribution,

$$\|h^2\nabla^3\tilde{u}^{\rm a}\|_{L^2(\Omega_h^{\rm c})} \qquad \text{and} \qquad N^{-1}\|h^2\nabla^2\tilde{u}^{\rm a}\|_{L^2(\mathcal{B}_N\setminus B_{N/2})}$$

remains small in comparison. We show that the scaling $h(x) \approx \left(\frac{|x|}{K}\right)^{\beta}$ is a suitable choice, with $1 < \beta < 3/2$, under which both terms become of order $O(K^{-3})$.

Thus, we have determined the approximation parameters (K, N, h) in terms of a single parameter K. The quasi-optimal relations for P2-FEM discretization of the Cauchy–Born model are summarised in Table 3.1.

Corollary 3.2.3. *Suppose that N, h satisfy the relations of Table 3.1, the consistency error estimate (3.2.3) in terms of the number of degrees of freedom $\mathcal{N}_h$ can be written as*

$$\|\delta\mathcal{E}^{\rm g23}(\Pi_h u^{\rm a})\|_{\mathcal{U}^{-1,2}} \lesssim \mathcal{N}_h^{-5/4}. \tag{3.2.5}$$

3.2.3.3 Error estimate

To complete our summary of results, we now use the Inverse Function Theorem to obtain error estimates for the strains and the energy.

Theorem 3.2.4. *Suppose that **(A0)**, **(A1)** and **(A2)** are satisfied and that the quasi-optimal scaling of N and h depending on K from Table 3.1 is satisfied. Then, for sufficiently large atomistic region size K, a solution $u_h^{\rm g23}$ to* (3.1.13) *exists which satisfies*

the error estimates

$$\|\nabla u^{\mathrm{a}} - \nabla u_h^{\mathrm{g23}}\|_{L^2} \lesssim \mathcal{N}_h^{-5/4}, \quad \textit{and} \tag{3.2.6}$$

$$\left|[\mathcal{E}^{\mathrm{a}}(u^{\mathrm{a}}) - f(u^{\mathrm{a}})] - [\mathcal{E}^{\mathrm{g23}}(u_h^{\mathrm{g23}}) - f(u^{\mathrm{g23}})]\right| \lesssim \mathcal{N}_h^{-7/4}, \tag{3.2.7}$$

where $\mathcal{N}_h$ is the number of degrees of freedom and scales as $\mathcal{N}_h \sim K^2$.

Remark 3.2.5. The analogous estimates of P1-GR23 to (3.2.6) and (3.2.7) are $\mathcal{N}_h^{-1}$ and $\mathcal{N}_h^{-2}$ respectively.

□

3.2.4 Setup of the numerical tests

For our numerical tests, we consider an anti-plane displacement $u : \Lambda \to \mathbb{R}$. We choose a hexagonal atomistic region Ω^{a} with side length K and one layer of atomistic sites outside Ω^{a} as the interface. To construct the finite element mesh, we add hexagonal layers of elements such that, for each layer j, $h(\text{layer } j) = (|x|/K)^\beta$, with $\beta = 1.4$; see Figure 3.5. The procedure is terminated once the radius of the domain exceeds $N = \lceil K^{5/2} \rceil$. This construction guarantees the quasi-optimal approximation parameter balance to optimise the P2-FEM error. The derivation is given in Section 3.5.7.

In our tests we compare the P2-G23 method against

(1) a pure atomistic model with clamped boundary condition: the construction of the domain is as in the P2-G23 method, but without continuum region;

(2) a P1-G23 method: the construction is again identical to that of the P2-G23 method, but the P2-FEM in the definition of $\mathcal{U}_h$ is replaced by a P1-FEM. The same mesh scaling as for P2 is used (see also [16] where this is shown to be quasi-optimal).

The site potential is given by a nearest-neighbour embedded atom toy model,

$$V(Du) := G\left(\sum_{i=1}^{6} \rho(|D_i u(\ell)|)\right)$$

with $G(s) := s + \frac{1}{2}s^2$ and $\rho(r) := \sin^2(r\pi)$. This is a simplified anti-plane toy model as used in [18], which absorbs the pair interaction into the embedding term.

The external potential is defined by $\langle f, u\rangle = 10(u(0,0) - u(1,0))$, which can be thought of as an elastic dipole. A standard steepest descent method, preconditioned with a finite element Laplacian (see, for example [3]) and fixed (manually tuned) step-size, is used to find a minimizer u_h^{g23} of $\mathcal{E}^{g23}(u) - f(u)$ (see (3.1.9) for the formulation of $\mathcal{E}^{g23}$) using $u_h = 0$ as the starting guess.

In order to compare the errors, we use a comparison solution with atomistic region size $3K$ and other computational parameters scaled as above.

The numerical results, with brief discussions, are shown in Figures 3.6–3.9. The two most important observations are the following:

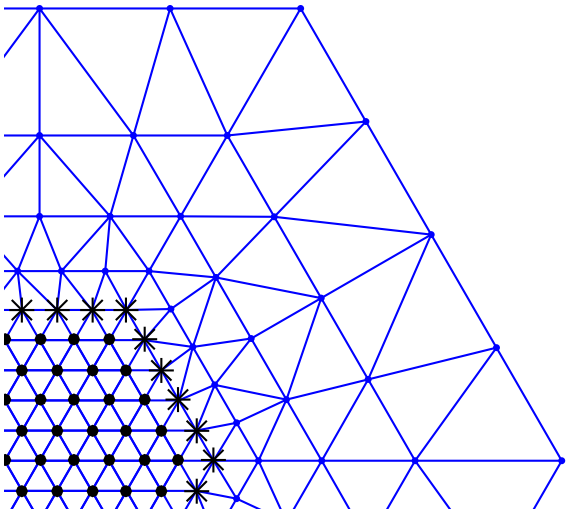

Figure 3.5: An example of the computatioanl mesh. The the vertices marked by "•" are the atomistic sites; the vertices marked by "∗" are the interface sites.

(1) the numerical tests confirm the analytical predictions for the geometry and the energy-norm errors, but the experimental rates for the energy error are better than the analytical rates. Similar observations were also made in [18].

(2) With our specific setup, the improvement of the P2-GR23 over P1-GR23 is clearly observed when plotting the error against $\#\mathcal{A} \propto \mathcal{N}_h$, but when plotted against $\mathcal{N}_h$ the improvement is only seen in the asymptotic regime. This indicates that further work is required, such as a posteriori adaption, to optimise the P2-GR23 in the pre-asymptotic regime as well.

3.2.5 Extension to high-order FEM

If we apply higher-order FEM in the continuum region, then to extend our error analysis we would need a smooth interpolant of $u \in \mathcal{U}_0$ with higher regularity than $\tilde{u} \in C^{2,1}(\mathbb{R}^2)$. A suitable extension given in [30] is, for arbitrary n, a $C^{n,1}$ piecewise polynomial of degree $2n+1$ with properties analogous to those stated in Lemma 3.5.1. The resulting higher-order decay rate $|\nabla^j \tilde{u}^{\rm a}(x)| \lesssim |x|^{-j-1}$ (cf. Corollary 3.2.1) indicates that the use of high-order FEM could be beneficial.

However, as we have pointed out in § 3.5.7, if we employ the mesh grading $h(x) = (|x|/K)^\beta$ with $1 < \beta < 3/2$ in the continuum region, the total approximation error cannot be improved by using Pp-FEM with $p > 2$, since the dominating term is the interface error $\|\nabla^2 \tilde{u}^{\rm a}\|_{L^2(\Omega^{\rm i})}$ for $p \geq 2$, which results from the construction of G23 coupling and is not affected by the choice of FEM.

If we consider a coarser mesh for high-order FEM in hopes of reducing the number of degrees of freedom, i.e., choosing $\beta \geq 3/2$, then applying analogous calculations to those in §3.5.7 gives us the following result:

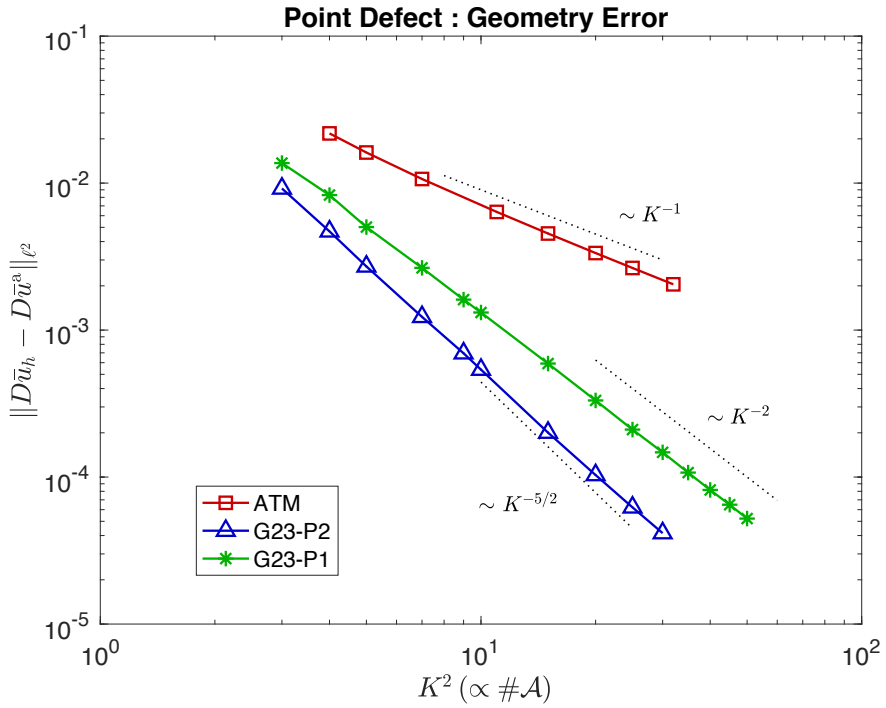

Figure 3.6: Error in energy norm plotted against $\#\mathcal{A}$. We clearly observe the predicted rate of convergence.

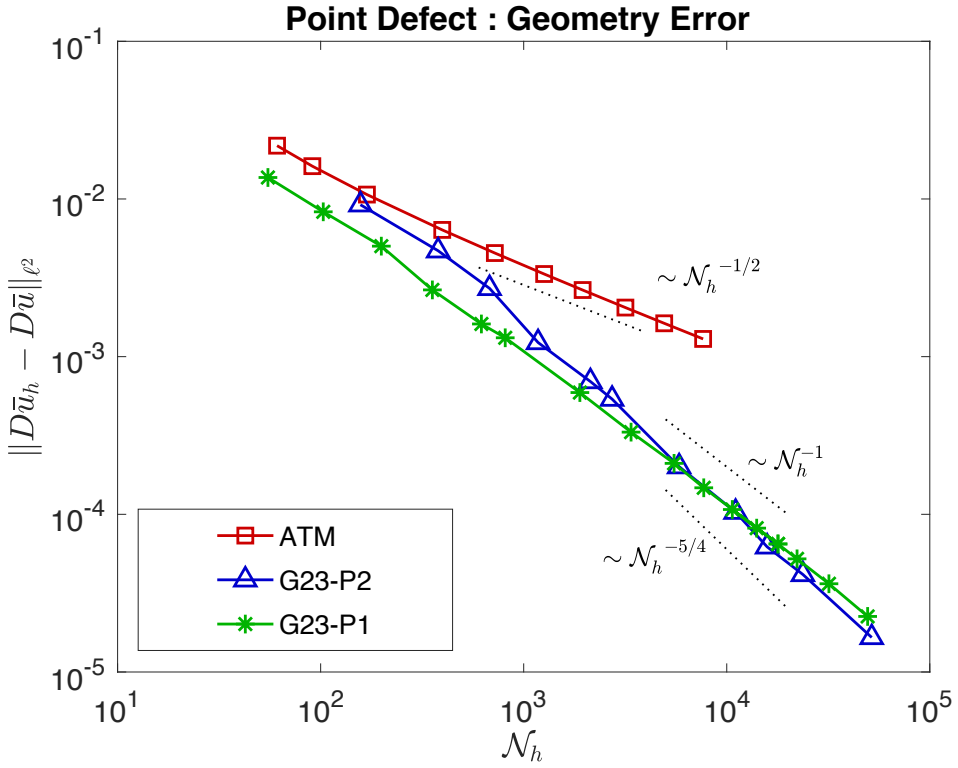

Figure 3.7: Error in energy norm plotted against the number of degrees of freedom. The improvement of P2-FEM is now only seen asymptotically.

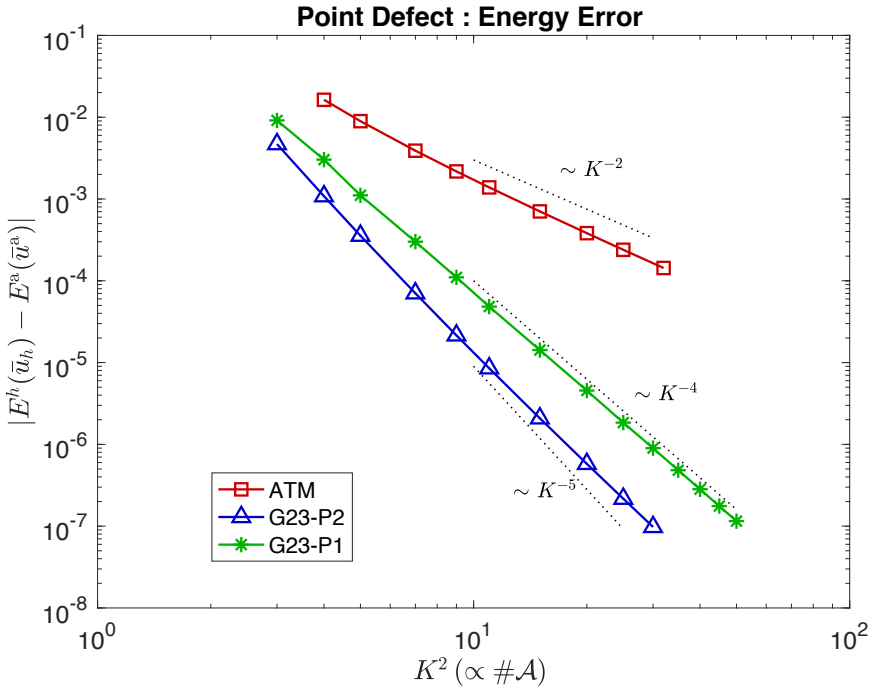

Figure 3.8: The energy error plotted against $\#\mathcal{A}$. The observed rate of convergence is better than the rate predicted in Theorem 3.2.4.

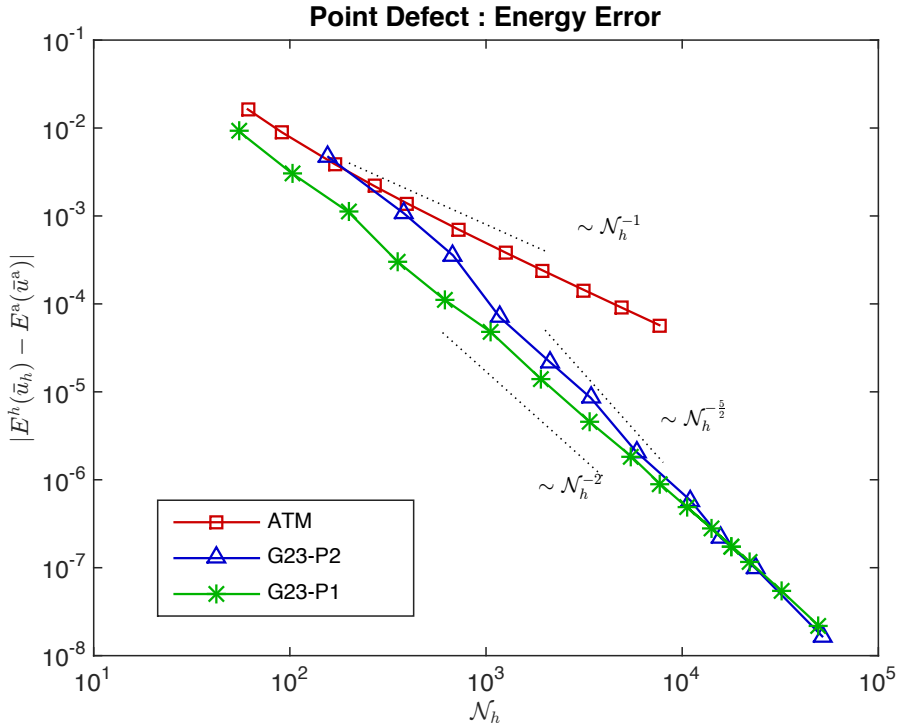

Figure 3.9: The energy error plotted against the number of degrees of freedom. The improvement of P2-FEM over P1-FEM can again only be observed asymptotically.

Employing Pp-FEM with $p \geq 2$, in order to match the convergence rate of the Cauchy–Born error term $\|\nabla^3 \tilde{u}^{\mathrm{a}}\|_{L^2(\Omega^{\mathrm{c}})} \sim K^{-3}$, the highest mesh coarsening rate is

$$\beta = \frac{5}{3} - \frac{1}{3p}.$$

This means that the optimal mesh grading that Pp-FEM can achieve without compromising accuracy is no greater than $\frac{5}{3}$. However, in that case, the number of degrees of freedom is always $\mathcal{O}(K^2)$. Thus higher-order FEM can at best improve the prefactor in the convergence rate.

3.3 Conclusion

We obtained a sharp energy-norm error estimate for the G23 coupling method with the P2-FEM discretisation of the continuum model. Furthermore, we demonstrated that, with the P1-FEM discretisation the FEM coarsening error is the dominating term in the consistency error estimate, whereas for the P2-FEM discretisation the interface error becomes the dominating term. In particular, a P2-FEM discretisation yields a more rapid decay of the error. Crucially though, since for Pp-FEM with $p \geq 2$ the interface contribution dominates, the total error the P2-FEM is already optimal. That is, increasing to $p > 2$ will not improve the rate of convergence, but increase the computational cost and algorithmic complexity.

Numerically, we observe that the improvement of P2-GR23 over P1-GR23 is only modest at moderate $\mathcal{N}_h$, hence a P2-GR23 scheme would be primarily of interest if very high accuracy of the solution is required. Purely according to our *a priori* error analysis, considering the additional algorithmic complexity, it is unclear how practically useful higher-order FEM in the context of A/C coupling are. However, before drawing such a universal conclusion, one should explore whether optimising the pre-asymptotic regime, using *hp* a posteriori mesh adaption, could lead to improved cost/error rates.

While our estimates for the error in energy-norm are sharp, our numerical results show that the estimates for the energy errors are suboptimal. We highlight the leading term in the error analysis which overestimates the error in Section 3.6.2. We are unable, at present, to obtain an optimal energy error estimate. This appears to be an open problem throughout the literature on hybrid atomistic multi-scale schemes; see e.g. [18].

In summary we conclude that using P2-FEM is a promising improvement to the efficiency of a/c coupling methods, but that some further work, both theoretical and for its implementation may be needed to exploit its full potential.

3.4 Reduction to consistency

Assuming the existence of an atomistic solution u^{a}, we seek to prove the existence of $u_h^{\mathrm{g23}} \in \mathcal{U}_h$ satisfying

$$\langle \delta \mathcal{E}^{\mathrm{g23}}(u_h^{\mathrm{g23}}), \varphi_h \rangle = \langle \delta f(u_h^{\mathrm{g23}}), \varphi_h \rangle, \quad \text{for all } \varphi_h \in \mathcal{U}_h, \tag{3.4.1}$$

and to estimate the error $\|u^{\mathrm{a}} - u_h^{\mathrm{g23}}\|$ in a suitable norm.

The error analysis consists of consistency and stability estimates. Once these are established we apply the following theorem to obtain the existence of a solution u_h^{g23} and the error estimate. The proof of this theorem is standard and can be found in various references, e.g. [46, Lemma 2.2].

Theorem 3.4.1 (The inverse function theorem). *Let $\mathcal{U}_h$ be a subspace of $\mathcal{U}$, equipped with $\|\nabla \cdot\|_{L^2}$, and let $\mathcal{G}_h \in C^1(\mathcal{U}_h, \mathcal{U}_h^*)$ with Lipschitz-continuous derivative $\delta \mathcal{G}_h$:*

$$\|\delta \mathcal{G}_h(u_h) - \delta \mathcal{G}_h(v_h)\|_{\mathcal{L}} \leq M \|\nabla u_h - \nabla v_h\|_{L^2} \quad \textit{for all } u_h, v_h \in \mathcal{U}_h,$$

where $\|\cdot\|_{\mathcal{L}}$ denotes the $\mathcal{L}(\mathcal{U}_h, \mathcal{U}_h^*)$-operator norm.

Let $\bar{u}_h \in \mathcal{U}_h$ satisfy

$$\|\mathcal{G}_h(\bar{u}_h)\|_{\mathcal{U}_h^*} \leq \eta, \tag{3.4.2}$$

$$\langle \delta \mathcal{G}_h(\bar{u}_h) v_h, v_h \rangle \geq \gamma \|\nabla v_h\|_{L^2}^2 \quad \textit{for all } v_h \in \mathcal{U}_h, \tag{3.4.3}$$

such that M, η, γ satisfy the relation

$$\frac{2M\eta}{\gamma^2} < 1.$$

Then there exists a (locally unique) $u_h \in \mathcal{U}_h$ such that $\mathcal{G}_h(u_h) = 0$,

$$\|\nabla u_h - \nabla \bar{u}_h\|_{L^2} \leq 2\frac{\eta}{\gamma}, \quad \textit{and}$$
$$\langle \delta \mathcal{G}_h(u_h) v_h, v_h \rangle \geq \left(1 - \frac{2M\eta}{\gamma^2}\right) \gamma \|\nabla v_h\|_{L^2}^2 \quad \textit{for all } v_h \in \mathcal{U}_h.$$

To ensure Dirichlet boundary conditions, we adapt the quasi-best approximation map defined in [18]. Let $\mu \in C^3(\mathbb{R}^2)$ be a cut-off function such that

$$\mu(x) = \begin{cases} 1 & 0 \leq x \leq \frac{1}{2}, \\ 0 & x \geq 1. \end{cases}$$

For $u : \Lambda \to \mathbb{R}^m$, define

$$\mathcal{L}u(x) := \mu\left(\frac{|x|}{N}\right)(\tilde{u}(x) - a_u), \text{ where } a_u := \frac{1}{|B_N \setminus B_{N/2}|}\int_{B_N \setminus B_{N/2}} \tilde{u}(y)\,\mathrm{d}y. \tag{3.4.4}$$

Let $\nu_{T,i}, i = 1, 2, 3$ be the vertices of T and m_e be the mid-point of an edge e. Then, the set of all *active* P2 finite element nodes is given by

$$\mathcal{N}_h := \{\nu_{T,i} \,|\, T \in \mathcal{T}_h, i = 1, 2, 3\} \cup \{m_e \,|\, e = T_1 \cap T_2, T_1, T_2 \in \mathcal{T}_h^c\}.$$

This includes all P1 nodes as well as the P2 nodes (edge midpoints) associated with edges entirely in the P2 region.

Furthermore, let $I_h^2 : C(\mathbb{R}^2; \mathbb{R}^m) \to \mathcal{U}_h$ be the interpolation operator such that, for $g \in C(\mathbb{R}^2; \mathbb{R}^m)$, $I_h^2(g)|_T \in \mathbb{P}^1(T)$ for $T \subset \mathcal{T}_h^a \cup \mathcal{T}_h^i$, $I_h^2(g)|_T \in \mathbb{P}^2(T)$ for $T \subset \mathcal{T}_h^c$, and

$$I_h^2(g)(x) = g(x) \qquad \text{for all } x \in \mathcal{N}_h.$$

Remark 3.4.2. We also introduce ghost nodes on the edges shared by interface and continuum elements:

$$\mathcal{N}_h^g := \{m_e \,|\, e = T_1 \cap T_2, T_1 \in \mathcal{T}_h^i, T_2 \in \mathcal{T}_h^c\}. \tag{3.4.5}$$

Then, for $x \in \mathcal{N}_h^g$, $I_h^2(g)(x) = (g(\nu_x^1) + g(\nu_x^2))/2$, where ν_x^1 and ν_x^2 are the vertices of the edge on which x lies. Hence, the P^1 and P^2 interpolants coincide on $\mathcal{N}_h^g$. □

We can now define the projection map (quasi-best approximation operator) $\Pi_h : \mathcal{U}_0 \to \mathcal{U}_h$ as

$$\Pi_h := I_h^2 \circ \mathcal{L}. \tag{3.4.6}$$

3.4.1 Stability

To put Theorem 3.4.1 (Inverse Function Theorem) into our context, let

$$\mathcal{G}_h(v) := \delta\mathcal{E}^{\mathrm{g23}}(v) - \delta f(v) \quad \text{and} \quad \bar{u}_h := \Pi_h u^{\mathrm{a}}.$$

To make (3.4.2) and (3.4.3) concrete we will show that there exist $\eta, \gamma > 0$ such that, for all $\varphi_h \in \mathcal{U}_h$,

$$\langle \delta\mathcal{E}^{\mathrm{g23}}(\Pi_h u^{\mathrm{a}}), \varphi_h\rangle - \langle \delta f(\Pi_h u^{\mathrm{a}}), \varphi_h\rangle \le \eta\|\nabla\varphi_h\|_{L^2}, \quad (\textit{consistency})$$
$$\langle \delta^2\mathcal{E}^{\mathrm{g23}}(\Pi_h u^{\mathrm{a}})\varphi_h, \varphi_h\rangle - \langle \delta^2 f(\Pi_h u^{\mathrm{a}})\varphi_h, \varphi_h\rangle \ge \gamma\|\nabla\varphi_h\|_{L^2}^2. \quad (\textit{stability})$$

Formally the inverse function theorem implies that, if η/γ is sufficiently small, then there exists $u_h^{\mathrm{g}23} \in \mathcal{U}_h$ such that

$$\begin{aligned}&\langle \delta\mathcal{E}^{\mathrm{g}23}(u_h^{\mathrm{g}23}), \varphi_h\rangle - \langle \delta f(u_h^{\mathrm{g}23}), \varphi_h\rangle = 0, \quad \forall \varphi_h \in \mathcal{U}_h, \quad \text{and}\\ &\|\nabla u_h^{\mathrm{g}23} - \nabla \Pi_h u^{\mathrm{a}}\|_{L^2} \leq 2\frac{\eta}{\gamma}.\end{aligned}$$

Finally adding the best approximation error $\|\nabla \Pi_h u^{\mathrm{a}} - \nabla u^{\mathrm{a}}\|_{L^2}$ gives the error estimate

$$\|\nabla u_h^{\mathrm{g}23} - \nabla u^{\mathrm{a}}\|_{L^2} \leq \|\nabla \Pi_h u^{\mathrm{a}} - \nabla u^{\mathrm{a}}\|_{L^2} + 2\frac{\eta}{\gamma}.$$

From the bounds (3.1.2) and (3.1.3) we can obtain the following Lipschitz continuity and stability results.

Lemma 3.4.3. *There exists $M > 0$ such that*

$$\|\delta\mathcal{G}_h(u_h) - \delta\mathcal{G}_h(v_h)\|_{\mathcal{L}} \leq M\|\nabla u_h - \nabla v_h\|_{L^2} \quad \textit{for all } u_h, v_h \in \mathcal{U}_h. \tag{3.4.7}$$

Proof. The result follows directly from (3.1.4) and the fact that $f \in C^r(\dot{\mathcal{U}}^{1,2})$ and that δf is compactly supported hence $\delta^2 f$ is also Lipschitz. Namely, for all $\varphi_h \in \mathcal{U}_h$,

$$\begin{aligned}&\langle (\delta\mathcal{G}_h(u_h) - \delta\mathcal{G}_h(v_h))\varphi_h, \varphi_h\rangle\\ =&\langle (\delta^2\mathcal{E}^{\mathrm{g}23}(u_h) - \delta^2\mathcal{E}^{\mathrm{g}23}(v_h))\varphi_h, \varphi_h\rangle + \langle (\delta^2 f(v_h) - \delta^2 f(u_h))\varphi_h, \varphi_h\rangle\\ \leq& C_{\mathrm{g}23}M_3\|\nabla u_h - \nabla v_h\|_{L^\infty}\|\nabla\varphi_h\|_{L^2}^2 + C_f\|u_h - v_h\|_{L^\infty(\mathcal{B}_{R_f})}\|\varphi_h\|_{L^2}^2\\ \lesssim& \|\nabla u_h - \nabla v_h\|_{L^2}\|\nabla\varphi_h\|_{L^2}^2 + \|\nabla u_h - \nabla v_h\|_{L^2(\mathcal{B}_{R_f})}\|\varphi_h\|_{L^2}^2,\end{aligned}$$

where $C_{\mathrm{g}23}$ is the constant resulting from the interface reconstruction and the linear elasticity formulation of Cauchy–Born in the continuum region, and C_f is the Lipschitz constant of $\delta^2 f$.

□

Lemma 3.4.4. *Under the assumptions **(A1)** and **(A2)**, if $\mathcal{G}_h(v) := \delta\mathcal{E}^{\mathrm{g}23}(v) - \delta f(v)$, then for any fixed mesh size h, there exists an independent constant $\gamma > 0$ such that, when K is sufficiently large,*

$$\langle \delta\mathcal{G}_h(\Pi_h u^{\mathrm{a}})\varphi_h, \varphi_h\rangle \geq \gamma\|\nabla\varphi_h\|_{L^2}^2 \quad \textit{for all } \varphi_h \in \mathcal{U}_h. \tag{3.4.8}$$

Proof. The proof of this result is a straightforward adaption of the proof of [30, Lemma 4.9], which is an analogous result for blending-type a/c coupling. The idea is to split the test function $\varphi_h \in \mathcal{U}_h$ into two parts: one that is supported only in Ω^{a} and one that is

supported further away when K increases. Let $L = \frac{1}{3}K$ and $\beta : \mathbb{R}^2 \to [0,1]$ be a smooth cut-off function such that

$$\beta(x) = \begin{cases} 1, & |x| < L+2 \\ 0, & |x| > 2L-2. \end{cases}$$

Define $z_a := \beta\varphi_h$ and $z_c := \varphi_h - z_a$. Then we have

$$\nabla z_a(x) = \begin{cases} \nabla\varphi_h(x), |x| \le L \\ 0, |x| \ge 2L \end{cases} \quad \text{and} \quad \nabla z_c(x) = \begin{cases} 0, |x| \le L \\ \nabla\varphi_h(x), |x| \ge 2L. \end{cases}$$

We observe that, when $K \to \infty$, $\nabla z_a \to \nabla\varphi_h$ and $\nabla z_c \rightharpoonup 0$ because $\langle \nabla z_c, \nabla\varphi_h\rangle \to 0$ when Ω^{a} is infinitely large. Then the second variation of the coupling energy can be written as

$$\begin{aligned} \langle \delta\mathcal{G}_h(\Pi_h u^{\mathrm{a}})\varphi_h, \varphi_h\rangle =& \langle \delta\mathcal{G}_h(\Pi_h u^{\mathrm{a}})z_a, z_a\rangle + \langle \delta\mathcal{G}_h(\Pi_h u^{\mathrm{a}})z_c, z_c\rangle \\ &+ 2\langle \delta\mathcal{G}_h(\Pi_h u^{\mathrm{a}})z_a, z_c\rangle \\ =:& \, a + b + c. \end{aligned}$$

We already know that ∇z_a is only supported in Ω^{a} and $\Pi_h u^{\mathrm{a}} = u^{\mathrm{a}}$ in Ω^{a} , which by **(A1)** gives

$$a = \langle \delta\mathcal{E}^{\mathrm{a}}(u^{\mathrm{a}})z_a, z_a\rangle \ge C_0 \|\nabla z_a\|_{L^2}^2.$$

For b, recalling the Lipschitz property (3.4.7) of $\delta\mathcal{G}_h$ we have, since $\nabla z_c \rightharpoonup 0$,

$$|b - \langle \delta\mathcal{G}_h(0)z_c, z_c\rangle| \le M\|\nabla\Pi_h u^{\mathrm{a}}\|_{L^2(\Omega_h\setminus B_L)}\|\nabla z_c\|^2_{L^2(\Omega_h\setminus B_L)} \to 0 \quad \text{as } L = \frac{1}{3}K \to \infty.$$

Recalling **(A2)**, we obtain that when K is sufficiently large, there exists some $C_0^{\mathrm{g23}} > C_b > 0$ such that

$$b \ge (C_0^{\mathrm{g23}} - C_b)\|\nabla z_c\|_{L^2}^2.$$

For c, we know that when $K \to \infty$, $\nabla z_a \to \nabla\varphi_h$ and $\nabla z_c \rightharpoonup 0$, hence we have $c \to 0$ as $K \to \infty$.

Combining a, b, c together, we have the result. □

3.5 Consistency estimate with a P2-FEM

3.5.1 Outline of the consistency estimate

We begin by decomposing the consistency error into

$$\begin{aligned} \langle \delta\mathcal{E}^{\mathrm{g23}}(\Pi_h u^{\mathrm{a}}), \varphi_h\rangle - \langle \delta f(\Pi_h u^{\mathrm{a}}), \varphi_h\rangle =& \left\{\langle \delta\mathcal{E}^{\mathrm{g23}}(\Pi_h u^{\mathrm{a}}), \varphi_h\rangle - \langle \delta\mathcal{E}^{\mathrm{a}}(u^{\mathrm{a}}), \varphi\rangle\right\} \\ &+ \left\{\langle \delta f(\Pi_h u^{\mathrm{a}}), \varphi_h\rangle - \langle \delta f(u^{\mathrm{a}}), \varphi\rangle\right\} \\ =:& \, \eta_{\mathrm{int}} + \eta_{\mathrm{ext}}, \end{aligned} \tag{3.5.1}$$

where $\varphi_h \in \mathcal{U}_h$ is given and we can choose $\varphi \in \mathcal{U}_0$ arbitrarily.

For $\varphi_h \in \mathcal{U}_h$, $\varphi_h|_T \in \mathbb{P}^2(T)$ for $T \in \mathcal{T}_h^c$. But the test function φ in $\langle \delta\mathcal{E}^{\rm a}(u^{\rm a}), \varphi\rangle$ is a piecewise linear lattice function. While we postpone the construction of φ, we will ensure that it is defined in such a way that $\varphi(\ell) = \varphi_h(\ell)$ for all $\ell \in \mathcal{A} \cup \mathcal{I} \cup \mathcal{I}^+$, where $\mathcal{I}^+$ is an extra layer of atomistic sites outside $\mathcal{I}$. With this assumption in place, we can further decompose $\eta_{\rm int}$ into the following parts,

$$\begin{aligned}
\eta_{\rm int} &= \int_{\Omega^{\rm c}} \partial_{\mathsf{F}} W(\nabla \tilde{u}^{\rm a}) : (\nabla \varphi_h - \nabla \varphi) \\
&\quad + \int_{\Omega^{\rm c}} (\partial_{\mathsf{F}} W(\nabla \Pi_h u^{\rm a}) - \partial_{\mathsf{F}} W(\nabla \tilde{u}^{\rm a})) : \nabla \varphi_h \\
&\quad + \int_{\Omega^{\rm c}} \big[\partial_{\mathsf{F}} W(\nabla \tilde{u}^{\rm a}) - \partial_{\mathsf{F}} W(\nabla u^{\rm a})\big] : \nabla \varphi \\
&\quad + \langle \delta\mathcal{E}^{\rm g23}(u^{\rm a}) - \delta\mathcal{E}^{\rm a}(u^{\rm a}), \varphi\rangle \\
&=: \delta_1 + \delta_2 + \delta_3 + \delta_4,
\end{aligned} \tag{3.5.2}$$

where $\tilde{u}^{\rm a}$ is the smooth interpolant of $u^{\rm a}$ defined in Lemma 3.5.1 below. By $\nabla\varphi$ in δ_1 we mean the gradient of the canonical linear interpolant of φ. To estimate δ_2 we require an approximation error estimate for $\Pi_h u - u$. To estimate δ_3 we will exploit the fact that the atomistic triangulation $\mathcal{T}$ is uniform to prove a super-convergence estimate. Finally, for the modelling error, δ_4, we employ the techniques developed in [44].

To define the smooth interpolant $\tilde{u}^{\rm a}$, we use the construction from [30], namely a $C^{2,1}$-conforming multi-quintic interpolant. Although the interpolant defined in [30] is for lattice functions on $\mathbb{Z}^2$, we can use the linear transformation from $\mathbb{Z}^2$ to $\Lambda = \mathsf{A}\mathbb{Z}^2$ to obtain a modified interpolant.

Lemma 3.5.1. *(a) For each $u : \Lambda \to \mathbb{R}^m$, there exists a unique $\tilde{u} \in C^{2,1}(\mathbb{R}^2;\mathbb{R}^m)$ such that, for all $\ell \in \Lambda$,*

$$\begin{aligned}
\tilde{u}|_{\ell+\mathsf{A}(0,1)^2} &\text{ is a polynomial of degree 5,} \\
\tilde{u}(\ell) &= u(\ell), \\
\partial_{a_i}\tilde{u}(\ell) &= \tfrac{1}{2}\left(u(\ell + a_i) - u(\ell - a_i)\right), \\
\partial_{a_i}^2\tilde{u}(\ell) &= u(\ell + a_i) - 2u(\ell) + u(\ell - a_i),
\end{aligned}$$

where $i \in \{1,2\}$ and ∂_{a_i} is the derivative in the direction of a_i.

(b) Moreover, for $q \in [1,\infty]$, $0 \le j \le 3$,

$$\|\nabla^j \tilde{u}\|_{L^q(\ell+\mathsf{A}(1,0)^2)} \lesssim \|D^j u\|_{\ell^q(\ell+\mathsf{A}\{-1,0,1,2\}^2)} \quad \text{and} \quad |D^j u(\ell)| \lesssim \|\nabla^j \tilde{u}\|_{L^1(\ell+\mathsf{A}(-1,1)^2)}, \tag{3.5.3}$$

where D is the difference operator defined in (3.1.1)*. In particular,*

$$\|\nabla \tilde{u}\|_{L^q} \lesssim \|\nabla u\|_{L^q} \lesssim \|\nabla \tilde{u}\|_{L^q},$$

where u is identified with its piecewise affine interpolant.

Proof. Let $v : \mathbb{Z}^2 \to \mathbb{R}^m$ and $v(\xi) := u(\mathsf{A}\xi)$ for all $\xi \in \mathbb{Z}$. Then [30, Lemma 1] shows that

there exists a unique $\tilde{v} \in C^{2,1}(\mathbb{R}^2;\mathbb{R}^m)$ such that, for $\xi \in \mathbb{Z}^2$,

$$\begin{aligned}
\tilde{v}|_{\xi+(0,1)^2} &\text{ is a polynomial of degree 5,}\\
\tilde{v}(\xi) &= v(\xi),\\
\partial_{e_i}\tilde{v}(\xi) &= \tfrac{1}{2}\left(v(\xi+e_i) - v(\xi-e_i)\right),\\
\partial^2_{e_i}\tilde{v}(\xi) &= v(\xi+e_i) - 2v(\xi) + v(\xi-e_i) \quad i=1,2,
\end{aligned}$$

Defining $\tilde{u}(x) := \tilde{v}(\mathsf{A}^{-1}x)$ for all $x \in \mathbb{R}^2$ proves part(a).

For part (b), [30, Lemma 1] establishes also that there exists a constant C_j' such that, for $\xi \in \mathbb{Z}^2$, $1 \le j \le 3$, $q \in [1,\infty]$,

$$\|\nabla^j \tilde{v}\|_{L^q(\xi+(1,0)^2)} \le C_j' \|\hat{D}^j v\|_{\ell^q(\xi+\{-1,0,1,2\}^2)},$$

where $\hat{D}$ represents the 4-stencil difference operator in $\mathbb{Z}^2$: let $\mathcal{R} := \{\rho \in \mathbb{Z}^2 \,|\, |\rho| = 1\}$, then $\hat{D}v(\ell) := (\hat{D}_\rho v(\ell))_{\rho\in\mathcal{R}}$ with $\hat{D}_\rho v(\ell) := v(\ell+\rho) - v(\ell)$. After transformation, we have, for $\xi = \mathsf{A}\ell \in \Lambda$,

$$\hat{D}v(\ell) = (D_i u(\xi))_{i=1,2,4,5}.$$

By adding the additional stencil elements D_3, D_6 we obtain

$$\begin{aligned}
C_j''\|\nabla^j \tilde{u}\|_{L^q(\xi+\mathsf{A}(1,0)^2)} &\le \|\nabla^j \tilde{v}\|_{L^q(\ell+(1,0)^2)}\\
&\le C_j'\|\hat{D}^j v\|_{\ell^q(\ell+\{-1,0,1,2\}^2)} \le C_j'''\|D^j u\|_{\ell^q(\xi+\mathsf{A}\{-1,0,1,2\}^2)},
\end{aligned}$$

where C_j'' and C_j''' only depend on j. Writing $C := \max_{1\le j\le 3}\left(\frac{C_j'''}{C_j''}\right)$ yields the first inequality of (3.5.3). Following a similar argument the second inequality also holds. □

3.5.2 Construction of φ and estimation of δ_1

Recall that

$$\delta_1 := \int_{\Omega^{\mathrm{c}}} \partial_{\mathsf{F}} W(\nabla \tilde{u}^{\mathrm{a}}) : (\nabla\varphi_h - \nabla\varphi).$$

We adapt the modified quasi-interpolation operator introduced in [5] to approximate a test function $\varphi_h \in \mathcal{U}_h$. The advantage of this interpolation operator is that by using the setting of a partition of unity the approximation error has a local average zero. Consequently we can apply the Poincaré inequality on patches to obtain local estimates.

We think of the construction of φ as a Dirichlet boundary problem with the outer boundary $\partial\Omega_h$ and the inner boundary $\partial\Omega^{\mathrm{c}}$. Let ϕ_ℓ be the piecewise linear hat-functions on the canonical triangulation $\mathcal{T}$ associated with $\ell \in \Lambda$. Define

$$\phi_\ell^{\mathrm{PU}} := \frac{\phi_\ell}{\sum_{k\in\mathcal{C}\cap\Omega_h}\phi_k}, \quad \forall \ell \in \mathcal{C},$$

where $\mathcal{C}$ is the continuum lattice sites as defined in §3.1.4. It is clear that $\{\phi_\ell^{\mathrm{PU}}\}_{\ell\in\mathcal{C}\cap\Omega_h}$ is a partition of unity.

Now we refer to [5] for the contruction of a linear interpolant of $\varphi_h \in \mathcal{U}_h$. We shall define the interpolant as follows:

$$\Pi_h^* \varphi_h(x) := \varphi(x) := \varphi_1(x) + \varphi_2(x), \quad \forall x \in \mathbb{R}^2, \tag{3.5.4}$$

where

$$\begin{aligned}
\varphi_1(\ell) &:= \begin{cases} \varphi_h(\ell), & \ell \in \mathcal{A} \cup \mathcal{I} \cup \mathcal{I}^+, \\ \frac{\int_{\mathbb{R}^2} \phi_\ell \varphi_h}{\int_{\mathbb{R}^2} \phi_\ell}, & \ell \in \mathcal{C} \setminus \mathcal{I}^+, \end{cases} \\
\varphi_1(x) &:= \sum_{\ell \in \Lambda} \varphi_1(\ell) \phi_\ell(x), \quad \forall x \in \mathbb{R}^2, \\
\varphi_2(\ell) &:= \begin{cases} \frac{\int_{\mathbb{R}^2} (\varphi_h - \varphi_1) \phi_\ell^{\mathrm{PU}}}{\int_{\mathbb{R}^2} \phi_\ell}, & \ell \in \mathcal{C} \setminus \mathcal{I}^+, \\ 0, & \ell \in \mathcal{A} \cup \mathcal{I} \cup \mathcal{I}^+, \end{cases} \\
\varphi_2(x) &:= \sum_{\ell \in \Lambda} \varphi_2(\ell) \phi_\ell(x), \quad \forall x \in \mathbb{R}^2.
\end{aligned}$$

Observe that φ_h and φ both are supported on a finite domain, hence we can use Theorem 3.1 in [5] to conclude that

$$\|\nabla \varphi\|_{L^2(\mathbb{R}^2)} \lesssim \|\nabla \varphi_h\|_{L^2(\mathbb{R}^2)}, \quad \forall \varphi_h \in \mathcal{U}_h.$$

Let $g := -\mathrm{div}\,[\partial_{\mathsf{F}} W(\nabla \tilde{u}^{\mathrm{a}})]$. Then

$$\delta_1 = \int_{\Omega^{\mathrm{c}}} g \cdot (\varphi_h - \varphi)\,\mathrm{d}x = \int_{\Omega^{\mathrm{c}}} g \cdot ((\varphi_h - \varphi_1) - \varphi_2)\,\mathrm{d}x$$

Since φ_2 is a piecewise-linear quasi-interpolant of $\varphi_h - \varphi_1$ as defined in [5], a direct consequence of Theorem 3.1 in [5] is that there exists $C > 0$ such that, recalling $\Omega_h^{\mathrm{a}} := \bigcup \mathcal{T}_h^{\mathrm{a}}$,

$$\delta_1 \leq C \|\nabla(\varphi_h - \varphi_1)\|_{L^2(\mathbb{R}^2 \setminus \Omega_h^{\mathrm{a}})} \left(\sum_{\ell \in \mathcal{C} \cap \Omega_h} d_\ell^2 \int_{w_\ell} \phi_\ell^{\mathrm{PU}} |g - \langle g \rangle_\ell|^2 \,\mathrm{d}x \right)^{1/2},$$

where $w_\ell := \mathrm{supp}(\phi_\ell)$, $\langle g \rangle_\ell := 1/|w_\ell| \int_{w_\ell} g(x)\,\mathrm{d}x$ and $d_\ell := \mathrm{diam}(w_\ell) = 1$. With the sharp Poincaré constant derived by [1] , we have

$$\int_{w_\ell} \phi_\ell^{\mathrm{PU}} |g - \langle g \rangle_\ell|^2 \,\mathrm{d}x \leq \int_{w_\ell} |g - \langle g \rangle_\ell|^2 \,\mathrm{d}x \leq \tfrac{1}{4} d_\ell^2 \|\nabla g\|_{L^2(w_\ell)}^2.$$

On the other hand, φ_1 is a standard quasi-interpolant of φ_h in $\bigcup \mathcal{T}_h^c$, which implies that there exists $C' > 0$ such that

$$\|\nabla(\varphi_h - \varphi_1)\|_{L^2(\mathbb{R}^2 \setminus \Omega_h^{\mathrm{a}})} \leq C' \|\nabla \varphi_h\|_{L^2(\mathbb{R}^2 \setminus \Omega_h^{\mathrm{a}})}. \tag{3.5.5}$$

Due to the fact that $d_\ell = 1$ and that each point in $\mathbb{R}^2 \setminus \Omega_h^{\mathrm{a}}$ is covered by at most

three w_ℓ, we have

$$\begin{aligned}\delta_1 &\le C \max_\ell d_\ell^2 \|\nabla g\|_{L^2(\mathbb{R}^2\setminus\Omega_h^{\mathrm{a}})} \|\nabla\varphi_h\|_{L^2(\mathbb{R}^2\setminus\Omega_h^{\mathrm{a}})} \\ &\le C\left(M_2\|\nabla^3\tilde{u}^{\mathrm{a}}\|_{L^2(\mathbb{R}^2\setminus\Omega_h^{\mathrm{a}})} + M_3\|\nabla^2\tilde{u}^{\mathrm{a}}\|^2_{L^4(\mathbb{R}^2\setminus\Omega_h^{\mathrm{a}})}\right)\|\nabla\varphi_h\|_{L^2(\mathbb{R}^2\setminus\Omega_h^{\mathrm{a}})}, \end{aligned} \tag{3.5.6}$$

where we used the following estimate, for some $c > 0$,

$$\begin{aligned}\|\nabla g\|_{L^2(\Omega_h)} &= \|\nabla \mathrm{div}[\partial_{\mathsf{F}} W(\nabla\tilde{u}^{\mathrm{a}})]\|_{L^2(\mathbb{R}^2\setminus\Omega_h^{\mathrm{a}})} \\ &= \|\nabla\left(\partial^2_{\mathsf{F}} W(\nabla\tilde{u}^{\mathrm{a}})\nabla^2\tilde{u}^{\mathrm{a}}\right)\|_{L^2(\mathbb{R}^2\setminus\Omega_h^{\mathrm{a}})} \\ &= \left\|\partial^2_{\mathsf{F}} W(\nabla\tilde{u}^{\mathrm{a}})\nabla^3\tilde{u}^{\mathrm{a}} + \partial^3_{\mathsf{F}} W(\nabla\tilde{u}^{\mathrm{a}})\left(\nabla^2\tilde{u}^{\mathrm{a}}\right)^2\right\|_{L^2(\mathbb{R}^2\setminus\Omega_h^{\mathrm{a}})} \\ &\le c\left(M_2\|\nabla^3\tilde{u}^{\mathrm{a}}\|_{L^2(\mathbb{R}^2\setminus\Omega_h^{\mathrm{a}})} + M_3\|\nabla^2\tilde{u}^{\mathrm{a}}\|^2_{L^4(\mathbb{R}^2\setminus\Omega_h^{\mathrm{a}})}\right),\end{aligned}$$

employing the global bounds (3.1.2) and (3.1.3). This completes the estimate for δ_1.

3.5.3 Estimation of δ_2

Recall that

$$\delta_2 := \int_{\Omega^{\mathrm{c}}} (\partial_{\mathsf{F}} W(\nabla\Pi_h u^{\mathrm{a}}) - \partial_{\mathsf{F}} W(\nabla\tilde{u}^{\mathrm{a}})) : \nabla\varphi_h.$$

We start with estimating the best approximation error.

Lemma 3.5.2. *Let $T \in \mathcal{T}_h^c$, $u \in \dot{\mathcal{U}}^{1,2}$ and $v \in W^{3,2}(\mathbb{R}^2)$. Then we have the following estimates.*

(a) Denote $h_T := \mathrm{diam}(T)$, then

$$\|\nabla v - \nabla I_h^2 v\|_{L^2(T)} \lesssim h_T^2 \|\nabla^3 v\|_{L^2(T)}.$$

(b) There exists a constant $C > 0$ such that, for any domain $S \supset \mathcal{B}_N$,

$$\|\nabla\mathcal{L}u - \nabla\tilde{u}\|_{L^2(S)} \le C\|\nabla\tilde{u}\|_{L^2\left(S\setminus\mathcal{B}_{N/2}\right)},$$

where $\mathcal{L}$ is the cut-off function defined by (3.4.4).

(c) Furthermore, we have the best approximation error estimate

$$\begin{aligned}\|\nabla\Pi_h u - \nabla\tilde{u}\|_{L^2(\Omega^{\mathrm{c}})} \lesssim &\|h^2\nabla^3\tilde{u}^{\mathrm{a}}\|_{L^2(\Omega_h^{\mathrm{c}})} + \|\nabla\tilde{u}^{\mathrm{a}}\|_{L^2\left(\mathbb{R}^2\setminus\mathcal{B}_{N/2}\right)} \\ &+ N^{-1}\|h^2\nabla^2\tilde{u}\|_{L^2(\mathcal{B}_N\setminus\mathcal{B}_{N/2})},\end{aligned} \tag{3.5.7}$$

where $h(x) := \mathrm{diam}(T)$ with $x \in T$.

Proof. Recall the uniform shape regularity assumption (3.1.11).

Part (a) follows directly from the Bramble–Hilbert Lemma.

For Part (b), we use a variation of Theorem 2.1 in [42]. Applying Poincaré's inequality gives

$$\begin{aligned}\|\nabla\mathcal{L}(u)-\nabla\tilde{u}\|_{L^2(S)} &= \big\|N^{-1}\mu'(\tilde{u}-a)+(\mu-1)\nabla\tilde{u}\big\|_{L^2(S)}\\ &\le N^{-1}C_\mu\|\tilde{u}-a\|_{L^2(S)}+\|(1-\mu)\nabla\tilde{u}\|_{L^2(S\setminus B_{N/2})}\\ &\le C_pC_\mu\|\nabla\tilde{u}\|_{L^2(\mathcal{B}_N\setminus\mathcal{B}_{N/2})}+\|(1-\mu)\nabla\tilde{u}\|_{L^2(S\setminus\mathcal{B}_{N/2})}\\ &\le C\|\nabla\tilde{u}\|_{L^2(S\setminus\mathcal{B}_{N/2})}.\end{aligned}$$

For Part (c), we combine Part (a) and (b), that is

$$\begin{aligned}\|\nabla\Pi_h u-\nabla\tilde{u}\|_{L^2(\Omega^{\mathrm{c}})} &\le \|\nabla(I_h^2\circ\mathcal{L})(u)-\nabla\mathcal{L}(u)\|_{L^2(\Omega^{\mathrm{c}})}+\|\nabla\mathcal{L}(u)-\nabla\tilde{u}\|_{L^2(\Omega^{\mathrm{c}})}\\ &\lesssim \|h^2\nabla^3\mathcal{L}(u)\|_{L^2(\Omega^{\mathrm{c}})}+\|\nabla\tilde{u}\|_{L^2(\Omega^{\mathrm{c}}\setminus\mathcal{B}_{N/2})}\\ &= \left\|h^2\sum_{n=0}^{3}\frac{1}{N^n}\nabla^n\mu\nabla^{3-n}(\tilde{u}-a)\right\|_{L^2(\mathcal{B}_N\setminus\Omega^{\mathrm{a}})}+\|\nabla\tilde{u}\|_{L^2(\mathbb{R}^2\setminus\mathcal{B}_{N/2})}\\ &\lesssim \|h^2\nabla^3\tilde{u}\|_{L^2(\Omega_h^{\mathrm{c}})}+\|\nabla\tilde{u}\|_{L^2(\mathbb{R}^2\setminus\mathcal{B}_{N/2})}+\frac{1}{N}\|h^2\nabla^2\tilde{u}\|_{L^2(\mathcal{B}_N\setminus B_{N/2})}.\end{aligned}$$

The last line only contains the terms with $n=0,1$. The term for $n=2$ is

$$N^{-2}\|h^2\nabla\tilde{u}\|_{L^2(\mathcal{B}_N\setminus B_{N/2})},$$

but since $N^{-2}h^2\lesssim 1$ this is absorved into $\|\nabla\tilde{u}\|_{L^2(\mathbb{R}^2\setminus\mathcal{B}_{N/2})}$. For $n=3$, using Poincaré's inequality a similar argument applies. □

The estimate for δ_2 is now a consequence of the best approximation error estimate:

$$\begin{aligned}\delta_2 &\le \|\partial_{\mathsf{F}}W(\nabla\Pi_h u^{\mathrm{a}})-\partial_{\mathsf{F}}W(\nabla\tilde{u}^{\mathrm{a}})\|_{L^2(\Omega^{\mathrm{c}})}\|\nabla\varphi_h\|_{L^2(\Omega^{\mathrm{c}})}\\ &\le M_2\|\nabla\Pi_h u^{\mathrm{a}}-\nabla\tilde{u}^{\mathrm{a}}\|_{L^2(\Omega^{\mathrm{c}})}\|\nabla\varphi_h\|_{L^2(\Omega^{\mathrm{c}})}\\ &\lesssim \Big(\|h^2\nabla^3\tilde{u}^{\mathrm{a}}\|_{L^2(\Omega_h^{\mathrm{c}})}+\|\nabla\tilde{u}^{\mathrm{a}}\|_{L^2\left(\mathbb{R}^2\setminus\mathcal{B}_{N/2}\right)}+N^{-1}\|h^2\nabla^2\tilde{u}\|_{L^2(\mathcal{B}_N\setminus B_{N/2})}\Big)\|\nabla\varphi_h\|_{L^2(\Omega^{\mathrm{c}})}.\end{aligned}\tag{3.5.8}$$

3.5.4 Estimation of δ_3

Recall that

$$\delta_3=\int_{\Omega^{\mathrm{c}}}\left[\partial_{\mathsf{F}}W(\nabla\tilde{u}^{\mathrm{a}})-\partial_{\mathsf{F}}W(\nabla u^{\mathrm{a}})\right]:\nabla\varphi,$$

where φ is a lattice function with compact support and $\nabla\varphi$ denotes the gradient of its piecwise linear interpolant. To estimate this term we observe that u^{a} can be interpreted as the P1 nodal interpolant of $\tilde{u}^{\mathrm{a}}$. Although this indicates a first-order estimate only, we can exploit mesh regularity to obtain a second-order superconvergence estimate.

To that end, we rewrite the integral over the domain as a summation of elements. Let $\mathring{E}$ be the union of edges that are shared by two continuum elements, and ω_e be the

union of said elements, i.e.,

$$\mathring{E} := \{e = T_1 \cap T_2 \,|\, T_1, T_2 \in \mathcal{T}_\mathcal{C}\}.$$
$$\omega_e := T_1 \cup T_2, \quad \text{where } T_1 \cap T_2 = e.$$

Recall that $W(\mathsf{F}) \equiv \frac{1}{\Omega_0} V(\mathsf{F} \cdot \mathbf{a})$. Observe that for a pair of T_1, T_2 sharing a common edge e which has the direction of a_j, $\nabla_{a_j}\varphi(T_1) = \nabla_{a_j}\varphi(T_2)$, which allows us to re-group integration over elements as integration of patches ω_e *except* for elements near the interface. After simplifying the notation by writing $\tilde{V}_j := \partial_j V(\nabla \tilde{u} \cdot \boldsymbol{a})$ and $V_j := \partial_j V(\nabla u \cdot \mathbf{a})$, we can rewrite δ_3 as follows:

$$\begin{aligned}
\delta_3 &= \frac{1}{\Omega_0} \sum_{T \in \mathcal{T}_\mathcal{C} \cup \mathcal{T}_\mathcal{I}} \sum_{j=1}^{6} \int_{T \cap \Omega^{\mathrm{c}}} \big[\tilde{V}_j - V_j\big] \cdot \nabla_{a_j}\varphi(T) \\
&= \frac{1}{\Omega_0} \sum_{j=1}^{6} \sum_{e \in \mathring{E}_j} \int_{\omega_e} \big[\tilde{V}_j - V_j\big] \cdot \nabla_{a_j}\varphi \\
&\qquad + \frac{1}{\Omega_0} \sum_{T \in \mathcal{T}_\mathcal{C} \cup \mathcal{T}_\mathcal{I}} \sum_{j=1}^{6} c_{T,j} \int_{T \cap \Omega^{\mathrm{c}}} \big[\tilde{V}_j - V_j\big] \cdot \nabla_{a_j}\varphi(T) \\
&=: \tau_1 + \tau_2,
\end{aligned}$$

where $\mathring{E}_j := \{e \in \mathring{E} \,|\, e \text{ is in the direction of } a_j\}$ and $c_{T,j}$ is defined as follows,

$$c_{T,j} = \begin{cases} 0, & \exists e \in \mathring{E}_j \cap T, \\ 1, & \text{otherwise.} \end{cases}$$

Observe that for $T \in \mathcal{T}_\mathcal{C}$, $c_{T,j}$ is only non-zero near the interface. So we have

$$\tau_2 \leq \frac{1}{\Omega_0} \int_{\Omega^i_+} M_2 |\nabla \tilde{u}^{\mathrm{a}} - \nabla u^{\mathrm{a}}| \, |\nabla \varphi| \lesssim \|\nabla^2 \tilde{u}^{\mathrm{a}}\|_{L^2(\Omega^i_+)} \|\nabla \varphi\|_{L^2(\Omega^i_+)}, \tag{3.5.9}$$

where $\Omega^i_+ := \bigcup \{T \in \mathcal{T}_\mathcal{C} \,|\, \mathrm{dist}(T, \Omega^i) \leq 1/2\}$. Note that the second-order error $\nabla^2 \tilde{u}^{\mathrm{a}}$ results from the fact that u^{a} is a piecewise linear nodal interpolant of $\tilde{u}^{\mathrm{a}}$ on a uniform mesh.

To estimate τ_1, we employ the following second-order mid-point estimate.

Lemma 3.5.3. *Suppose $f \in W^{2,\infty}(T_1 \cup T_2; \mathbb{R})$ where $T_1, T_2 \in \mathcal{T}$ such that they share an edge e and let m_e be the mid-point of e, then*

$$\left| \int_{T_1 \cup T_2} f(\xi) - f(m_e) \, \mathrm{d}\xi \right| \lesssim \|\nabla^2 f\|_{L^\infty(T_1 \cup T_2)}.$$

Then we can write

$$\tau_1 = \frac{1}{\Omega_0} \sum_{j=1}^{6} \sum_{e \in \mathring{E}_j} \int_{\omega_e} \Big[(\tilde{V}_j - \tilde{V}_j(m_e)) - (V_j - \tilde{V}_j(m_e))\Big] \cdot \nabla_{a_j}\varphi. \tag{3.5.10}$$

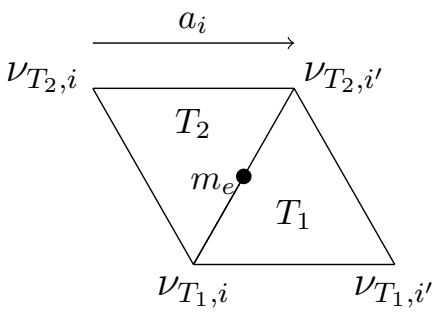

Figure 3.10: An illustration of the mid-point rule.

By Lemma 3.5.3 we have

$$\begin{aligned}\left|\int_{\omega_e}\big(\tilde{V}_j-\tilde{V}_j(m_e)\big)\right| &\lesssim \|\nabla^2\partial_j V(\nabla\tilde{u}^{\mathrm{a}}\cdot\mathbf{a}))\|_{L^\infty(\omega_e)}\\ &\lesssim \Big(M_3\|\nabla^2\tilde{u}^{\mathrm{a}}\|^2_{L^\infty(\omega_e)}+M_2\|\nabla^3\tilde{u}^{\mathrm{a}}\|_{L^\infty(\omega_e)}\Big)\\ &\lesssim \|\nabla^2\tilde{u}^{\mathrm{a}}\|^2_{L^4(\omega_e)}+\|\nabla^3\tilde{u}^{\mathrm{a}}\|_{L^2(\omega_e)},\end{aligned}\tag{3.5.11}$$

where the last line comes from the fact that $\tilde{u}^{\mathrm{a}}$ is a polynomial of degree 5 on each T, hence on each patch ω_e the norms are equivalent.

On the other hand, for $i=1,...6$ we denote $\nu_{T,i}$ and $\nu_{T,i'}$ as the vertices of T with $\nu_{T,i}+a_i=\nu_{T,i'}$. Then on $T\supset e$, we have, using Taylor expansion,

$$\nabla u^{\mathrm{a}}|_T\cdot a_i-\nabla\tilde{u}^{\mathrm{a}}(m_e)\cdot a_i=\tilde{u}^{\mathrm{a}}(\nu_{T,i'})-\tilde{u}^{\mathrm{a}}(\nu_{T,i})-\nabla\tilde{u}^{\mathrm{a}}(m_e)\cdot a_i=\tau_e,$$

where $|\tau_e|\lesssim\|\nabla^3\tilde{u}^{\mathrm{a}}\|_{L^\infty(\omega_e)}$. Then for T_1 and T_2 with $T_1\cap T_2=e=[\nu_{T,i},\nu_{T,i'}]$, we have

$$[\nabla u^{\mathrm{a}}(T_1)\cdot a_i-\nabla\tilde{u}^{\mathrm{a}}(m_e)\cdot a_i]+[\nabla u^{\mathrm{a}}(T_2)\cdot a_i-\nabla\tilde{u}^{\mathrm{a}}(m_e)\cdot a_i]=2\tau_e.$$

(See also Figure 3.10.) Hence, we can estimate

$$\begin{aligned}&\left|\int_{\omega_e}V_j-\tilde{V}_j(m_e)\right|\\ =&\Big||T_1|(V_j|_{T_1}-\tilde{V}_j(m_e))+|T_2|(V_j|_{T_2}-\tilde{V}_j(m_e))\Big|\\ =&|T_1|\left|\sum_{i=1}^6\partial_{j,i}V(\nabla\tilde{u}^a(m_e)\cdot\mathbf{a})\Big[\nabla u^{\mathrm{a}}|_{T_1}\cdot a_i-\nabla\tilde{u}^{\mathrm{a}}(m_e)\cdot a_i\right.\\ &\qquad\qquad\left.+\nabla u^{\mathrm{a}}|_{T_2}\cdot a_i-\nabla\tilde{u}^{\mathrm{a}}(m_e)\cdot a_i\Big]\right.\\ &\qquad\left.+\mathcal{O}\big(M_3\|\nabla^2\tilde{u}^{\mathrm{a}}\|^2_{L^\infty(\omega_e)}\big)\right|\\ \lesssim& M_2\|\nabla^3\tilde{u}^{\mathrm{a}}\|_{L^\infty(\omega_e)}+M_3\|\nabla^2\tilde{u}^{\mathrm{a}}\|^2_{L^\infty(\omega_e)}.\end{aligned}$$

Combining this estimate with (3.5.11), we have

$$\tau_1 \lesssim \Big\{ \|\nabla^2 \tilde{u}^{\mathrm{a}}\|^2_{L^4(\Omega^{\mathrm{c}})} + \|\nabla^3 \tilde{u}^{\mathrm{a}}\|_{L^2(\Omega^{\mathrm{c}})} \Big\} \|\nabla \varphi\|_{L^2(\Omega^{\mathrm{c}})}.$$

Finally, combining the last estimate with (3.5.9) we obtain

$$\delta_3 \lesssim \Big\{ \|\nabla^2 \tilde{u}^{\mathrm{a}}\|_{L^2(\Omega^i_+)} + \|\nabla^2 \tilde{u}^{\mathrm{a}}\|^2_{L^4(\Omega^{\mathrm{c}})} + \|\nabla^3 \tilde{u}^{\mathrm{a}}\|_{L^2(\Omega^{\mathrm{c}})} \Big\} \|\nabla \varphi\|_{L^2(\Omega^{\mathrm{c}})}. \tag{3.5.12}$$

3.5.5 Estimation of δ_4

We observe that δ_4 requires the estimation of pure modelling errors regardless of the choice of finite element approximation or domain truncation. This term was the main focus of [44], where the following result was proven.

Theorem 3.5.4 (Theorem 5.1 [44]). *Let $u : \Lambda \to \mathbb{R}^m$ and let $\varphi : \Lambda \to \mathbb{R}^m$ with compact support, then*

$$\begin{aligned} &\langle \delta\mathcal{E}^{\mathrm{g23}}(u^{\mathrm{a}}) - \delta\mathcal{E}^{\mathrm{a}}(u^{\mathrm{a}}), \varphi \rangle \\ &\qquad \lesssim \Big(M_2 \|D^2 u^{\mathrm{a}}\|_{\ell^2(\mathcal{I}^{\mathrm{ext}})} + M_2 \|D^3 u^{\mathrm{a}}\|_{\ell^2(\mathcal{C})} + M_3 \|D^2 u^{\mathrm{a}}\|^2_{\ell^4(\mathcal{C})} \Big) \|D\varphi\|_{\ell^2(\Lambda \setminus \mathcal{A})}, \end{aligned}$$

where $\mathcal{I}^{\mathrm{ext}} := \{\ell \in \Lambda \,|\, \mathrm{dist}(\ell, \mathcal{I}) \leq 1\}$.

By the construction of the smooth interpolant $\tilde{u}$ in Lemma 3.5.1 we therefore conclude that

$$\delta_4 \lesssim (\|\nabla^2 \tilde{u}^{\mathrm{a}}\|_{L^2(\Omega^{\mathrm{i}})} + \|\nabla^3 \tilde{u}^{\mathrm{a}}\|_{L^2(\Omega^{\mathrm{c}})} + \|\nabla^2 \tilde{u}^{\mathrm{a}}\|^2_{L^4(\Omega^{\mathrm{c}})}) \|\nabla \varphi\|_{L^2(\mathbb{R}^2 \setminus \Omega^{\mathrm{a}})}. \tag{3.5.13}$$

3.5.6 Proof of Theorem 3.2.2

Recall from (3.5.1) the splitting of the consistency error into η_{ext} and η_{int}. From the definition of φ in (3.5.4) it follows that $\eta_{\mathrm{ext}} = 0$.

In (3.5.2) the term η_{int} is further split into $\delta_1, \ldots, \delta_4$ which are respectively estimated in (3.5.6), (3.5.8), (3.5.12) and (3.5.13). Combining these four estimates, the stated result (3.2.3) follows.

3.5.7 Proof of the estimate (3.2.5)

A key aspect of our analysis is the optimisation of the approximation parameters: First, we determine a mesh size h so that the finite element error is balanced with the modelling error. Secondly, the domain radius N and the atomistic radius K will be balanced. Finally, in order to compare the efficiency against different methods, we will express the convergence rate of the total error in terms of numbers of degree of freedom only.

We first estimate the decay rate of each term in the consistency estimate (3.2.3). Recall that Corollary 3.2.1 implies $|\nabla^j \tilde{u}^{\mathrm{a}}(x)| \lesssim |x|^{-1-j}$. Hence, we can estimate the

interface error by

$$\|\nabla^2 \tilde{u}^{\mathrm{a}}\|_{L^2(\Omega^{\mathrm{i}})} \lesssim \left(\int_{\Omega^{\mathrm{i}}} |x|^{-6}\right)^{\frac{1}{2}} \lesssim (K \cdot K^{-6})^{\frac{1}{2}} \lesssim K^{-5/2}. \tag{3.5.14}$$

Similarly, we have

$$\begin{aligned}
\|\nabla^3 \tilde{u}^{\mathrm{a}}\|_{L^2(\Omega^{\mathrm{c}})} &\lesssim \left(\int_{\Omega^{\mathrm{c}}} |x|^{-8}\,\mathrm{d}x\right)^{\frac{1}{2}} \lesssim \left(\int_K^\infty r \cdot r^{-8}\,\mathrm{d}r\right)^{\frac{1}{2}} \lesssim K^{-3}, \\
\|\nabla^2 \tilde{u}^{\mathrm{a}}\|^2_{L^4(\Omega^{\mathrm{c}})} &\lesssim \left(\int_{\Omega^{\mathrm{c}}} |x|^{-12}\,\mathrm{d}x\right)^{\frac{1}{2}} \lesssim \left(\int_K^\infty r \cdot r^{-12}\,\mathrm{d}r\right)^{\frac{1}{2}} \lesssim K^{-5}, \\
\|\nabla \tilde{u}^{\mathrm{a}}\|_{L^2(\mathbb{R}\setminus\mathcal{B}_{N/2})} &\lesssim \left(\int_{\mathbb{R}^2\setminus\mathcal{B}_{N/2}} |x|^{-4}\,\mathrm{d}x\right)^{\frac{1}{2}} \lesssim \left(\int_{N/2}^\infty r \cdot r^{-4}\,\mathrm{d}r\right)^{\frac{1}{2}} \lesssim N^{-1}.
\end{aligned} \tag{3.5.15}$$

We observe that the interface term (3.5.14) dominates the consistency error. Balancing this with the far-field term (3.5.15) gives

$$N^{-1} \approx K^{-5/2}, \quad \text{i.e.,} \quad N \approx K^{5/2}.$$

To determine the mesh size h, we write $h(x) := \left(\frac{|x|}{K}\right)^\beta$. Then we have

$$\begin{aligned}
\|h^2\nabla^3 \tilde{u}^{\mathrm{a}}\|_{L^2(\Omega^{\mathrm{c}}_h)} &\lesssim \left(\int_{\Omega^{\mathrm{c}}_h} \frac{|x|^{4\beta}}{K^{4\beta}} |x|^{-8}\,\mathrm{d}x\right)^{1/2} \\
&= \frac{1}{K^{2\beta}} \left(\int_K^N r \cdot r^{4\beta-8}\,\mathrm{d}r\right)^{1/2} \\
&= \frac{1}{K^{2\beta}} \left(\Big[r^{4\beta-6}\Big]_{r=K}^{r=N}\right)^{1/2} \\
&\approx K^{-3}, \quad \text{provided that } 4\beta - 6 < 0.
\end{aligned}$$

The final remaining term is

$$\begin{aligned}
N^{-1}\|h^2\nabla^2 \tilde{u}^{\mathrm{a}}\|_{L^2(\mathcal{B}_N\setminus B_{N/2})} &\lesssim N^{-1} \left(\int_{\mathcal{B}_N\setminus B_{N/2}} \frac{|x|^{4\beta}}{K^{4\beta}} |x|^{-6}\,\mathrm{d}x\right)^{1/2} \\
&\lesssim N^{2\beta-3} K^{-2\beta} \approx K^{3\beta-\frac{15}{2}}.
\end{aligned}$$

Since we chose $\beta < 3/2$, it follows that K^{-3} dominates $K^{3\beta-\frac{15}{2}}$.

Therefore, the error rate for the optimal finite element coarsening is K^{-3} and to attain it we must choose

$$h(x) \approx \left(\frac{|x|}{K}\right)^\beta, \quad \text{where } \beta < \frac{3}{2}.$$

Finally, we estimate the relationship between the number of degrees of freedom $\mathcal{N}_h$

and the atomistic radius K. It is easy to see that the number of degrees of freedom in the atomistic domain satisfies $\mathcal{N}_{\rm a} \approx K^2$. Next, one can estimate the degrees of freedom in the continuum domain $\mathcal{N}_{\rm c}$ by considering each hexagonal layer of the mesh. On each layer with radius r, $\mathcal{N}_{\rm layer} \approx \frac{r}{h(r)}$. Summing over all layers in the continuum region gives

$$\begin{aligned}
\mathcal{N}_{\rm c} &\approx \sum_{\text{layers in } \Omega_{\rm c}} \left(h\frac{1}{h}\right)\frac{r}{h} \\
&\approx \int_K^N \frac{r}{h(r)^2}\,{\rm d}r \\
&\approx \int_K^N r^{1-2\beta}K^{2\beta}\,{\rm d}r \\
&\approx (-N^{2-2\beta} + K^{2-2\beta})K^{2\beta}, \qquad \text{provided that } 2-2\beta < 0, \\
&\approx K^2.
\end{aligned}$$

Therefore, we deduce that the mesh grading should satisfy $1 < \beta < \frac{3}{2}$ to obtain the optimal cost/accuracy ratio for the error in the energy-norm, $K^{-5/2} \approx \mathcal{N}_h^{-5/4}$. The table in § 3.2.3.2 summarises the derivation of this section.

3.6 Proof of Theorem 3.2.4

3.6.1 Existence and error in energy norm

We refer to the inverse function theorem, Theorem 3.4.1. Let $\delta\mathcal{G}_h := \delta\mathcal{E}^{\rm g23} - \delta f$ and $\bar{u}_h := \Pi_h u^{\rm a}$. We have already shown in Theorem 3.2.2 and Lemma 3.4.4 that

$$\begin{aligned}
\|\mathcal{G}_h(\bar{u}_h)\|_{\mathcal{U}_h^*} &\le \eta, \\
\langle \delta\mathcal{G}_h(\bar{u}_h)v_h, v_h\rangle &\ge \gamma\|\nabla v_h\|_{L^2}^2 \quad \text{for all } v_h \in \mathcal{U}_h,
\end{aligned}$$

with $\eta = \eta_{\rm int} + \eta_{\rm ext}$ and

$$\begin{aligned}
\eta_{\rm int} &\lesssim \|\nabla^2\tilde{u}^{\rm a}\|_{L^2(\Omega^{\rm i})} + \|\nabla^3\tilde{u}^{\rm a}\|_{L^2(\Omega^{\rm c})} + \|\nabla^2\tilde{u}^{\rm a}\|_{L^4(\Omega^{\rm c})}^2 \\
&\qquad + \|h^2\nabla^3\tilde{u}^{\rm a}\|_{L^2(\Omega_h^{\rm c})} + \|\nabla\tilde{u}^{\rm a}\|_{L^2(\mathbb{R}^2\setminus\mathcal{B}_{N/2})} + N^{-1}\|h^2\nabla^2\tilde{u}^{\rm a}\|_{L^2(\mathcal{B}_N\setminus B_{N/2})} \\
&\lesssim \mathcal{N}_h^{-5/4}.
\end{aligned}$$

For $\eta_{\rm ext}$, recall that $\partial_{u(\ell)}f(u) = 0$ for all $|\ell| \ge R_f$, and that $K \ge R_f$. We have, on $\operatorname{supp}(\partial_{u(\ell)}f(u))$, $\nabla\Pi_h u^{\rm a} = \nabla u^{\rm a}$ and $\nabla\varphi_h = \nabla\varphi$. Thus $\eta_{\rm ext} = 0$ and

$$\eta = \eta_{\rm int} \lesssim \mathcal{N}_h^{-5/4}.$$

Using also the Lipscthiz bound from Lemma 3.4.3 Theorem 3.4.1 implies, for K

sufficiently large, that there exists a strongly stable minimizer $u_h^{\mathrm{g23}} \in \mathcal{U}_h$ such that

$$\langle \delta \mathcal{E}^{\mathrm{g23}}(u_h^{\mathrm{g23}}), \varphi_h \rangle - \langle \delta f(u_h^{\mathrm{g23}}), \varphi_h \rangle = 0, \quad \forall \varphi_h \in \mathcal{U}_h,$$

and

$$\begin{aligned}
\|\nabla u_h^{\mathrm{g23}} - \nabla \Pi_h u^{\mathrm{a}}\|_{L^2} &\leq 2\frac{\eta}{\gamma} \\
&\lesssim \|\nabla^2 \tilde{u}^{\mathrm{a}}\|_{L^2(\Omega^{\mathrm{i}})} + \|\nabla^3 \tilde{u}^{\mathrm{a}}\|_{L^2(\Omega^{\mathrm{c}})} + \|\nabla^2 \tilde{u}^{\mathrm{a}}\|_{L^4(\Omega^{\mathrm{c}})}^2 \\
&\quad + \|h^2 \nabla^3 \tilde{u}^{\mathrm{a}}\|_{L^2(\Omega^{\mathrm{c}})} + \|\nabla \tilde{u}^{\mathrm{a}}\|_{L^2(\mathbb{R}^2 \setminus \mathcal{B}_{N/2})} \\
&\lesssim \mathcal{N}_h^{-5/4}.
\end{aligned}$$

Adding the best approximation error (3.5.7) gives

$$\begin{aligned}
\|\nabla u_h^{\mathrm{g23}} - \nabla u^{\mathrm{a}}\|_{L^2} &\leq \|\nabla u_h^{\mathrm{g23}} - \nabla \Pi_h u^{\mathrm{a}}\|_{L^2} + \|\nabla \Pi_h u^{\mathrm{a}} - \nabla u^{\mathrm{a}}\|_{L^2} \\
&\lesssim \mathcal{N}_h^{-5/4} + \|h^2 \nabla^3 \tilde{u}\|_{L^2(\bigcup \mathcal{T}_h^{\mathrm{c}})} + \|\nabla \tilde{u}\|_{L^2(\mathbb{R}^2 \setminus \mathcal{B}_{N/2})} \\
&\lesssim \mathcal{N}_h^{-5/4}.
\end{aligned}$$

This completes the proof of Theorem 3.2.4.

3.6.2 The energy error

In this section we prove the energy error estimates stated in Theorem 3.2.4. For the sake of notational simplicity we define $\mathcal{E}_f^{\mathrm{a}} := \mathcal{E}^{\mathrm{a}} - f$ and $\mathcal{E}_f^{\mathrm{g23}} := \mathcal{E}^{\mathrm{g23}} - f$.

First, we observe that

$$\begin{aligned}
|\mathcal{E}_f^{\mathrm{g23}}(u_h^{\mathrm{g23}}) - \mathcal{E}_f^{\mathrm{a}}(u^{\mathrm{a}})| &\leq |\mathcal{E}_f^{\mathrm{g23}}(u_h^{\mathrm{g23}}) - \mathcal{E}_f^{\mathrm{g23}}(\Pi_h u^{\mathrm{a}})| + |\mathcal{E}_f^{\mathrm{g23}}(\Pi_h u^{\mathrm{a}}) - \mathcal{E}_f^{\mathrm{a}}(u^{\mathrm{a}})| \\
&=: e_1 + e_2.
\end{aligned}$$

The first term can be estimated by (3.2.6) and the fact that $\langle \delta \mathcal{E}_f^{\mathrm{g23}}(u_h^{\mathrm{g23}}), \varphi_h \rangle = 0$ for all $\varphi_h \in \mathcal{U}_h$:

$$\begin{aligned}
e_1 &\leq \left| \langle \delta \mathcal{E}_f^{\mathrm{g23}}(u_h^{\mathrm{g23}}), \Pi_h u^{\mathrm{a}} - u_h^{\mathrm{g23}} \rangle \right| \\
&\quad + \left| \int_0^1 (1-t) \langle \delta^2 \mathcal{E}_f^{\mathrm{g23}}(u_h^{\mathrm{g23}} + t(\Pi_h u^{\mathrm{a}} - u_h^{\mathrm{g23}}))(\Pi_h u^{\mathrm{a}} - u_h^{\mathrm{g23}}), (\Pi_h u^{\mathrm{a}} - u_h^{\mathrm{g23}}) \rangle \, dt \right| \\
&\lesssim \|\nabla \Pi_h u^{\mathrm{a}} - \nabla u_h^{\mathrm{g23}}\|_{L^2}^2 \lesssim K^{-5} \lesssim \mathcal{N}_h^{-5/2}. \qquad (3.6.1)
\end{aligned}$$

For the second term we use the fact that $\mathcal{E}^{\mathrm{g23}}(0) = \mathcal{E}^{\mathrm{a}}(0)$, and hence $\mathcal{E}_f^{\mathrm{g23}}(0) = \mathcal{E}_f^{\mathrm{a}}(0)$, to

estimate

$$\begin{aligned} e_2 &\le |\mathcal{E}_f^{\mathrm{g}23}(0) - \mathcal{E}_f^{\mathrm{a}}(0)| + \left| \int_0^1 \langle \delta\mathcal{E}_f^{\mathrm{g}23}(t\Pi_h u^{\mathrm{a}}), \Pi_h u^{\mathrm{a}} \rangle \, dt - \int_0^1 \langle \delta\mathcal{E}_f^{\mathrm{a}}(tu^{\mathrm{a}}), u^{\mathrm{a}} \rangle \, dt \right| \\ &\le \left| \int_0^1 \langle \delta\mathcal{E}_f^{\mathrm{g}23}(t\Pi_h u^{\mathrm{a}}), \Pi_h u^{\mathrm{a}} \rangle - \langle \delta\mathcal{E}_f^{\mathrm{a}}(tu^{\mathrm{a}}), v \rangle \, \mathrm{d}t \right| + \left| \int_0^1 \langle \delta\mathcal{E}_f^{\mathrm{a}}(tu^{\mathrm{a}}), v - u^{\mathrm{a}} \rangle \, \mathrm{d}t \right| \\ &=: e_{21} + e_{22}, \end{aligned}$$

where $v : \Lambda \to \mathbb{R}^m$ is an arbitrary test function.

3.6.2.1 Estimate for e_{21}

To exploit the consistency error estimate we choose $v := \Pi_h^* \Pi_h u^{\mathrm{a}}$ defined in (3.5.4). In this case, similar to estimating η_{int}, we obtain

$$\begin{aligned} e_{21} &\lesssim \int_0^1 \tilde{\eta}_{\mathrm{int}}(t) \, \mathrm{d}t \, \|\nabla \Pi_h u^{\mathrm{a}}\|_{L^2(\mathbb{R}^2 \setminus \Omega_h^{\mathrm{a}})}, \qquad \text{where} \\ \tilde{\eta}_{\mathrm{int}}(t) &= \|\nabla^2 t\tilde{u}^{\mathrm{a}}\|_{L^2(\Omega^{\mathrm{i}})} + \|\nabla^3 t\tilde{u}^{\mathrm{a}}\|_{L^2(\Omega^{\mathrm{c}})} + \|\nabla^2 t\tilde{u}^{\mathrm{a}}\|_{L^4(\Omega^{\mathrm{c}})}^2 + \|h^2 \nabla^3 t\tilde{u}^{\mathrm{a}}\|_{L^2(\Omega_h^{\mathrm{c}})} \\ &\quad + \|\nabla t\tilde{u}^{\mathrm{a}}\|_{L^2(\mathbb{R}^2 \setminus \mathcal{B}_{N/2})} + N^{-1} \|h^2 \nabla^2 t\tilde{u}\|_{L^2(\mathcal{B}_N \setminus B_{N/2})} \\ &\lesssim tK^{-5/2}. \end{aligned}$$

From Corollary 3.2.1 and 3.5.2 it follows that $|\nabla \Pi_h v^{\mathrm{a}}(x)| \lesssim |x|^{-2}$ hence we can deduce that

$$e_{21} \lesssim K^{-5/2} K^{-1} = K^{-7/2} \lesssim \mathcal{N}_h^{-7/4}. \tag{3.6.2}$$

3.6.2.2 Estimate for e_{22}

First we observe that by Trapezoidal rule, if $\zeta \in C^2(\mathbb{R})$ and $\zeta(0) = \zeta(1) = 0$, then we have for some $\theta \in [0, 1]$,

$$\int_0^1 \zeta(t) \, \mathrm{d}t = -\frac{1}{12} \zeta''(\theta).$$

Let $\zeta(t) := \langle \delta\mathcal{E}_f^{\mathrm{a}}(tu^{\mathrm{a}}), v - u^{\mathrm{a}} \rangle$. Then $\zeta(1) = 0$ since $\delta\mathcal{E}_f^{\mathrm{a}}(u^{\mathrm{a}}) = 0$ and $\zeta(0) = 0$ since $\delta\mathcal{E}^{\mathrm{a}}(0) = 0$ and $\partial_{u(\ell)} f(u) = 0$ outside defect core while $v = u^{\mathrm{a}}$ in the defect core.

Having $e_{22} = \int_0^1 \zeta(t) \, \mathrm{d}t$ we obtain

$$\begin{aligned} e_{22} &\lesssim \delta^3 \mathcal{E}^{\mathrm{a}}(\theta u^{\mathrm{a}})[u^{\mathrm{a}}, u^{\mathrm{a}}, v - u^{\mathrm{a}}] \\ &\lesssim M_3 \sum_{\ell \in \Lambda \setminus \mathcal{A}} |Du^{\mathrm{a}}(\ell)|^2 |Dv(\ell) - Du^{\mathrm{a}}(\ell)| \\ &\lesssim \int_{R^2 \setminus \Omega^{\mathrm{a}}} |\nabla \tilde{u}^{\mathrm{a}}|^2 |\nabla v - \nabla u^{\mathrm{a}}|, \end{aligned}$$

where we recall that $v := \Pi_h^* \Pi_h u^{\mathrm{a}}$. Using the stability (3.5.5) we obtain

$$\begin{aligned} e_{22} &\lesssim \|\nabla \tilde{u}^{\mathrm{a}}\|^3_{L^3(\mathbb{R}^2 \setminus \Omega^{\mathrm{a}})} + \|\nabla \tilde{u}^{\mathrm{a}}\|^2_{L^4(\mathbb{R}^2 \setminus \Omega^{\mathrm{a}})} \|\nabla \Pi_h u^{\mathrm{a}}\|_{L^2(\mathbb{R}^2 \setminus \Omega^{\mathrm{a}})} \\ &\lesssim \int_K r r^{-6} \, \mathrm{d}r + \left(\int_K r r^{-8} \, \mathrm{d}r \right)^{1/2} \left(\int_K r r^{-4} \, \mathrm{d}r \right)^{1/2} \\ &\lesssim K^{-4} + K^{-3} K^{-1} = K^{-4}. \end{aligned} \tag{3.6.3}$$

Combining (3.6.1), (3.6.2) and (3.6.3) completes the proof of the energy error estimate (3.2.7) and therefore of our main result, Theorem 3.2.4.

Chapter 4

A/C coupling with boundary element methods

4.1 Introduction

This chapter explores the feasibility and effectiveness of employing boundary elements in addition to the existing a/c framework to better approximate the far-field energy which is typically truncated. Specifically we combine the quasi-nonlocal (QNL) type method from Chapter 3 with a BEM, in a 2D model problem.

The boundary element method is a numerical method for solving linear partial differential equations by discretising the boundary integral formulation. For a general introduction and analysis we refer to [51]. In the present work we first approximate a nonlinear elasticity model by a quadratic energy functional which is then discretised by the BEM.

The idea of employing a BEM-like scheme to model the elastic far-field is not new. For example, in [26, 50] an atomistic Green's function method is employed to determine a far-field boundary condition which yields a *sequential* multi-scale scheme, while [54, 29] formulate *concurrent* multi-scale schemes coupling atomistic mechanics to a Green's function method. In this setting, a preliminary error analysis can already be found in [18]. By contrast, our new scheme employs a BEM, i.e., a continuum elasticity Green's function approach to model the elastic far-field. Moreover, our formulation allows a seemless transition between atomistic mechanics, nonlinear continuum mechanics (FEM) and linearised continuum mechanics (BEM). This flexibility is particularly interesting for an error analysis since we are able to determine quasi-optimal error balancing between the three different models (atomistic, Cauchy–Born, linearised elasticity).

To conclude the introduction we remark that the BEM far-field boundary condition can of course be employed for other A/C coupling schemes as well as more complex (in terms of geometry and interaction law) atomistic models, but in particular the latter generalisation requires some additional work. With this in mind, the present chapter may be considered a proof of concept.

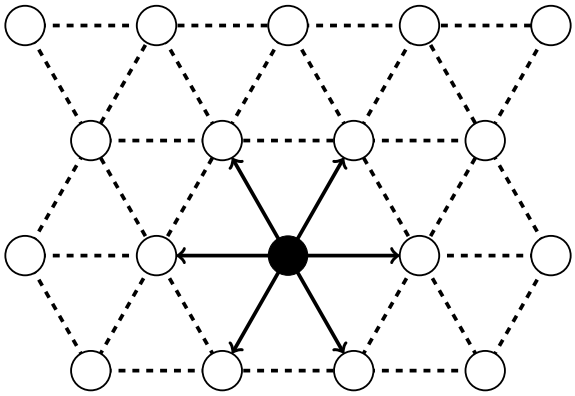

Figure 4.1: The lattice (circles), its canonical triangulation (dashed lines) and the six nearest-neighbour directions (arrows). This illustration is taken from Chapter 3.

4.1.1 Outline

In the present chapter we estimate the accuracy of a QNL-type atomistic/continuum coupling method employing a P1 FEM in the continuum region and P0 BEM on the boundary against an exact solution obtained from a fully atomistic model. We review the atomistic model in § 4.2.1, the QNL coupling scheme in § 4.2.2 and § 4.2.3, and the modification to incorporate a BEM for the elastic far-field in § 4.2.4. In §4.3 we collect notation, assumptions and preliminary results required to state the main results in § 4.4. We then deduce the optimal approximation parameters (atomistic region size, continuum region size, FEM and BEM meshes) in §4.4.4. We will conclude that formally omitting the FEM region entirely yields the best possible convergence rate. In practice, it is necessary to admit one layer of FEM in order to couple BEM on the boundary without incurring ghost forces.

4.2 Method Formulation

4.2.1 Atomistic model

In order to employ the G23 coupling in [44] and Chapter 3, we follow the same model construction therein. We consider an infinite 2D triangular lattice as our model geometry,

$$\Lambda := \mathsf{A}\mathbb{Z}^2, \quad \text{with } \mathsf{A} = \begin{pmatrix} 1 & \cos(\pi/3) \\ 0 & \sin(\pi/3) \end{pmatrix}.$$

We define the six nearest-neighbour lattice directions by $a_1 := (1, 0)$, and $a_j := Q_6^{j-1} a_1, j \in \mathbb{Z}$, where Q_6 denotes the rotation through the angle $\pi/3$. We equip Λ with an *atomistic triangulation*, as shown in Figure 4.1, which will be used in both error analysis and numerical simulations. We denote this triangulation by $\mathcal{T}$ and its elements by $T \in \mathcal{T}$. In addition, we denote $\boldsymbol{a} := (a_j)_{j=1}^6$, and $\mathsf{F}\boldsymbol{a} := (\mathsf{F}a_j)_{j=1}^6$, for $\mathsf{F} \in \mathbb{R}^{m\times 2}$.

We identify a discrete displacement map $u : \Lambda \to \mathbb{R}$ with its continuous piecewise

affine interpolant, with weak derivative ∇u, which is also the pointwise derivative on each element $T \in \mathcal{T}$. For $m = 1, 2, 3$, we define the spaces of displacements as

$$\begin{aligned} \mathcal{U}_0 &:= \big\{ u : \Lambda \to \mathbb{R}^m \,|\, \mathrm{supp}(\nabla u) \text{ is compact} \big\}, \quad \text{and} \\ \dot{\mathcal{U}}^{1,2} &:= \big\{ u : \Lambda \to \mathbb{R}^m \,|\, \nabla u \in L^2 \big\}. \end{aligned}$$

We equip $\dot{\mathcal{U}}^{1,2}$ with the H^1-semi norm and denote $\|u\|_{\mathcal{U}^{1,2}} := \|\nabla u\|_{L^2(\mathbb{R}^2)}$. From [40] we know that $\mathcal{U}_0$ is dense in $\dot{\mathcal{U}}^{1,2}$ in the sense that, if $u \in \dot{\mathcal{U}}^{1,2}$, then there exist $u_j \in \mathcal{U}_0$ such that $\nabla u_j \to \nabla u$ strongly in L^2.

A *homogeneous displacement* is a map $u_{\mathsf{F}} : \Lambda \to \mathbb{R}^m, u_{\mathsf{F}}(x) := \mathsf{F}x$, where $\mathsf{F} \in \mathbb{R}^{m\times 2}$.

For a map $u : \Lambda \to \mathbb{R}^m$, we define the finite difference operator

$$\begin{aligned} D_j u(x) &:= u(x + a_j) - u(x), \quad x \in \Lambda, j \in \{1, 2, ..., 6\}, \quad \text{and} \\ Du(x) &:= (D_j u(x))_{j=1}^6. \end{aligned} \tag{4.2.1}$$

Note that $Du_{\mathsf{F}}(x) = \mathsf{F}\boldsymbol{a}$.

We assume that the atomistic interaction is represented by a nearest-neighbour many-body site energy potential $V \in C^r(\mathbb{R}^{m\times 6})$,$r \geq 5$, with $V(\mathbf{0}) = 0$ and $\nabla^j V \in L^\infty(\mathbb{R}^{m\times 6})$ for $j = 2, \ldots, 5$. In addition, we assume that V satisfies the *point symmetry*

$$V((-g_{j+3})_{j=1}^6) = V(\boldsymbol{g}) \quad \forall \boldsymbol{g} \in \mathbb{R}^{m\times 6}.$$

Because $V(\mathbf{0}) = 0$, the energy of a displacement $u \in \mathcal{U}_0$

$$\mathcal{E}^{\mathrm{a}}(u) := \sum_{\ell\in\Lambda} V(Du(\ell)),$$

is well-defined. We need the following lemma to extend $\mathcal{E}^{\mathrm{a}}$ to $\dot{\mathcal{U}}^{1,2}$ to formulate a variational problem in the energy space $\dot{\mathcal{U}}^{1,2}$,

Lemma 4.2.1. *$\mathcal{E}^{\mathrm{a}} : (\mathcal{U}_0, \|\nabla \cdot\|_{L^2}) \to \mathbb{R}$ is continuous and has a unique continuous extension to $\dot{\mathcal{U}}^{1,2}$, which we still denote by $\mathcal{E}^{\mathrm{a}}$. Moreover, the extended $\mathcal{E}^{\mathrm{a}} : (\dot{\mathcal{U}}^{1,2}, \|\nabla \cdot\|_{L^2}) \to \mathbb{R}$ is r-times continuously Fréchet differentiable.*

Proof. See Lemma 2.1 in [18]. □

We model a point defect by including an external potential $f \in C^r(\dot{\mathcal{U}}^{1,2})$ with $\partial_{u(\ell)} f(u) = 0$ for all $|\ell| \geq R_f$, where R_f is the defect core radius, and $f(u + c) = f(u)$ for all constants c. For instance, we can think of f modelling a substitutional impurity. See also [30, 39] for similar approaches.

Then we seek the solution to

$$u^{\mathrm{a}} \in \arg\min \big\{ \mathcal{E}^{\mathrm{a}}(u) - f(u) \,|\, u \in \dot{\mathcal{U}}^{1,2} \big\}. \tag{4.2.2}$$

For $u, \varphi, \psi \in \dot{\mathcal{U}}^{1,2}$ we define the *first and second variations* of $\mathcal{E}^{\rm a}$ by

$$\langle \delta \mathcal{E}^{\rm a}(u), \varphi \rangle := \lim_{t \to 0} t^{-1} \left(\mathcal{E}^{\rm a}(u + t\varphi) - \mathcal{E}^{\rm a}(u) \right),$$
$$\langle \delta^2 \mathcal{E}^{\rm a}(u)\varphi, \psi \rangle := \lim_{t \to 0} t^{-1} \left(\langle \delta \mathcal{E}^{\rm a}(u + t\varphi), \psi \rangle - \langle \delta \mathcal{E}^{\rm a}(u), \psi \rangle \right).$$

We define analogously all energy functionals introduced in later sections.

For the sake of analysis we need the following global bounds on the partial derivatives of V. For $\boldsymbol{g} \in \mathbb{R}^{m \times 6}$, define the first and second partial derivatives, for $i, j = 1, \ldots, 6$, by

$$\partial_j V(\boldsymbol{g}) := \frac{\partial V(\boldsymbol{g})}{\partial g_j} \in \mathbb{R}^m, \quad \text{and} \quad \partial_{i,j} V(\boldsymbol{g}) := \frac{\partial^2 V(\boldsymbol{g})}{\partial g_i \partial g_j} \in \mathbb{R}^{m \times m},$$

and similarly for the third derivatives $\partial_{i,j,k} V(\boldsymbol{g}) \in \mathbb{R}^{m \times m \times m}$. We assumed in § 4.2.1 that second and higher derivatives are bounded, hence we can define the constants

$$M_2 := \sum_{i,j=1}^{6} \sup_{\boldsymbol{g} \in \mathbb{R}^{m \times 6}} \sup_{\substack{h_1, h_2 \in \mathbb{R}^2, \\ |h_1| = |h_2| = 1}} \partial_{i,j} V(\boldsymbol{g})[h_1, h_2] < \infty, \quad \text{and} \tag{4.2.3}$$

$$M_3 := \sum_{i,j,k=1}^{6} \sup_{\boldsymbol{g} \in \mathbb{R}^{m \times 6}} \sup_{\substack{h_1, h_2, h_3 \in \mathbb{R}^2, \\ |h_1| = |h_2| = |h_3| = 1}} \partial_{i,j,k} V(\boldsymbol{g})[h_1, h_2, h_3] < \infty. \tag{4.2.4}$$

With the above bounds it is easy to show that

$$\begin{aligned} \sum_{i=1}^{6} |\partial_i V(\boldsymbol{g}) - \partial_i V(\boldsymbol{h})| &\le M_2 \max_{j=1,\ldots,6} |g_j - h_j|, \quad \text{and} \\ \sum_{i,j=1}^{6} |\partial_{i,j} V(\boldsymbol{g}) - \partial_{i,j} V(\boldsymbol{h})| &\le M_3 \max_{k=1,\ldots,6} |g_k - h_k|, \quad \text{for } \boldsymbol{g}, \boldsymbol{h} \in \mathbb{R}^{m \times 6}. \end{aligned} \tag{4.2.5}$$

4.2.2 GR-AC coupling

The Cauchy–Born strain energy function [33, 17], corresponding to the interatomic potential V is

$$W(\mathsf{F}) := \frac{1}{\Omega_0} V(\mathsf{F}\boldsymbol{a}), \qquad \text{for } \mathsf{F} \in \mathbb{R}^{m \times 2},$$

where $\Omega_0 := \sqrt{3}/2$ is the volume of a unit cell of the lattice Λ. Hence $W(\mathsf{F})$ is the energy per volume of the homogeneous lattice $\mathsf{F}\Lambda$. It is shown in [24] that, in a triangular lattice with anti-plane elasticity, $\nabla^2 W(\mathbf{0}) = \mu I^{2\times 2}$ for some constant $\mu > 0$ (the shear modulus), which will be used in the formulation of BEM in later sections.

Let $\mathcal{A} \subset \Lambda$ be the set of all lattices sites for which we require full atomistic accuracy.

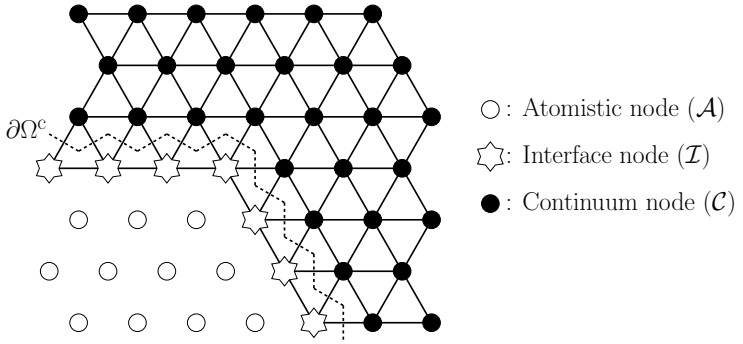

Figure 4.2: The domain decomposition with a layer of interface atoms. This illustration is taken from [12].

We define the set of interface lattice sites as

$$\mathcal{I} := \left\{ \ell \in \Lambda \setminus \mathcal{A} \,\middle|\, \ell + a_j \in \mathcal{A} \text{ for some } j \in \{1, \dots, 6\} \right\}$$

and we define the remaining lattice sites as $\mathcal{C} := \Lambda \setminus (\mathcal{A} \cup \mathcal{I})$. Let Ω_ℓ be the Voronoi cell associated with site ℓ. We define the continuum region $\Omega^{\mathrm{c}} := \mathbb{R}^2 \setminus \bigcup_{\ell \in \mathcal{A} \cup \mathcal{I}} \Omega_\ell$; see Figure 4.2. We also define Ω^{a} and Ω^{i} analogously.

A general form for the GRAC-type a/c coupling energy [16, 44] is

$$\mathcal{E}^{\mathrm{ac}}(u) = \sum_{\ell \in \mathcal{A}} V(Du(\ell)) + \sum_{\ell \in \mathcal{I}} V\left((\mathcal{R}_\ell D_j u(\ell))_{j=1}^6 \right) + \int_{\Omega^{\mathrm{c}}} W(\nabla u(x))\, \mathrm{d}x, \tag{4.2.6}$$

where $\mathcal{R}_\ell D_j u(\ell) := \sum_{i=1}^6 C_{\ell,j,i} D_i u(\ell)$. The parameters $C_{\ell,j,i}$ are determined such that the coupling scheme satisfies the "patch tests":

$\mathcal{E}^{\mathrm{ac}}$ is *locally energy consistent* if, for all $\mathsf{F} \in \mathbb{R}^{m \times 2}$,

$$V_\ell^i(\mathsf{F}\boldsymbol{a}) = V(\mathsf{F}\boldsymbol{a}) \quad \forall \ell \in \mathcal{I}. \tag{4.2.7}$$

$\mathcal{E}^{\mathrm{ac}}$ is *force consistent* if, for all $\mathsf{F} \in \mathbb{R}^{m \times 2}$,

$$\delta \mathcal{E}^{\mathrm{ac}}(u_{\mathsf{F}}) = 0, \quad \text{where} \quad u_{\mathsf{F}}(x) := \mathsf{F}x. \tag{4.2.8}$$

$\mathcal{E}^{\mathrm{ac}}$ is *patch test consistent* if it satisfies both (4.2.7) and (4.2.8).

For simplicity we write

$$V_\ell^i(Du(\ell)) := V\left((\mathcal{R}_\ell D_j u(\ell))_{j=1}^6 \right).$$

Following [44] we make the following standing assumption (see Figure 4.3 for examples).

(A0) *Each vertex $\ell \in \mathcal{I}$ has exactly two neighbours in $\mathcal{I}$, and at least one neighbour in $\mathcal{C}$.*

Under this assumption, the geometry reconstruction operator $\mathcal{R}_\ell$ is then defined

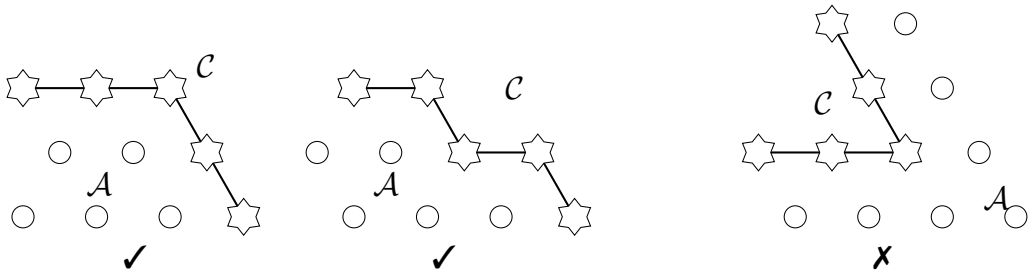

Figure 4.3: The first two configurations are allowed. The third configuration is not allowed as the interface atom at the corner has no nearest neighbour in the continuum region, and should instead be taken as an atomistic site. This illustration is taken from [12].

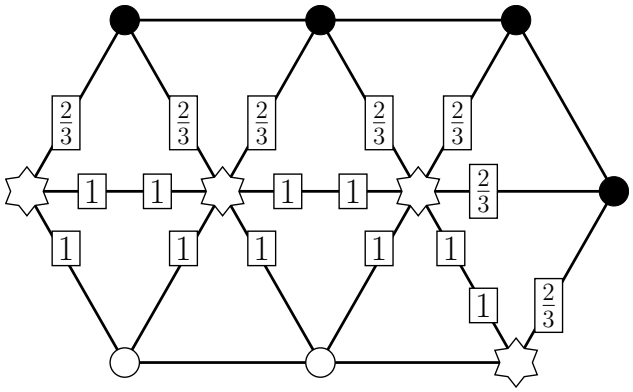

Figure 4.4: The geometry reconstruction coefficents $\lambda_{x,j}$ at the interface sites. This illustration is taken from [12].

by

$$\mathcal{R}_\ell D_j y(\ell) := (1-\lambda_{\ell,j})D_{j-1}y(\ell) + \lambda_{\ell,j} D_j y(\ell) + (1-\lambda_{\ell,j})D_{j+1}y(\ell),$$
$$\lambda_{x,j} := \begin{cases} 2/3, & x + a_j \in \mathcal{C} \\ 1, & \text{otherwise} \end{cases};$$

see Figure 4.4. The resulting a/c coupling method is called G23 and the corresponding energy functional $\mathcal{E}^{\mathrm{g23}}$. It is proven in [44] that this choice of coefficients (and only this choice) leads to patch test consistency (4.2.7) and (4.2.8).

For future reference we decompose the canonical triangulation $\mathcal{T}$ as follows:

$$\begin{aligned} \mathcal{T}_\mathcal{A} &:= \{T \in \mathcal{T} \,|\, T \cap (\mathcal{I} \cup \mathcal{C}) = \emptyset, \}, \\ \mathcal{T}_\mathcal{C} &:= \{T \in \mathcal{T} \,|\, T \cap (\mathcal{I} \cup \mathcal{A}) = \emptyset, \} \quad \text{and} \\ \mathcal{T}_\mathcal{I} &:= \mathcal{T} \setminus (\mathcal{T}_\mathcal{C} \cup \mathcal{T}_\mathcal{A}). \end{aligned} \tag{4.2.9}$$

4.2.3 The finite element scheme

In the atomistic region Ω^{a} and the interface region Ω^{i}, the interactions are represented by discrete displacement maps, which are identified with their linear interpolant. In these regions there is no approximation error.

On the other hand, as formulated in (4.2.6), the interactions are approximated by

the Cauchy–Born energy in the continuum region $\Omega_h^{\rm c}$.

Let $K > 0$ be the inner radius of the atomistic region,

$$K := \sup\big\{r > 0 \,|\, \mathcal{B}_r \cap \Lambda \subset \mathcal{A}\big\},$$

where $\mathcal{B}_r$ denotes the ball of radius r centred at 0. We assume throughout that $K \geq R_f$ to ensure that the defect core is contained in the atomistic region.

Let Ω_h be the entire finite computational domain and $N > 0$ be the inner radius of Ω_h, i.e.,

$$N := \sup\big\{r > 0 \,|\, \mathcal{B}_r \subset \Omega_h\big\}.$$

Let $\mathcal{T}_h$ be a finite element triangulation of Ω_h which satisfies, for $T \in \mathcal{T}_h$,

$$T \cap (\mathcal{A} \cup \mathcal{I}) \neq \emptyset \quad \Rightarrow \quad T \in \mathcal{T}.$$

In other words, $\mathcal{T}_h$ and $\mathcal{T}$ coincide in the atomistic and interface regions, whereas in the continuum region the mesh size may increase towards the domain boundary.

We observe that the concrete construction of $\mathcal{T}_h$ will be based on the choice of the domain parameters K and N; hence we will write $\mathcal{T}_h(K, N)$ to emphasize this dependence. To eliminate the possibility of extreme angles on elements, we assume throughout that the family $(\mathcal{T}_h(K, N))_{K,N}$ is *uniformly shape-regular*, i.e., there exists $c > 0$ such that,

$$\operatorname{diam}(T)^2 \leq c|T|, \quad \forall T \in \mathcal{T}_h(K, N), \forall K \leq N, \tag{4.2.10}$$

and that the induced mesh on $\Gamma_h := \partial\Omega_h$ is uniformly quasi-uniform.

Hence in the analysis we can avoid deteriorated constants in finite element interpolation error estimates. In later sections we will again drop the parameters from the notation by writing $\mathcal{T}_h \equiv \mathcal{T}_h(K, N)$ but implicitly will always keep the dependence.

Similar to (4.2.9), we denote the atomistic, interface and continuum elements by $\mathcal{T}_h^a, \mathcal{T}_h^i$ and $\mathcal{T}_h^c$, respectively. We observe that $\mathcal{T}_h^a = \mathcal{T}_\mathcal{A}$ and $\mathcal{T}_h^i = \mathcal{T}_\mathcal{I}$. We also let $\mathcal{N}_h$ be the number of degrees of freedom of $\mathcal{T}_h$.

We define the finite element space of admissible displacements as

$$\mathcal{U}_h := \big\{u \in C(\mathbb{R}^2; \mathbb{R}^m) \,|\, u|_T \in \mathbb{P}^1(T) \text{ for } T \subset \mathcal{T}_h\big\}. \tag{4.2.11}$$

4.2.4 GR-AC coupling with BEM

In [12], we employed finite element methods to approximate the solution. We applied P2-FEM with Dirichlet boundary conditions. To improve the far-field description, we now consider applying a boundary element method to approximate the far-field energy.

Recall that the general form (4.2.6) of the GR-AC type coupling energy is

$$\mathcal{E}^{\rm ac}(u) = \sum_{\ell \in \mathcal{A}} V(Du(\ell)) + \sum_{\ell \in \mathcal{I}} V_\ell^{\rm i}(Du(\ell)) + \int_{\Omega^{\rm c}} W(\nabla u(x))\,{\rm d}x.$$

In the far-field we can approximate the Cauchy–Born energy by the linearization (recall that $\nabla^2 W(0) = \mu I_{2\times 2}$), for $u \in \dot{\mathcal{U}}^{1,2}$ and $\Omega_h^{\rm c} := \Omega_h \cap \Omega^{\rm c}$,

$$\begin{aligned}\mathcal{E}_{\rm lin}^{\rm ac}(u) &= \sum_{\ell\in\mathcal{A}} V(Du(\ell)) + \sum_{\ell\in\mathcal{I}} V_\ell^{\rm i}(Du(\ell)) + \int_{\Omega_h^{\rm c}} W(\nabla u(x))\,{\rm d}x + \int_{\mathbb{R}^2\setminus\Omega_h} \frac{\mu}{2}|\nabla u|^2 \\ &=: \mathcal{E}_h^{\rm ac}(u) + \int_{\mathbb{R}^2\setminus\Omega_h} \frac{\mu}{2}|\nabla u|^2.\end{aligned} \tag{4.2.12}$$

We seek the minimizer of above energy functional

$$u^* := \arg\min\{\mathcal{E}_{\rm lin}^{\rm ac}(u) - f(u) \,:\, u \in \dot{\mathcal{U}}^{1,2}\}.$$

For numerical simulations, we exploit the boundary integral to represent the quadratic term $\int_{\mathbb{R}^2\setminus\Omega_h} \frac{\mu}{2}|\nabla u|^2$.

In preparation, let $\Gamma_h := \partial\Omega_h$, $\gamma_0^{\rm int} : C(\Omega_h) \to C(\Gamma_h)$ and $\gamma_0^{\rm ext} : C(\Omega_h^{\complement}) \to C(\Gamma_h)$ be the interior and exterior trace operators respectively, then we define, for $u, v \in \dot{\mathcal{U}}^{1,2}$,

$$\mathcal{E}_*^{\rm ac}(u) := \mathcal{E}_h^{\rm ac}(u) + \inf_{\gamma_0^{\rm ext} v = \gamma_0^{\rm int} u} \frac{\mu}{2} \int_{\Omega_h^{\complement}} |\nabla v|^2. \tag{4.2.13}$$

Let

$$\bar{u}_h := \arg\min\{\mathcal{E}_*^{\rm ac}(u) : u \in \mathcal{U}_h\}$$

and

$$\begin{aligned} v_h &:= \arg\min\left\{ \int_{\Omega_h^{\complement}} |\nabla v|^2 \,:\, v \in \dot{H}^1(\Omega_h^{\complement}), \gamma_0^{\rm ext} v = \gamma_0^{\rm int} \bar{u}_h \right\}, \\ u_h^* &:= \arg\min\left\{ \mathcal{E}_{\rm lin}^{\rm ac}(u) - f(u) \,:\, u \in \dot{H}^1(\mathbb{R}^2), u|_{\Omega_h} \in \mathcal{U}_h \right\}, \end{aligned} \tag{4.2.14}$$

then clearly $u_h^* = \bar{u}_h$ in Ω_h while $u_h^* = v_h$ in $\Omega_h^{\complement}$. The inf-problem (4.2.14) can be expressed as an exterior Laplace problem

$$\begin{aligned} -\Delta v &= 0, \quad \text{in } \Omega_h^{\complement} \\ v &= \gamma_0^{\rm int} \bar{u}_h, \quad \text{on } \Gamma_h \\ |v(x) - u_0| &= \mathcal{O}\left(\frac{1}{|x|}\right) \quad \text{as } |x| \to \infty, \end{aligned} \tag{4.2.15}$$

where u_0 is a constant determined by the inner boundary condition $v = \gamma_0^{\rm int} \bar{u}_h$ on Γ_h. This exterior Laplace problem can be solved by boundary integrals and be approximated by boundary element methods.

4.2.4.1 Boundary integrals

In this section, we formally outline how we combine the BEM with a/c coupling. Technical details will be presented in later sections. For a complete introduction to BEM we refer

to [51].

To define Sobolev spaces of fractional order, we use the Slobodeckij semi-norm.

Definition 4.2.1. *Let $\Gamma \subset \mathbb{R}^d$ be a Lipschitz boundary, then for $0 < s < 1$, we define*

$$
\begin{aligned}
|v|_{H^s(\Gamma)} &:= \left(\int_\Gamma \int_\Gamma \frac{[v(x) - v(y)]^2}{|x-y|^{d-1+2s}} \mathrm{d}S(x) \mathrm{d}S(y) \right)^{1/2}, \\
\|v\|_{H^s(\Gamma)} &:= \left(\|v\|^2_{L^2(\Gamma)} + |v|^2_{H^s(\Gamma)} \right)^{1/2}, \quad \textit{and} \\
H^s_{(\Gamma)} &:= \left\{ u \in L^2(\Gamma) \,|\, |v|_{H^s(\Gamma)} < \infty \right\}.
\end{aligned}
$$

For $0 < s < 1$, $H^{-s}(\Gamma)$ is defined as the dual space of $H^s(\Gamma)$:

$$
\|v\|_{H^{-s}(\Gamma)} := \sup_{0 \neq w \in H^s(\Gamma)} \frac{\langle v, w \rangle_\Gamma}{\|w\|_{H^s(\Gamma)}},
$$

with respect to the duality pairing

$$
\langle v, w \rangle_\Gamma := \int_\Gamma v(x) w(x) \, \mathrm{d}x.
$$

Using the Trace Theorem (see Theorem 4.3.2), we can conclude that for $u_h \in \mathcal{U}_h \subset H^1(\Omega_h)$,

$$
\gamma_0^{\mathrm{int}} u_h \in H^{1/2}(\Gamma_h) \quad \text{and} \quad \|\gamma_0^{\mathrm{int}} u_h\|_{H^{1/2}(\Gamma_h)} \leq C_{\Omega_h} \|u_h\|_{H^1(\Omega_h)}.
$$

In addition to the trace operators γ_0^{int} and γ_0^{ext}, we define the interior and exterior conormal derivative, for $x \in \Gamma_h$ and $u \in \dot{H}^1(\mathbb{R}^2)$, by

$$
\begin{aligned}
\gamma_1^{\mathrm{int}} u(x) &:= \lim_{\Omega_h \ni y \to x \in \Gamma_h} n(x) \cdot \nabla u(y), \quad \text{and} \\
\gamma_1^{\mathrm{ext}} u(x) &:= \lim_{\Omega_h^{\mathfrak{C}} \ni y \to x \in \Gamma_h} n(x) \cdot \nabla u(y),
\end{aligned}
$$

where n is the outward unit normal vector to Ω_h, i.e. pointing *into* $\Omega_h^{\mathfrak{C}}$.

Denote the fundamental solution to the Laplace operator in 2D by $G(x, y)$, i.e.

$$
G(x, y) := -\frac{1}{2\pi} \log |x - y|.
$$

For $y_0 \in \Omega_h$ and $R > 2\mathrm{diam}(\Omega_h)$, let $B_R(y_0)$ be a ball centred at y_0 with radius R. Then, by Green's First Identity, we can solve the exterior Laplace problem (4.2.15) using the following representation formula, for $x \in B_R(y_0) \setminus \bar{\Omega}_h$,

$$
\begin{aligned}
v(x) = &\int_{\Gamma_h} (\gamma_0^{\mathrm{ext}} \bar{u}_h)(y) \gamma_{1,y}^{\mathrm{ext}} G(x, y) \mathrm{d}S(y) - \int_{\Gamma_h} G(x, y) \gamma_1^{\mathrm{ext}} v(y) \mathrm{d}S(y) + \\
&+ \int_{\partial B_R(y_0)} G(x, y) \gamma_{1, \partial B_R(y_0)}^{\mathrm{int}} v(y) \mathrm{d}S(y) - \int_{\partial B_R(y_0)} \gamma_{1, \partial B_R(y_0), y}^{\mathrm{ext}} G(x, y) \gamma_0^{\mathrm{int}} v(y) \mathrm{d}S(y),
\end{aligned}
$$

where $\gamma^{\text{int}}_{1,\partial B_R(y_0)}$ and $\gamma^{\text{ext}}_{1,\partial B_R(y_0)}$ are the conormal derivatives on $\partial B_R(y_0)$. Taking limit $R \to \infty$ gives, for $x \in \Omega_h^{\complement}$,

$$v(x) = u_0 + \int_{\Gamma_h} (\gamma_0^{\text{ext}} \bar{u}_h)(y) \gamma_{1,y}^{\text{ext}} G(x,y) \mathrm{d}S(y) - \int_{\Gamma_h} G(x,y) \gamma_1^{\text{ext}} v(y) \mathrm{d}S(y), \tag{4.2.16}$$

where u_0 is the far-field constant in (4.2.15).

Let us define the following boundary integrals, for $x \in \mathbb{R}^2 \setminus \Gamma_h$,

$$\begin{aligned} A\psi(x) &:= \int_{\Gamma_h} G(x,y)\psi(y)\mathrm{d}S(y) \quad \text{(single layer potential)}, \\ B\psi(x) &:= \int_{\Gamma_h} \psi(y) \gamma_{1,y}^{\text{int}} G(x,y)\mathrm{d}S(y) \quad \text{(double layer potential)}. \end{aligned}$$

Then for $x \in \Gamma_h$ we define

$$\begin{aligned} Vu(x) &:= \gamma_0^{\text{int}}(Au)(x), \quad Ku(x) := \gamma_0^{\text{int}}(Bu)(x), \\ K'u(x) &:= \gamma_1^{\text{int}}(Au)(x), \quad Du(x) := -\gamma_1^{\text{int}}(Bu)(x). \end{aligned}$$

We refer to Theorem 4.3.3 and 4.3.4 for properties and spaces of V, K, K' and D. Applying the exterior trace operator and the exterior conormal operator to (4.2.16) gives, for $x \in \Gamma_h$,

$$\gamma_0^{\text{int}} v(x) = u_0 + \lambda(x)\gamma_0^{\text{int}}\bar{u}_h + (K\gamma_0^{\text{int}}\bar{u}_h)(x) - V(\gamma_1^{\text{ext}} v)(x), \tag{4.2.17}$$

$$\gamma_1^{\text{ext}} v(x) = (1-\lambda(x))\gamma_1^{\text{ext}} v(x) - (K'\gamma_1^{\text{ext}}(v)(x) - (D\gamma_0^{\text{int}}\bar{u}_h)(x), \tag{4.2.18}$$

where by Lemma 6.8 in [51]

$$\lambda(x) := \lim_{\epsilon \to 0} \frac{1}{2\pi\epsilon} \int_{y \ni \Omega_h : |y-x| = \epsilon} \mathrm{d}S(y) = \frac{1}{2} \text{ a.e.}$$

We observe that the Neumann data $\gamma_1^{\text{ext}} v$ can be obtained from the Dirichlet data $\gamma_0^{\text{int}}\bar{u}_h$ via (4.2.17) and (4.2.18) up to constant u_0. To make sure that the operator V is bijective, we need the following restriction on the boundary spaces.

Let us define subspaces

$$\begin{aligned} H_*^{-1/2}(\Gamma_h) :=& \{w \in H^{-1/2}(\Gamma_h) : \langle w, 1\rangle_{\Gamma_h} = 0\} \quad \text{and} \\ H_*^{1/2}(\Gamma_h) :=& \{v \in H^{1/2}(\Gamma_h) : v = V(w) \text{ for some } w \in H_*^{-1/2}\}. \end{aligned}$$

Then Lemma 4.3.8 shows that $V : H_*^{-1/2}(\Gamma_h) \to H_*^{1/2}(\Gamma_h)$ is an isomorphism and consequently $u_0 = 0$.

Remark 4.2.2. For any Lipschitz boundary Γ, there exist an unique $w_\Gamma \in H^{-1/2}(\Gamma) \setminus H_*^{-1/2}(\Gamma)$ such that $\langle w_\Gamma, 1\rangle_\Gamma = 1$ and

$$u - \langle u, w_\Gamma\rangle_\Gamma \in H_*^{1/2}(\Gamma), \qquad \text{for any } u \in H^{1/2}(\Gamma). \tag{4.2.19}$$

Its derivation is shown in [51, §6.6.1]. □

Therefore from (4.2.18) and (4.2.17) we have

$$-\gamma_1^{\text{ext}} v = \big[D + (K' - \tfrac{1}{2}I)V^{-1}(K - \tfrac{1}{2}I)\big]\gamma_0^{\text{int}}\bar{u}_h, \quad \text{if } \gamma_0^{\text{int}}\bar{u}_h \in H_*^{1/2}(\Gamma_h).$$

Denote $g^{-1} := D + (K' - \frac{1}{2}I)V^{-1}(K - \frac{1}{2}I)$, which is called *Steklov–Poincaré operator* and was proposed by [7]. The significance of this formulation is symmetry, which is essential for the Galerkin matrices in energy calculations. Then the total energy (4.2.13) is equivalent to, for $u \in \mathcal{U}_h \cap H_*^{1/2}(\Gamma_h)$,

$$\mathcal{E}_*^{\text{ac}}(u) \equiv \mathcal{E}^{\text{tot}}(u) := \mathcal{E}_h^{\text{ac}}(u) + \frac{\mu}{2}\int_{\Gamma_h} (\gamma_0^{\text{int}} u) g^{-1}(\gamma_0^{\text{int}} u). \tag{4.2.20}$$

Theorem 4.3.9 establishes that Steklov–Poincaré operator $g^{-1} : H_*^{1/2}(\Gamma_h) \to H_*^{-1/2}(\Gamma_h)$ is positive definite. Lemma 4.3.10 shows that g^{-1} is in fact in-variant under rescaling. In addition, in order to ensure that the regularity constants are independent of the size of the boundary Γ_h, we employ a rescaling argument in Section 4.3.2 to introduce another fractional norm on the boundary: for $u \in H^{1/2}(\Gamma_h)$

$$\|u\|^2_{H^{1/2}_{\Gamma_h}} := \big[\tfrac{1}{2}\text{diam}(\Gamma_h)\big]^{-1}\|u\|^2_{L^2(\Gamma_h)} + |u|^2_{H^{1/2}(\Gamma_h)}.$$

By Lemma 4.3.11 we have that for all $u \in H_*^{1/2}(\Gamma_h)$

$$\langle g^{-1}u, u\rangle \geq C_1\|u\|^2_{H^{1/2}_{\Gamma_h}} \quad \text{and} \quad \|g^{-1}u\|_{H^{-1/2}_{\Gamma_h}} \leq C_2\|u\|_{H^{-1/2}_{\Gamma_h}},$$

where C_1 and C_2 are independent of the radius of Ω_h.

Now we take into account the displacement inside Ω_h to introduce the following norm for the error analysis. For $u \in \mathcal{U}_h \cap H_*^{1/2}(\Gamma_h)$, define

$$\|u\|_E^2 := \|\nabla u\|^2_{L^2(\Omega_h)} + \|u\|^2_{H^{1/2}_{\Gamma_h}}. \tag{4.2.21}$$

It is clear that this norm is rescale in-variant.

4.2.4.2 Boundary element method

We introduce a numerical discretization scheme to approximate the boundary integral equations. Let

$$S_h^0(\Gamma_h) = \text{span}\big\{\phi_k^0\big\}_{k=1}^M \subset H_*^{-1/2}(\Gamma_h),$$
$$S_h^1(\Gamma_h) = \text{span}\big\{\phi_k^1\big\}_{k=1}^M \subset H_*^{1/2}(\Gamma_h),$$

where ϕ_k^0 are piecewise constant basis functions and ϕ_k^1 are piecewise linear hat functions on the discretized boundary with elements $\mathcal{T}_h \cap \Gamma_h$. For a Dirichlet datum $u \in H_*^{1/2}(\Gamma_h)$,

we define $g_h^{-1}u := \bar{v}_h \in S_h^0(\Gamma_h)$ as the solution to

$$\langle \bar{v}_h, \tau_h \rangle = \langle Du, \tau_h \rangle + \langle V^{-1}(K - \tfrac{1}{2}I)u, (K - \tfrac{1}{2}I)\tau_h \rangle, \quad \text{for all } \tau_h \in S_h^1(\Gamma_h). \tag{4.2.22}$$

Then we define

$$\mathcal{E}_h^{\rm tot}(u_h) := \mathcal{E}_h^{\rm ac}(u_h) + \frac{\mu}{2} \int_{\Gamma_h} (\gamma_0^{\rm int} u_h) g_h^{-1} (\gamma_0^{\rm int} u_h), \tag{4.2.23}$$

where $\gamma_0^{\rm int} u_h \in S_h^1(\Gamma_h)$. We seek the solution to

$$u_h := \arg\min\{\mathcal{E}_h^{\rm tot}(u) - f(u) \,:\, u \in \mathcal{U}_h^*\}, \tag{4.2.24}$$

where

$$\mathcal{U}_h^* := \big\{ u_h \in \mathcal{U}_h \cap S_h^1(\Gamma_h) \,:\, u_h|_{\Gamma_h} \in H_*^{1/2}(\Gamma_h) \big\},$$

and the error estimate $\|\nabla u_h - \nabla \tilde{u}^{\rm a}\|$ in a suitable norm.

For the simplicity of analysis, we impose the following assumption on the boundary Γ_h and the atomistic triangulation $\mathcal{T}$:

(B3) The boundary Γ_h is aligned with the canonical triangulation $\mathcal{T}$ in the sense that, for all $T \in \mathcal{T}$,

(a) $T \cap \Gamma_h \neq \emptyset \implies \mathrm{int}(T) \cap \Gamma_h = \emptyset$.

(b) Let $\mathcal{V}_{\rm FEM}$ be the set of vertices of $\mathcal{T}_h$, and $\mathcal{V}_{\rm can}$ be the set of vertices of $\mathcal{T}$, then $\mathcal{V}_{\rm FEM} \cap \Gamma_h \subset \mathcal{V}_{\rm can}$.

(B3) is employed in § 4.7.1.1 for the construction of a dual interpolant. We expect that, without it, the main results are still true, but would require some additional technicalities to prove. For the sake of clarity we therefore impose **(B3)** to emphasize the main concepts of the error analysis.

4.3 Preliminaries

In order to measure the "smoothness" of displacement maps $u \in \dot{\mathcal{U}}^{1,2}$, we review from [30] a smooth interpolant $\tilde{u}$, namely a $C^{2,1}$-conforming multi-quintic interpolant.

Lemma 4.3.1. *(a) For each $u : \Lambda \to \mathbb{R}^m$, there exists a unique $\tilde{u} \in C^{2,1}(\mathbb{R}^2; \mathbb{R}^m)$ such that, for all $\ell \in \Lambda$,*

$$\begin{aligned} \tilde{u}|_{\ell + \mathsf{A}(0,1)^2} &\text{ is a polynomial of degree 5,} \\ \tilde{u}(\ell) &= u(\ell), \\ \partial_{a_i} \tilde{u}(\ell) &= \tfrac{1}{2}\left(u(\ell + a_i) - u(\ell - a_i)\right), \\ \partial_{a_i}^2 \tilde{u}(\ell) &= u(\ell + a_i) - 2u(\ell) + u(\ell - a_i), \end{aligned}$$

where $i \in \{1, 2\}$ and ∂_{a_i} is the derivative in the direction of a_i.

(b) Moreover, for $q \in [1,\infty]$, $0 \le j \le 3$,

$$\|\nabla^j \tilde{u}\|_{L^q(\ell+\mathsf{A}(1,0)^2)} \lesssim \|D^j u\|_{\ell^q(\ell+\mathsf{A}\{-1,0,1,2\}^2)} \quad \textit{and} \quad |D^j u(\ell)| \lesssim \|\nabla^j \tilde{u}\|_{L^1(\ell+\mathsf{A}(-1,1)^2)}, \tag{4.3.1}$$

where D is the difference operator defined in (4.2.1)*. In particular,*

$$\|\nabla \tilde{u}\|_{L^q} \lesssim \|\nabla u\|_{L^q} \lesssim \|\nabla \tilde{u}\|_{L^q},$$

where u is identified with its piecewise affine interpolant.

Proof. This is the same proof as Lemma 6.1 in Chapter 3. □

4.3.1 Properties of Steklov–Poincaré operator

As mentioned in Section 4.2.4, we require some regularity properties of the Steklov–Poincaré operator g^{-1}. First of all we have the following trace theorem.

Theorem 4.3.2 (Trace Theorem). *For $\frac{1}{2} < s \le 1$, the interior trace operator*

$$\gamma_0 : H^s(\Omega_h) \to H^{s-1/2}(\Gamma_h)$$

is bounded satisfying

$$\|\gamma_0 v\|_{H^{s-1/2}(\Gamma_h)} \le c_T \|v\|_{H^s(\Omega_h)}, \quad \forall v \in H^s(\Omega_h).$$

Proof. This is a standard result, see for example [2]. □

The boundedness and ellipticity of the boundary integrals are proved in [8] for Lipschitz domains.

Theorem 4.3.3 (Boundedness). *The boundary integral operators*

$$\begin{aligned} V &: H^{-1/2+s}(\Gamma_h) \to H^{1/2+s}(\Gamma_h), \\ K &: H^{1/2+s}(\Gamma_h) \to H^{1/2+s}(\Gamma_h), \\ K' &: H^{1/2+s}(\Gamma_h) \to H^{1/2+s}(\Gamma_h), \\ D &: H^{1/2+s}(\Gamma_h) \to H^{-1/2+s}(\Gamma_h) \end{aligned}$$

are bounded for all $s \in \left(-\frac{1}{2}, \frac{1}{2}\right)$.

Proof. See Theorem 1 in [8]. □

Theorem 4.3.4 (Ellipticity). *The operators V and D are strongly elliptic in the sense that there exist $C^V, C^D > 0$ such that for all $v \in H_*^{-1/2}(\Gamma_h), u \in H_*^{1/2}(\Gamma_h)$*

$$\langle Vv, v\rangle \geq C^V \|v\|^2_{H^{-1/2}(\Gamma_h)}, \tag{4.3.2}$$

$$\langle Du, u\rangle \geq C^D \|u\|^2_{H^{1/2}(\Gamma_h)}. \tag{4.3.3}$$

This is a special case of Theorem 2 in [8]. In 2D, the far-field constant u_0 vanishes only if the Dirichlet data is in the subspace $H_*^{1/2}(\Gamma_h)$. To construct the proofs for Theorem 4.3.4, we need several intermediate results from the literature.

Lemma 4.3.5. *Suppose $v \in H_*^{-1/2}(\Gamma_h)$, $y_0 \in \Omega_h$ and $u(x) = (Av)(x)$ for $x \in \mathbb{R}^2 \setminus \Gamma_h$ then we have*

$$|u(x)| \leq c_1 \frac{1}{|x - y_0|} \quad \textit{and}$$
$$|\nabla u(x)| \leq c_2 \frac{1}{|x - y_0|^2}, \quad \textit{for } |x - y_0| > \max\{1, 2\mathrm{diam}(\Omega_h)\}.$$

Proof. See Lemma 6.21 in [51]. □

Lemma 4.3.6. *For $w \in H^{-1/2}(\Gamma_h)$ and $u = Aw$, we have the following jump relation:*

$$\gamma_1^{\mathrm{int}} u - \gamma_1^{\mathrm{ext}} u = w. \tag{4.3.4}$$

Proof. See Lemma 4 in [8]. □

Lemma 4.3.7. *The interior and exterior conormal derivatives $\gamma_1^{\mathrm{int}} : H^1(\Omega_h) \to H^{-1/2}(\Gamma_h)$ and $\gamma_1^{\mathrm{ext}} : H^1(\Omega_h^{\complement}) \to H^{-1/2}(\Gamma_h)$ are continuous in the sense that*

$$\|\gamma_1^{\mathrm{int}} u\|_{H^{-1/2}(\Gamma_h)} \leq c^{\mathrm{int}} \|\nabla u\|_{L^2(\Omega_h)} \tag{4.3.5}$$

$$\|\gamma_1^{\mathrm{ext}} u\|_{H^{-1/2}(\Gamma_h)} \leq c^{\mathrm{ext}} \|\nabla u\|_{L^2(\Omega_h^{\complement})}. \tag{4.3.6}$$

Proof. See Lemma 3.2 in [8]. □

Proof of Theorem 4.3.4. It is clear that if $v \in H_*^{1/2}(\Gamma)$, $u = Av(x)$ is a solution to the interior Dirichlet boundary value problem

$$-\Delta u = 0, \quad \text{in } \Omega_h,$$
$$u = \gamma_0^{\mathrm{int}}(Av)(x) = (Vv)(x), \quad \text{on } \Gamma_h.$$

By choosing $w \in H^1(\Omega_h)$ we integrate by part to get

$$a_{\Omega_h}(u,w) := \int_{\Omega_h} \nabla u(x) \nabla w(x)\,\mathrm{d}x = \langle \gamma_1^{\mathrm{int}} u, \gamma_0^{\mathrm{int}} w \rangle_{\Gamma_h}. \tag{4.3.7}$$

On the other hand, for $y_0 \in \Omega_h$ and $R > 2\mathrm{diam}(\Omega_h)$, let $B_R(y_0)$ be a ball centred at y_0 with radius R. Then $u = Av(x)$ is also the unique solution to the exterior Dirichlet boundary value problem

$$\begin{aligned} -\Delta u &= 0, \quad \text{in } B_R(y_0) \setminus \bar{\Omega}_h, \\ u &= \gamma_0^{\mathrm{ext}}(Av)(x) = (Vv)(x), \quad \text{on } \Gamma_h, \\ u &= (Av)(x), \quad \text{on } \partial B_R(y_0). \end{aligned}$$

We also integrate by part and get

$$a_{B_R(y_0)\setminus\bar{\Omega}_h}(u,w) := \int_{B_R(y_0)\setminus\bar{\Omega}_h} \nabla u(x)\nabla w(x)\,\mathrm{d}x = -\langle \gamma_1^{\mathrm{ext}} u, \gamma_0^{\mathrm{ext}} w\rangle_{\Gamma_h} + \langle \gamma_1^{\mathrm{int}} u, \gamma_0^{\mathrm{int}} w\rangle_{\partial B_R(y_0)}.$$

Since $u = Av(x)$ with $v \in H_*^{1/2}(\Gamma)$, by Lemma 4.3.5 we have

$$|\langle \gamma_1^{\mathrm{int}} u, \gamma_0^{\mathrm{int}} u\rangle_{\partial B_R(y_0)}| \le C \int_{|x-y_0|=R} \frac{1}{|x-y_0|^3}\,\mathrm{dS}(x) \le CR^{-2} \to 0, \text{ as } R \to \infty.$$

Thus we have

$$a_{\Omega_h^{\complement}}(u,w) = -\langle \gamma_1^{\mathrm{ext}} u, \gamma_0^{\mathrm{ext}} w\rangle_{\Gamma_h}. \tag{4.3.8}$$

Consequently we have by Lemma 4.3.6

$$a_{\Omega}(u,u) + a_{\Omega_h^{\complement}}(u,u) = \langle \gamma_1^{\mathrm{int}} u - \gamma_1^{\mathrm{ext}} u, \gamma_0^{\mathrm{int}} u\rangle_{\Gamma_h} = \langle v, \gamma_0^{\mathrm{int}} u\rangle_{\Gamma_h} = \langle Vv, v\rangle_{\Gamma_h}. \tag{4.3.9}$$

Applying (4.3.5) and (4.3.6) gives the ellipticity of V. Analogous argument follows for the ellipticity of D. □

Lemma 4.3.8. *$V : H_*^{-1/2}(\Gamma_h) \to H_*^{1/2}(\Gamma_h)$ is an isomorphism.*

Proof. This is a consequence of Theorems 4.3.3 and 4.3.4 and the Lax-Milgram Theorem. □

Therefore, with the boundedness and ellipticity, we can prove the positive definiteness of the Steklov–Poincaré operator.

Theorem 4.3.9. *The Steklov–Poincaré operator $g^{-1} : H_*^{1/2}(\Gamma_h) \to H_*^{-1/2}(\Gamma_h)$ is well-defined. Furthermore, there exist $C_1^g, C_2^g > 0$ such that for all $u \in H_*^{1/2}(\Gamma_h)$*

$$\langle g^{-1}u, u\rangle \ge C_1^g \|u\|^2_{H^{1/2}(\Gamma_h)} \quad \textit{and} \quad \|g^{-1}u\|_{H^{-1/2}(\Gamma_h)} \le C_2^g \|u\|_{H^{1/2}(\Gamma_h)}. \tag{4.3.10}$$

Proof. Since $V : H_*^{-1/2}(\Gamma_h) \to H_*^{1/2}(\Gamma_h)$ is an isomorphism and $K, K' : H^{1/2}(\Gamma_h) \to H^{1/2}(\Gamma_h)$ and $D : H^{1/2+s}(\Gamma_h) \to H^{-1/2+s}(\Gamma_h)$ are bounded, we have that $g^{-1} = D + (K' - \frac{1}{2}I)V^{-1}(K - \frac{1}{2}I)$ is well-defined. The upper bound C_2^g follows from the Lax-Milgram Theorem.

For positive-definiteness, we use the ellipticity of V^{-1} and D from Theorem 4.3.4 to obtain

$$\begin{aligned}\langle g^{-1}u, u\rangle &= \langle Du, u\rangle + \langle V^{-1}(K - \tfrac{1}{2}I)u, (K - \tfrac{1}{2}I)u\rangle \\ &\geq \langle Du, u\rangle \\ &\geq C^D \|u\|^2_{H^{1/2}(\Gamma_h)}. \quad \square\end{aligned}$$

4.3.2 Re-scaling of the boundary integrals

In the analysis of a/c coupling methods, we are concerned with the convergence rate against the size of the domain. Therefore, we need to explore how boundary integrals scale with the size of the domain.

Suppose that $f_1 : \Gamma_1 := \partial\Omega_1 \to \mathbb{R}^2$ and $f_1 \in H^{1/2}(\partial B_1)$, where Ω_1 is a Lipschitz domain with radius 1. Let $f_R : \Gamma_R := \partial\Omega_R \to \mathbb{R}^2$ and $f_R(x) := f_1(x/R)$, where $\Omega_R = R\Omega_1$. Then we have

$$\|f_R\|^2_{L^2(\Gamma_R)} = \int_{\Gamma_R} |f_R(x)|^2 \,\mathrm{d}x = \int_{\Gamma_R} |f_1(x/R)|^2 \,\mathrm{d}x = \int_{\Gamma_1} |f_1(y)|^2 R \,\mathrm{d}y = R\|f_1\|^2_{L^2(\Gamma_1)},$$

while

$$\begin{aligned}|f_R|^2_{H^{1/2}(\Gamma_R)} &:= \int_{\Gamma_R}\int_{\Gamma_R} \frac{[f_R(x) - f_R(y)]^2}{|x-y|^2} \mathrm{d}S(x)\mathrm{d}S(y) \\ &= \int_{\Gamma_R}\int_{\Gamma_R} \frac{[f_1(x/R) - f_1(y/R)]^2}{|x-y|^2} \mathrm{d}S(x)\mathrm{d}S(y) \\ &= \int_{\Gamma_1}\int_{\Gamma_1} \frac{[f_1(x') - f_1(y')]^2}{|Rx' - Ry'|^2} R^2 \mathrm{d}S(x')\mathrm{d}S(y') \\ &= \int_{\Gamma_1}\int_{\Gamma_1} \frac{[f_1(x') - f_1(y')]^2}{|x' - y'|^2} \mathrm{d}S(x')\mathrm{d}S(y') \\ &= |f_1|^2_{H^{1/2}(\Gamma_1)}.\end{aligned}$$

Thus we define a re-scaled norm in $H^{1/2}(\Gamma_h)$,

$$\|f\|^2_{H^{1/2}_{\Gamma_h}} := \left[\tfrac{1}{2}\mathrm{diam}(\Gamma_h)\right]^{-1} \|f\|^2_{L^2(\Gamma_h)} + |f|^2_{H^{1/2}(\Gamma_h)}, \tag{4.3.11}$$

then we have $\|f_1\|_{H^{1/2}(\Gamma_1)} = \|f_R\|_{H^{1/2}_{\Gamma_R}}$ with $R = \frac{1}{2}\mathrm{diam}(\Gamma_h)$. Similarly, we define a rescaled H^1 norm

$$\|f\|^2_{H^1_{\Gamma_h}} := \left[\tfrac{1}{2}\mathrm{diam}(\Gamma_h)\right]^{-1} \|f\|^2_{L^2(\Gamma_h)} + \left[\tfrac{1}{2}\mathrm{diam}(\Gamma_h)\right] \|\nabla f\|^2_{L^2(\Gamma_h)}. \tag{4.3.12}$$

Then we have $\|f_1\|_{H^1(\Gamma_1)} = \|f_R\|_{H^1_{\Gamma_h}}$ with $R = \frac{1}{2}\mathrm{diam}(\Gamma_h)$.

Lemma 4.3.10. *Let V_1, K_1, V_R, K_R be the boundary integrals V and K on Γ_1 and Γ_R respectively. Denote*

$$g_1^{-1} = D_1 + (K_1' - \tfrac{1}{2}I)V_1^{-1}(K_1 - \tfrac{1}{2}I) \quad \textit{and} \quad g_R^{-1} = D_R + (K_R' - \tfrac{1}{2}I)V_R^{-1}(K_R - \tfrac{1}{2}I).$$

Then for $u_1 \in H_*^{1/2}(\Gamma_1)$ and $u_R := u_1(x/R)$, we have $u_R \in H_*^{1/2}(\Gamma_R)$ and

$$\langle g_1^{-1}u_1, u_1\rangle_{\Gamma_1} = \langle g_R^{-1}u_R, u_R\rangle_{\Gamma_R}.$$

Proof. First we show that $u_R \in H_*^{1/2}(\Gamma_R)$. Since $u_1 \in H_*^{1/2}(\Gamma_1)$, there exists $\phi_1 \in H_*^{-1/2}(\Gamma_1)$ such that $V_1\phi_1 = u_1$. Let $\phi_R(x) := \frac{1}{R}\phi_1(x/R)$, then it is clear that $\phi_R \in H_*^{-1/2}(\Gamma_R)$. Then we can write

$$\begin{aligned}
u_R(x) = u_1(x/R) &= -\frac{1}{2\pi}\int_{\Gamma_1} \log\left|\frac{x}{R} - y\right| \phi_1(y)\,\mathrm{d}S(y) \\
&= -\frac{1}{2\pi}\int_{\Gamma_R} \log\left|\frac{x}{R} - \frac{y}{R}\right| \phi_1\left(\frac{y}{R}\right)\frac{1}{R}\mathrm{d}S(y) \\
&= -\frac{1}{2\pi}\int_{\Gamma_R} \log\left|\frac{x}{R} - \frac{y}{R}\right| \phi_R(y)\,\mathrm{d}S(y) \\
&= -\frac{1}{2\pi}\int_{\Gamma_R} (\log|x-y| - \log R)\phi_R(y)\,\mathrm{d}S(y) \\
&= -\frac{1}{2\pi}\int_{\Gamma_R} \log|x-y|\phi_R(y)\,\mathrm{d}S(y) = V_R\phi_R \in H_*^{1/2}(\Gamma_R),
\end{aligned}$$

where we used the fact that $\langle \phi_R, 1\rangle_{\Gamma_R} = 0$. By a similar argument of change of variables, we have

$$\begin{aligned}
(K_1 - \tfrac{1}{2}I)u_1 &= (K_R - \tfrac{1}{2}I)u_R, \\
D_1u_1 &= D_Ru_R.
\end{aligned}$$

Now we shall prove that V^{-1} is also scale in-variant. Let $\bar{u}_1$ be the solution to the homogeneous Laplace equation

$$\begin{aligned}
-\Delta\bar{u}_1 &= 0, \quad \text{in } \mathbb{R}^2 \setminus \Gamma_1, \\
\bar{u}_1 &= u_1, \quad \text{on } \Gamma_1, \\
|\bar{u}_1(x)| &= \mathcal{O}\left(\frac{1}{|x|}\right) \quad \text{as } |x| \to \infty.
\end{aligned}$$

Then $\bar{u}_R := \bar{u}_1(x/R)$ also solves

$$\begin{aligned} -\Delta \bar{u}_R &= 0, \quad \text{in } \mathbb{R}^2 \setminus \Gamma_R, \\ \bar{u}_R &= u_R, \quad \text{on } \Gamma_R, \\ |\bar{u}_R(x)| &= \mathcal{O}\left(\frac{1}{|x|}\right), \quad \text{as } |x| \to \infty. \end{aligned}$$

For $i = 1, R$, define v_i and $\bar{v}_i$ in the same way as u_i and $\bar{u}_i$. Then we can apply (4.3.7), (4.3.8) and the jump relation in Lemma 4.3.6 to get

$$\begin{aligned} \int_{\Omega_i} \nabla \bar{u}_i \nabla \bar{v}_i + \int_{\mathbb{R}^2 \setminus \Omega_i} \nabla \bar{u}_i \nabla \bar{v}_i &=: a_{\Omega_i(0}(\bar{u}_i, \bar{v}_i) + a_{\mathbb{R}^2 \setminus \Omega_i}(\bar{u}_i, \bar{v}_i) \\ &= \langle \gamma_1^{\text{int}} \bar{u}_i - \gamma_1^{\text{ext}} \bar{u}_i, \gamma_0^{\text{int}} \bar{v}_i \rangle_{\Gamma_i} \\ &= \langle \phi_i, v_i \rangle_{\Gamma_i} \\ &= \langle V_i^{-1} u_i, v_i \rangle_{\Gamma_i}, \quad \text{for } i = 1, R, \end{aligned}$$

where $\phi_i = V_i^{-1} u_i$. Clearly

$$a_{\Omega_1}(\bar{u}_1, \bar{v}_1) + a_{\mathbb{R}^2 \setminus \Omega_1}(\bar{u}_1, \bar{v}_1) = a_{\Omega_R}(\bar{u}_R, \bar{v}_R) + a_{\mathbb{R}^2 \setminus \Omega_R}(\bar{u}_R, \bar{v}_R).$$

Thus $\langle V_1^{-1} u_1, v_1 \rangle_{\Gamma_1} = \langle V_R^{-1} u_R, v_R \rangle_{\Gamma_R}$ and hence the result follows. □

Using the re-scaled norm we have the following lemma.

Lemma 4.3.11. *The Steklov–Poincaré operator $g^{-1} : H_*^{1/2}(\Gamma_h) \to H_*^{-1/2}(\Gamma_h)$ has the following regularity, for $u \in H_*^{1/2}(\Gamma_h)$*

$$\langle g^{-1} u, u \rangle \geq C_1 \|u\|^2_{H^{1/2}_{\Gamma_h}} \quad \textit{and} \quad \|g^{-1} u\|_{H^{-1/2}(\Gamma_h)} \leq C_2 \|u\|_{H^{1/2}_{\Gamma_h}}, \tag{4.3.13}$$

where C_1 and C_2 are independent of the radius of Ω_h.

Furthermore, the Galerkin operator g_h^{-1} is also coercive: for $u_h \in S_h^1(\Gamma_h)$ we have

$$\langle g_h^{-1} u_h, u_h \rangle \geq C_1^h \|u_h\|^2_{H^{1/2}_{\Gamma_h}}, \tag{4.3.14}$$

where C_1^h is independent of the radius of Ω_h.

Proof. The result 4.3.13 follows directly from Theorem 4.3.9 and Lemma 4.3.10. Due to the symmetry of g_h^{-1} analogous argument gives 4.3.14. □

4.3.3 Boundary element approximation error

We also need the following boundary element approximation error estimate to compare g^{-1} and g_h^{-1}.

Theorem 4.3.12. *If $u \in H_*^{1/2}(\Gamma_h)$, then the approximate solution $g_h^{-1}u$ to (4.2.22) exists and we have the stability property*

$$\|g_h^{-1}u\|_{H^{-1/2}(\Gamma_h)} \leq \frac{C_2}{C_1}\|u\|_{H^{1/2}_{\Gamma_h}}. \tag{4.3.15}$$

Furthermore, if $g^{-1}u \in H^1(\Gamma_h)$, then

$$\|g^{-1}u - g_h^{-1}u\|_{H^{-1/2}(\Gamma_h)} \leq Ch^{3/2}|g^{-1}u|_{H^1(\Gamma_h)}, \tag{4.3.16}$$

where h is the size of each boundary element and C is independent of the size of Γ_h.

Proof. Since $S_h^0(\Gamma_h)$ is a conforming trial space in $H^{-1/2}(\Gamma_h)$ and g^{-1} is bounded and elliptic according to Lemma 4.3.11, then by the Lax-Milgram Theorem $g_h^{-1}u$ exists and we have (4.3.15). For (4.3.16), by Cea's Lemma we have

$$\|g^{-1}u - g_h^{-1}u\|_{H^{-1/2}(\Gamma_h)} \leq \frac{C_2}{C_1}\inf_{v_h \in H^{-1/2}(\Gamma_h)}\|g^{-1}u - v_h\|_{H^{-1/2}(\Gamma_h)}.$$

By Theorem 10.4 in [51], we have

$$\inf_{v_h \in H^{-1/2}(\Gamma_h)}\|g^{-1}u - v_h\|_{H^{-1/2}(\Gamma_h)} \leq ch^{3/2}|g^{-1}u|_{H^1(\Gamma_h)}.$$

□

4.4 Main results

4.4.1 Regularity of u^{a}

The approximation error estimates in later sections requires the decay of the elastic fields away from the defect core which follows from a natural stability assumption:

(A1) The atomistic solution is strongly stable, that is, there exists $C_0 > 0$,

$$\langle \delta^2\mathcal{E}^{\mathrm{a}}(u^{\mathrm{a}})\varphi, \varphi\rangle \geq C_0\|\nabla\varphi\|_{L^2}^2, \quad \forall \varphi \in \dot{\mathcal{U}}^{1,2}, \tag{4.4.1}$$

where u^{a} is a solution to (4.2.2).

Corollary 4.4.1. *Suppose that* **(A1)** *is satisfied, then there exists a constant $C > 0$ such that, for $1 \leq j \leq 3$,*

$$|D^j u^{\mathrm{a}}(\ell)| \leq C|\ell|^{-1-j} \quad \textit{and} \quad |\nabla^j \tilde{u}^{\mathrm{a}}(x)| \leq C|x|^{-1-j}.$$

Proof. See Theorem 2.3 in [18]. □

4.4.2 Stability

In [41] it is proven that there is a "universal" instability in 2D interfaces for QNL-type a/c couplings. It is impossible to show that $\delta^2\mathcal{E}^{\mathrm{g23}}(u^{\mathrm{a}})$ is a positive definite operator for general cases, even with the assumption (4.4.1). In fact, this potential instability is universal to a wide class of generalized geometric reconstruction methods. Nevertheless, it is rarely observed in practice. To circumvent this difficulty, we make the following standing assumption:

(A2) The *homogeneous lattice* is strongly stable under the G23 approximation, that is, there exists $C_0^{\mathrm{ac}} > 0$ which is independent of K such that, for K sufficiently large,

$$\langle \delta^2\mathcal{E}_h^{\mathrm{ac}}(0)\varphi_h, \varphi_h\rangle \geq C_0^{\mathrm{ac}}\|\nabla\varphi_h\|_{L^2}^2, \quad \forall \varphi_h \in \mathcal{U}_h. \tag{4.4.2}$$

Because (4.4.2) does not depend on the solution it can be tested numerically. But a precise understanding under which conditions (4.4.2) is satisfied is still missing. In [41] a method of stabilizing 2D QNL-type schemes with flat interfaces is formulated, which could replace this assumption, but we are not yet able to extend this method to interfaces with corners, such as the configurations discussed in this paper. From these two assumptions, we can deduce the following stability result when the BEM formulation is added.

Lemma 4.4.2. *For any $\varphi_h \in \mathcal{U}_h^*$, we have*

$$\langle \delta^2\mathcal{E}_h^{\mathrm{tot}}(0)\varphi_h, \varphi_h\rangle \geq C_0^{\mathrm{tot}}\|\varphi_h\|_E^2, \tag{4.4.3}$$

where $\|\cdot\|_E^2$ is the norm defined in (4.2.21) *and C_0^{tot} is independent of the size of Ω_h.*

Proof. This is an immediate consequence of the property (4.3.14) of g_h^{-1}:

$$\begin{aligned}
\langle \delta^2\mathcal{E}_h^{\mathrm{tot}}(0)\varphi_h, \varphi_h\rangle &= \langle \delta^2\mathcal{E}_h^{\mathrm{ac}}(0)\varphi_h, \varphi_h\rangle + \mu\int_{\Gamma_h}\varphi_h g_h^{-1}\varphi_h \\
&\geq C^{\mathrm{ac}}\|\nabla\varphi_h\|_{L^2(\Omega_h)}^2 + C_1\|\varphi_h\|_{H^{1/2}_{\Gamma_h}}^2 \\
&\geq \min\{C^{\mathrm{ac}}, C_1\}\|\varphi_h\|_E^2.
\end{aligned}$$

□

Then we have the following stability estimate.

Theorem 4.4.3. *Under assumptions **(A1)** and **(A2)** there exists $\gamma > 0$ such that, when the atomistic region radius K is sufficiently large,*

$$\langle \delta\mathcal{G}_h(\Pi_h u^{\mathrm{a}})\varphi_h, \varphi_h\rangle \geq \gamma\|\varphi_h\|_E^2 \quad \text{for all } \varphi_h \in \mathcal{U}_h^*, \tag{4.4.4}$$

where Π_h is the best approximation operator defined in §4.6.1.

Proof. After employing Lemma 4.4.2 this is an analogous argument to the proof of Lemma 3.4.4, which is a straightforward adaption of the proof of [30, Lemma 4.9]. □

4.4.3 Main results

Our two main results are a consistency error estimate for the A/C+BEM coupling scheme and the resulting error estimate.

Theorem 4.4.4 (Consistency). *If u^{a} is a solution to* (4.2.2)*, then for all $v_h \in \mathcal{U}_h^*$*

$$\begin{aligned}
&\langle \delta\mathcal{E}_h^{\mathrm{tot}}(\Pi_h u^{\mathrm{a}}), v_h\rangle \\
&\quad \lesssim \Big(\|\nabla^2 \tilde{u}^{\mathrm{a}}\|_{L^2(\Omega^{\mathrm{i}})} + \|\nabla^3 \tilde{u}^{\mathrm{a}}\|_{L^2(\mathbb{R}^2\setminus\Omega^{\mathrm{a}})} + \|\nabla^2 \tilde{u}^{\mathrm{a}}\|^2_{L^4(\mathbb{R}^2\setminus\Omega^{\mathrm{a}})} \\
&\qquad + \|h\nabla^2 \tilde{u}^{\mathrm{a}}\|_{L^2(\Omega_h^{\mathrm{c}})} + \|h^{3/2}\nabla^2 \tilde{u}^{\mathrm{a}}\|_{L^2(\Gamma_h)} + N^{-3} \Big) \|v_h\|_E.
\end{aligned} \tag{4.4.5}$$

Proof. See Section 4.7.6. □

Combining Theorem 4.4.4 with the stability result Theorem 4.4.3, we obtain the following error estimate.

Theorem 4.4.5. *If u^{a} is a solution to* (4.2.2) *and Assumptions (A1) and (A2) are satisfied then, for K sufficiently large, there exists a solution $u_h \in \mathcal{U}_h^*$ to* (4.2.24) *satisfying*

$$\begin{aligned}
\|\tilde{u}^{\mathrm{a}} - u_h\|_E &\lesssim \|\nabla^2 \tilde{u}^{\mathrm{a}}\|_{L^2(\Omega^{\mathrm{i}})} + \|\nabla^3 \tilde{u}^{\mathrm{a}}\|_{L^2(\mathbb{R}^2\setminus\Omega^{\mathrm{a}})} + \|\nabla^2 \tilde{u}^{\mathrm{a}}\|^2_{L^4(\mathbb{R}^2\setminus\Omega^{\mathrm{a}})} \\
&\quad + \|h\nabla^2 \tilde{u}^{\mathrm{a}}\|_{L^2(\Omega_h^{\mathrm{c}})} + \|h^{3/2}\nabla^2 \tilde{u}^{\mathrm{a}}\|_{L^2(\Gamma_h)} + N^{-3}.
\end{aligned} \tag{4.4.6}$$

Proof. See Section 4.7.7. □

Remark 4.4.6. The term N^{-3} is in fact the linearization error. Recall that in (4.2.12) we approximate the Cauchy–Born strain energy $W(\nabla u)$ by the linearised elasticity strain energy $\frac{1}{2}\mu|\nabla u|^2$. The linearization error in first variation can (formally) be estimated by

$$\int_{\Omega_h^{\mathfrak{C}}} [\partial_{\mathsf{F}} W(\nabla u)\nabla v - \mu \nabla u \cdot \nabla v] \lesssim \int_{\Omega_h^{\mathfrak{C}}} |\nabla u|^2 |\nabla v| \lesssim \|\nabla u\|^2_{L^4(\Omega_h^{\mathfrak{C}})} \|\nabla v\|_{L^2(\Omega_h^{\mathfrak{C}})}.$$

Taking account of the decay of $\tilde{u}^{\mathrm{a}}$ from Corollary 4.4.1, we have

$$\|\nabla \tilde{u}^{\mathrm{a}}\|^2_{L^4(\Omega_h^{\mathfrak{C}})} \lesssim N^{-3}.$$

For technical reasons we cannot directly perform such an estimate, but the $O(N^{-3})$ term arises in an indirect way; cf. §4.7.5.3 and 4.7.5.4. □

4.4.4 Optimal approximation parameters

In Chapter 3 we discussed the optimization of mesh parameters for P1-FEM and P2-FEM. We now perform a similar analysis for the setting of the present work, including the BEM approximation of the elastic far-field.

Recall that K is the radius of atomistic region $\Omega^{\rm a}$ and N is the radius of Ω_h. To simplify the discussion we assume that the FE mesh grading is linear, $|h(x)| \approx |x|/K$, which unsures quasi-optimal computational cost, up to logarithmic terms. In this setting it is easy to see that the various error contributions in (4.4.6) are bounded by

$$\begin{aligned}
\text{Modelling error:} \quad & \|\nabla^2 \tilde{u}^{\rm a}\|_{L^2(\Omega^{\rm i})} + \|\nabla^3 \tilde{u}^{\rm a}\|_{L^2(\mathbb{R}^2\setminus\Omega^{\rm a})} + \|\nabla^2 \tilde{u}^{\rm a}\|^2_{L^4(\mathbb{R}^2\setminus\Omega^{\rm a})} \lesssim K^{-5/2}, \\
\text{FEM error:} \quad & \|h\nabla^2 \tilde{u}^{\rm a}\|_{L^2(\Omega_h^{\rm c})} \lesssim K^{-2}\Big(1 - (K/N)^2\Big)^{1/2}, \\
\text{BEM error:} \quad & \|h^{3/2}\nabla^2 \tilde{u}^{\rm a}\|_{L^2(\Gamma_h)} \lesssim K^{-3/2}N^{-1}, \qquad \text{and} \\
\text{Linearisation error:} \quad & N^{-3}.
\end{aligned}$$

The key observation is that the modelling error, which cannot be reduced by choice of N or h is $O(K^{-5/2})$. By choosing $N \leq K + C$ for some fixed constant, both the FEM and the BEM errors also become $O(K^{-5/2})$, whereas for $N \gg K$, we obtain that the FEM error contribution becomes $O(K^{-2})$ which is strictly larger.

This quasi-optimal balance of approximation parameters means that we ought to remove the nonlinear elasticity region and directly couple the atomistic model to the BEM. The resulting error estimate is

$$\|\tilde{u}^{\rm a} - u_h\|_E \lesssim K^{-5/2}, \tag{4.4.7}$$

which is the best possible rate that can be achieved for a sharp-interface coupling method.

We remark, however, that the interface region (and therefore a thin layer of Cauchy–Born elasticity) cannot be removed entirely since the BEM must be coupled to a local elasticity model (FEM) rather than directly to the atomistic model. Coupling directly to the atomistic model would lead to a new consistency error usually dubbed "ghost forces".

4.5 Conclusion

In this work we have explored the natural combination of atomistic, finite element and boundary element modelling from the perspective of error analysis. The conclusion is an interesting, albeit not entirely unexpected, one. The rapid decay of elastic fields in the point defect case $|\nabla^j \tilde{u}(x)| \lesssim |x|^{-1-j}$ means that the continuum model error $|\nabla^3 \tilde{u}|$ and and linearisation error $|\nabla \tilde{u}|^2$ are balanced. It is therefore reasonble to entirely bypass the nonlinear elasticity model and couple the atomistic region directly to a linearised elasticity model. This observation, as well as additional complexities due to finite element and boundary element discretisation errors are made precise in Theorem 4.4.5 and in the

discussion in § 4.4.4.

Because the characteristic decay of elastic fields is different for different material defects (or other materials modelling situations) our conclusion cannot immediately applied to other contexts. However in those sitations our analysis can still provide guidance on how to generalise our results and optimally balance approximation errors due to continuum approximations, linearisation, finite element and boundary element approximations.

4.6 Proofs: Reduction to consistency

Assuming the existence of an atomistic solution $u^{\rm a}$ to (4.2.2), we seek to prove the existence of $u_h^{\rm ac} \in \mathcal{U}_h^*$ satisfying

$$\langle \delta \mathcal{E}_h^{\rm tot}(u_h^{\rm ac}), \varphi_h \rangle = \langle \delta f(u_h), \varphi_h \rangle, \quad \text{for all } \varphi_h \in \mathcal{U}_h^*, \tag{4.6.1}$$

and to estimate the error $\|u^{\rm a} - u_h^{\rm ac}\|_E$.

The error analysis consists of a best-approximation analysis (§ 4.6.1), consistency and stability estimates (§ **??**). Once these are established we apply a formulation of the inverse function theorem (§ 4.6.2) to obtain the existence of a solution $u_h^{\rm ac}$ and the error estimate.

4.6.1 The best approximation operator

We define a quasi-best approximation map $\Pi_h : C(\mathbb{R}^2;\mathbb{R}^m) \to \mathcal{U}_h$ to be the nodal interpolation operator, i.e., for $f \in C(\mathbb{R}^2;\mathbb{R}^m)$, $\Pi_h(f)|_T \in \mathbb{P}^1(T)$ for $T \subset \mathcal{T}_h$ and

$$\Pi_h(f)(x) = f(x) - f_0 \qquad \text{for all } x \in \mathcal{N}_h,$$

where f_0 is a constant such that $f(x) - f_0 \in H_*^{1/2}(\Gamma_h)$ for $x \in \Gamma_h$. Then it is clear that $\Pi_h u^{\rm a} \in \mathcal{U}_h^*$.

4.6.2 Inverse Function Theorem

The proof of this theorem is standard and can be found in various references, e.g. [46, Lemma 2.2].

Theorem 4.6.1 (The inverse function theorem). *Let $\mathcal{U}_h$ be a subspace of $\mathcal{U}$, equipped with $\|\nabla \cdot\|_{L^2}$, and let $\mathcal{G}_h \in C^1(\mathcal{U}_h, \mathcal{U}_h^*)$ with Lipschitz-continuous derivative $\delta\mathcal{G}_h$:*

$$\|\delta\mathcal{G}_h(u_h) - \delta\mathcal{G}_h(v_h)\|_{\mathcal{L}} \le M \|\nabla u_h - \nabla v_h\|_{L^2} \quad \textit{for all } u_h, v_h \in \mathcal{U}_h,$$

where $\|\cdot\|_{\mathcal{L}}$ denotes the $\mathcal{L}(\mathcal{U}_h, \mathcal{U}_h^*)$-operator norm.

Let $\bar{u}_h \in \mathcal{U}_h$ satisfy

$$\|\mathcal{G}_h(\bar{u}_h)\|_{\mathcal{U}_h^*} \leq \eta, \tag{4.6.2}$$

$$\langle \delta\mathcal{G}_h(\bar{u}_h)v_h, v_h\rangle \geq \gamma\|\nabla v_h\|_{L^2}^2 \quad \textit{for all } v_h \in \mathcal{U}_h, \tag{4.6.3}$$

such that M, η, γ satisfy the relation

$$\frac{2M\eta}{\gamma^2} < 1.$$

Then there exists a (locally unique) $u_h \in \mathcal{U}_h$ such that $\mathcal{G}_h(u_h) = 0$,

$$\|\nabla u_h - \nabla \bar{u}_h\|_{L^2} \leq 2\frac{\eta}{\gamma}, \quad \textit{and}$$
$$\langle \delta\mathcal{G}_h(u_h)v_h, v_h\rangle \geq \left(1 - \frac{2M\eta}{\gamma^2}\right)\gamma\|\nabla v_h\|_{L^2}^2 \quad \textit{for all } v_h \in \mathcal{U}_h.$$

To put Theorem 4.6.1 (Inverse Function Theorem) into our context, let

$$\mathcal{G}_h(v) := \delta\mathcal{E}_h^{\mathrm{tot}}(v) - \delta f(v) \quad \text{and} \quad \bar{u}_h := \Pi_h u^{\mathrm{a}},$$

where u^{a} is a solution to (4.2.2).

To make (4.6.2) and (4.6.3) concrete we will show that there exist $\eta, \gamma > 0$ such that, for all $\varphi_h \in \mathcal{U}_h^*$,

$$\langle \delta\mathcal{E}^{\mathrm{tot}}(\Pi_h u^{\mathrm{a}}), \varphi_h\rangle - \langle \delta f(\Pi_h u^{\mathrm{a}}), \varphi_h\rangle \leq \eta\|\varphi_h\|_E, \quad (\textit{consistency})$$
$$\langle \delta^2\mathcal{E}^{\mathrm{tot}}(\Pi_h u^{\mathrm{a}})\varphi_h, \varphi_h\rangle - \langle \delta^2 f(\Pi_h u^{\mathrm{a}})\varphi_h, \varphi_h\rangle \geq \gamma\|\varphi_h\|_E^2. \quad (\textit{stability})$$

Formally the inverse function theorem implies that, if η/γ is sufficiently small, then there exists $u_h^{\mathrm{ac}} \in \mathcal{U}_h^*$ such that

$$\langle \delta\mathcal{E}^{\mathrm{tot}}(u_h^{\mathrm{ac}}), \varphi_h\rangle - \langle \delta f(u_h^{\mathrm{ac}}), \varphi_h\rangle = 0, \quad \forall \varphi_h \in \mathcal{U}_h^*, \quad \text{and}$$
$$\|u_h^{\mathrm{ac}} - \Pi_h u^{\mathrm{a}}\|_E \leq 2\frac{\eta}{\gamma}.$$

Finally adding the best approximation error $\|\Pi_h u^{\mathrm{a}} - u^{\mathrm{a}}\|_{H_*}$ gives the error estimate

$$\|u_h^{\mathrm{ac}} - u^{\mathrm{a}}\|_E \leq \|\Pi_h u^{\mathrm{a}} - u^{\mathrm{a}}\|_E + 2\frac{\eta}{\gamma}.$$

We can now obtain the following Lipschitz continuity and stability results from the bounds (4.2.3) and (4.2.4).

Lemma 4.6.2. *There exists $M > 0$ such that*

$$\|\delta\mathcal{G}_h(u_h) - \delta\mathcal{G}_h(v_h)\|_{\mathcal{L}} \leq M\|u_h - v_h\|_E \quad \textit{for all } u_h, v_h \in \mathcal{U}_h^*, \tag{4.6.4}$$

where $\|\cdot\|_{\mathcal{L}}$ *denotes the operator norm associated with* $\|\cdot\|_E$.

4.7 Proofs: Consistency

4.7.1 Interpolants

In this section we introduce two interpolants that are necessary tools for our analysis.

4.7.1.1 Test function v

The consistency error $\delta\mathcal{E}_h^{\mathrm{tot}}(\Pi_h u^{\mathrm{a}})$ will be bounded by estimating

$$\langle \delta\mathcal{E}_h^{\mathrm{tot}}(\Pi_h u^{\mathrm{a}}), v_h\rangle - \langle \delta\mathcal{E}^{\mathrm{tot}}(u^{\mathrm{a}}), v\rangle \leq \eta_h \|v_h\|_E \qquad \forall v_h \in \mathcal{U}_h^*,$$

with $v \in \dot{\mathcal{U}}^{1,2}$ is constructed based on v_h. The purpose of this section is to construct such $v = \Pi_h^* v_h$, where $\Pi_h^* : \mathcal{U}_h^* \to \dot{\mathcal{U}}^{1,2}$.

Given some $v_h \in \mathcal{U}_h^*$ the first step is to extend v_h to $\mathbb{R}^2$. Let v_h^E be the solution to the exterior Dirichlet problem

$$\begin{aligned} -\Delta v_h^E &= 0, \quad \text{in } \Omega_h^{\mathfrak{C}}, \\ v_h^E &= v_h, \quad \text{on } \partial\Omega_h, \\ v_h^E &= v_h, \quad \text{in } \Omega_h, \\ |v_h^E(x)| &= \mathcal{O}\left(\frac{1}{|x|}\right) \quad \text{as } |x| \to \infty, \end{aligned} \tag{4.7.1}$$

where we note that the last condition can be imposed because $v_h \in \mathcal{U}_h^*$.

Next, we adapt the quasi-interpolation operator introduced in [5] to "project" v_h^E to $\dot{\mathcal{U}}^{1,2}$. Let ϕ_ℓ be the piecewise linear hat-functions on the atomistic triangulation $\mathcal{T}$, i.e., the canonical triangulation associated with Λ. Define

$$\phi_\ell^{\mathrm{PU}} := \frac{\phi_\ell}{\sum_{k\in\mathcal{C}} \phi_k} \qquad \forall \ell \in \mathcal{C},$$

where $\mathcal{C}$ is the continuum lattice sites as defined in Section 4.2.2. It is clear that $\{\phi_\ell^{\mathrm{PU}}\}_{\ell\in\mathcal{C}}$ is a partition of unity of $\mathbb{R}^2 \setminus (\Omega^{\mathrm{a}} \cup \Omega^{\mathrm{i}})$.

In order to estimate the interpolation error and modelling error in (4.7.10), we need $v - v_h^E$ to vanish in $\Omega^{\mathrm{a}} \cup \Omega^{\mathrm{i}}$ and on Γ_h. This is made possible due to assumption **(B3)**.

Now we refer to [5] for the contruction of a linear interpolant of $v_h^E \in \mathcal{U}_h$. We shall define the interpolant as follows:

$$\Pi_h^* v_h(x) := v(x) := v_1(x) + v_2(x), \quad \forall x \in \mathbb{R}^2, \tag{4.7.2}$$

where

$$v_1(\ell) := \begin{cases} v_h(\ell), & \ell \in \mathcal{A} \cup \mathcal{I} \cup \mathcal{I}^+ \cup (\Gamma_h \cap \mathcal{C}), \\ \frac{\int_{\mathbb{R}^2} \phi_\ell v_h^E}{\int_{\mathbb{R}^2} \phi_\ell}, & \ell \in \mathcal{C} \setminus (\mathcal{I}^+ \cup \Gamma_h), \end{cases}$$

$$v_1(x) := \sum_{\ell \in \Lambda} v_1(\ell)\phi_\ell(x), \quad \forall x \in \mathbb{R}^2,$$

$$v_2(\ell) := \begin{cases} \frac{\int_{\mathbb{R}^2} (v_h^E - v_1)\phi_\ell^{\mathrm{PU}}}{\int_{\mathbb{R}^2} \phi_\ell}, & \ell \in \mathcal{C} \setminus (\mathcal{I}^+ \cup \Gamma_h), \\ 0, & \ell \in \mathcal{A} \cup \mathcal{I} \cup \mathcal{I}^+ \cup (\Gamma_h \cap \mathcal{C}), \end{cases}$$

$$v_2(x) := \sum_{\ell \in \Lambda} v_2(\ell)\phi_\ell(x), \quad \forall x \in \mathbb{R}^2.$$

Note that with the assumption **(B3)**, we have

$$v(x) - v_h(x) = 0, \quad \forall x \in \Gamma_h.$$

We can use [5, Theorem 3.1] to conclude that

$$\|\nabla v\|_{L^2(\mathbb{R}^2)} \lesssim \|\nabla v_h^E\|_{L^2(\mathbb{R}^2)}, \quad \forall v_h \in \mathcal{U}_h.$$

Furthermore, since v_h^E is the extension of v_h via the exterior Laplace problem (4.7.1), we can link its energy norm to boundary norm of v_h. By the regularity of g^{-1} in Lemma 4.3.11 we have

$$\|\nabla v_h^E\|^2_{L^2(\Omega_h^{\mathfrak{C}})} = \langle g^{-1} v_h, v_h \rangle \lesssim \|v_h\|^2_{H^{1/2}_{\Gamma_h}}. \tag{4.7.3}$$

Therefore we have

$$\|\nabla v\|_{L^2(\mathbb{R}^2)} \lesssim \|\nabla v_h\|_{L^2(\Omega_h)} + \|\nabla v_h^E\|_{L^2(\Omega_h^{\mathfrak{C}})} \lesssim \|\nabla v_h\|_{L^2(\Omega_h)} + \|v_h\|_{H^{1/2}_{\Gamma_h}} \lesssim \|v_h\|_E. \tag{4.7.4}$$

4.7.1.2 Linearized elasticity approximation w

Recall that $u^{\mathrm{a}} \in \dot{\mathcal{U}}^{1,2}$ is the exact atomistic solution, and Lemma 4.3.1 shows that there exists a $C^{2,1}$-regular interpolant $\tilde{u}^{\mathrm{a}}$ of u^{a}.

In order to make use of existing BEM approximation error estimates (4.3.16), we need the conormal derivative in $H^1(\Gamma_h)$ of a solution to Laplace's equation ($\tilde{u}^{\mathrm{a}}$ only solves Laplace's equation approximately). To that end, we introduce an intermediate problem on a domain with smooth boundary inside Ω_h. Let $\mathcal{B}_R \subset \Omega_h$ be a ball with radius $R = \frac{2}{3}N$. To ensure the appropriate Dirichlet boundary condition, we use (4.2.19) to define the following function: let u_0^{a} be a constant such that

$$u_R^{\mathrm{a}} := \tilde{u}^{\mathrm{a}} - u_0^{\mathrm{a}} \quad \text{and } u_R^{\mathrm{a}}|_{\partial\mathcal{B}_R} \in H^{1/2}_*(\partial\mathcal{B}_R).$$

Let w be the solution to the exterior Dirichlet problem

$$\begin{aligned} -\Delta w &= 0, \quad \text{in } \mathcal{B}_R^{\complement}, \\ w &= u_R^{\mathrm{a}}, \quad \text{on } \partial\mathcal{B}_R, \\ |w(x)| &= \mathcal{O}\left(\frac{1}{|x|}\right) \quad \text{as } |x| \to \infty. \end{aligned} \tag{4.7.5}$$

Lemma 4.7.1. *The Dirichlet problem* (4.7.5) *has a unique solution and*

$$\|\nabla w - \nabla \tilde{u}^{\mathrm{a}}\|_{L^2(\mathcal{B}_R^{\complement})} \lesssim R^{-3}. \tag{4.7.6}$$

Proof. From Section 4.3.1 we know that this exterior Dirichlet problem has a unique solution. To estimate (4.7.6), we let $\phi := \tilde{u}^{\mathrm{a}} - w$, extended by zero to $\mathcal{B}_R$ then

$$\begin{aligned} \|\nabla\phi\|^2_{L^2(\mathcal{B}_R^{\complement})} &= \int_{\mathcal{B}_R^{\complement}} (\nabla\tilde{u}^{\mathrm{a}} - \nabla w)\cdot\nabla\phi \\ &= \int_{\mathbb{R}^2} \nabla\tilde{u}^{\mathrm{a}}\cdot\nabla\phi =: B \end{aligned}$$

Next, we use the fact that B is a linearised continuum approximation to the atomistic equilibrium equations. Recalling that u^{a} is an atomistic solution, i.e.,

$$\langle \delta\mathcal{E}^{\mathrm{a}}(u^{\mathrm{a}}), \phi\rangle = 0 \qquad \forall \phi \in \dot{\mathcal{U}}^{1,2},$$

and that $\partial_{\mathsf{F}}^2 W(0) = \mu I$, we can split B into

$$\begin{aligned} B &= \int_{\mathbb{R}^2} \nabla\tilde{u}^{\mathrm{a}}\cdot\nabla\phi - \mu^{-1}\langle\delta\mathcal{E}^{\mathrm{a}}(u^{\mathrm{a}}),\phi\rangle \\ &= \left(\int_{\mathbb{R}^2} \nabla\tilde{u}^{\mathrm{a}}\cdot\nabla\phi - \mu^{-1}\int_{\mathbb{R}^2}\partial_{\mathsf{F}}W(\nabla\tilde{u}^{\mathrm{a}})\cdot\nabla\phi\right) \\ &\quad + \mu^{-1}\left(\int_{\mathbb{R}^2}\partial_{\mathsf{F}}W(\nabla\tilde{u}^{\mathrm{a}})\cdot\nabla\phi - \langle\delta\mathcal{E}^{\mathrm{a}}(u^{\mathrm{a}}),\phi\rangle\right) \\ &=: B_1 + B_2. \end{aligned}$$

For B_1, we apply Taylor's expansion and use $\partial_{\mathsf{F}}^2 W(0) = \mu I$ to obtain

$$\begin{aligned} |B_1| \leq& \left|\int_{\mathbb{R}^2}\left(\nabla\tilde{u}^{\mathrm{a}} - \mu^{-1}\partial_F W(0) - \mu^{-1}\partial_F^2 W(0)\nabla\tilde{u}^{\mathrm{a}}\right)\cdot\nabla\phi\right| + C\int_{\mathbb{R}^2}|D\tilde{u}^{\mathrm{a}}|^2\,|\nabla\phi| \\ =& C\int_{\mathbb{R}^2}|\nabla\tilde{u}^{\mathrm{a}}|^2\,|\nabla\phi| \leq C\|\nabla\tilde{u}^{\mathrm{a}}\|^2_{L^4(\mathcal{B}_R^{\complement})}\|\nabla\phi\|_{L^2} \leq CR^{-3}\|\nabla\phi\|_{L^2}, \end{aligned}$$

where the constant C is independent of $\tilde{u}^{\mathrm{a}}$ and ϕ.

B_2 is the Cauchy–Born modelling error which is well understood, e.g., in [44] it is proven that

$$B_2 \leq \int_{\mathbb{R}^2}(C_1|\nabla^3\tilde{u}^{\mathrm{a}}| + C_2|\nabla^2\tilde{u}^{\mathrm{a}}|^2)|\nabla\phi|.$$

Hence we obtain

$$\begin{aligned} B_2 &\leq \left(\|\nabla^3 \tilde{u}^{\mathrm{a}}\|_{L^2(\mathcal{B}_R^{\complement})} + \|\nabla^2 \tilde{u}^{\mathrm{a}}\|^2_{L^4(\mathcal{B}_R^{\complement})} \right) \|\nabla \phi\|_{L^2} \\ &\leq \left(R^{-3} + R^{-5} \right) \|\nabla \phi\|_{L^2}. \end{aligned}$$

Combining the estimates for B_1 and B_2 yields the stated result. □

The second estimate we require for w is for the decay of $\nabla^2 w$.

Lemma 4.7.2. *Let w be given by (4.7.5), and $R \leq \frac{2}{3}N$, where N is the inner radius of Ω_h, then*

$$|\nabla^2 w(x)| \lesssim |x|^{-3} \qquad \text{for } |x| \geq N \tag{4.7.7}$$

and in particular,

$$\|\nabla^2 w\|_{L^2(\Omega_h^{\complement})} \lesssim N^{-5/2} \tag{4.7.8}$$

Proof. Since the auxiliary problem (4.7.5) involves a circular boundary $\partial\Omega_R^{\complement}$, we can exploit separation of variables and Fourier series to estimate $\nabla^2 w$. We write $\tilde{u}^{\mathrm{a}}$ and w in polar coordinates as

$$\begin{aligned} \tilde{u}^{\mathrm{a}}(r,\theta) &= \sum_{k\in\mathbb{Z}} \hat{a}_k(r) e^{ik\cdot\theta}, \\ w(r,\theta) &= \sum_{k\in\mathbb{Z}} \hat{W}_k(r) e^{ik\cdot\theta}. \end{aligned} \tag{4.7.9}$$

The boundary condition $w = \tilde{u}^{\mathrm{a}}$ on $\partial\mathcal{B}_R$ becomes

$$w(R,\theta) = \tilde{u}^{\mathrm{a}}(R,\theta), \quad \text{i.e.,} \qquad \hat{W}_k(R) = \hat{a}_k(R).$$

The Laplace operator in polar coordinates in 2D is given by

$$-\Delta_{x,y} = -r^{-1}\partial_r(r^{-1}\partial_r) - r^{-2}\partial_\theta^2.$$

Substituting (4.7.9) we obtain

$$\sum_{k\in\mathbb{Z}} \partial_r^2 \hat{W}_k + r^{-1}\partial_r \hat{W}_k - k^2 r^{-2} \hat{W}_k = 0.$$

Solving the resulting ODE for each $\hat{W}_k$ and taking into account the decay and boundary condition from (4.7.5), we deduce that

$$w(r,\theta) = \sum_{k\in\mathbb{Z}} \hat{a}_k(R) \left(\frac{r}{R}\right)^{-|k|} e^{ik\cdot\theta}.$$

Using the fact that, for $p \in \mathbb{N}$ and $q \geq 1 + \epsilon$,

$$\sum_{k \in \mathbb{Z}} |k|^p q^{-2|k|} \leq C_{p,\epsilon} q^2.$$

We can now estimate

$$\begin{aligned}
\left|\nabla_r^2 w(r,\theta)\right| &= \left| r^{-2} \sum_{k \in \mathbb{Z}} |k|(|k|+1)\hat{a}_k(R) \left(\frac{r}{R}\right)^{-|k|} e^{ik\cdot\theta} \right| \\
&\leq r^{-2} \left(\sum_{k \in \mathbb{Z}} |\hat{a}_k(R)|^2 \right)^{1/2} \left(\sum_{k \in \mathbb{Z}} |k|^4 \left(\frac{r}{R}\right)^{-2|k|} \right)^{1/2} \\
&\lesssim r^{-2} (r/R)^2 \left(\frac{1}{R} \int_{\partial \mathcal{B}_R} |\tilde{u}^{\mathrm{a}}|^2 \right)^{1/2},
\end{aligned}$$

where in the last line we also used Plancherel's Theorem. Using the fact that $|\tilde{u}^{\mathrm{a}}(x)| \lesssim |x|^{-1}$ we finally obtain

$$\left|\nabla_r^2 w(r,\theta)\right| \lesssim (r/R)^{-3}.$$

Analogous arguments for $\nabla_\theta^2 w$ and $\nabla_r \nabla_\theta w$ yield

$$\left|\nabla^2 w(r,\theta)\right| \lesssim (r/R)^{-3}.$$

The first result (4.7.7) follows from the assumption that $R \leq \frac{2}{3}N$. The second result (4.7.8) is an immediate consequence of (4.7.7). □

4.7.2 Consistency decomposition

Given a solution u^{a} to (4.2.2) and a discrete test function v_h, let $\Pi_h u^{\mathrm{a}}$ be as defined in § 4.6.1, let $v = \Pi_h^* v_h$ be defined by (4.7.2), and let w be given by (4.7.5). Moreover, let

$$\tilde{u}_h^{\mathrm{a}} := \tilde{u}^{\mathrm{a}} - c_h \quad \text{such that} \quad \tilde{u}_h^{\mathrm{a}}|_{\Gamma_h} \in H_*^{1/2}(\Gamma_h),$$

then we decompose the consistency error into

$$\begin{aligned}
\langle \delta\mathcal{E}_h^{\mathrm{tot}}(\Pi_h u^{\mathrm{a}}), v_h \rangle &= \langle \delta\mathcal{E}_h^{\mathrm{tot}}(\Pi_h u^{\mathrm{a}}), v_h \rangle - \langle \delta\mathcal{E}^{\mathrm{a}}(u^{\mathrm{a}}), v \rangle \\
&= \langle \delta\mathcal{E}_h^{\mathrm{ac}}(\Pi_h u^{\mathrm{a}}), v_h \rangle + \mu \langle g_h^{-1} \Pi_h u^{\mathrm{a}}, v_h \rangle_{\Gamma_h} - \langle \delta\mathcal{E}^{\mathrm{a}}(u^{\mathrm{a}}), v \rangle \\
&= \underbrace{\langle \delta\mathcal{E}_h^{\mathrm{ac}}(\Pi_h u^{\mathrm{a}}), v_h \rangle - \langle \delta\mathcal{E}_h^{\mathrm{ac}}(\tilde{u}^{\mathrm{a}}), v \rangle}_{\text{interpolation error}} \\
&\quad + \underbrace{\langle \delta\mathcal{E}^{\mathrm{ac}}(\tilde{u}^{\mathrm{a}}) - \delta\mathcal{E}^{\mathrm{a}}(u^{\mathrm{a}}), v \rangle - \int_{\Omega_h^{\mathfrak{C}}} (\partial W(\nabla \tilde{u}^{\mathrm{a}}) - \mu \nabla \tilde{u}^{\mathrm{a}}) \cdot \nabla v}_{\text{modelling error}} \\
&\quad + \underbrace{\mu \langle g_h^{-1} \Pi_h u^{\mathrm{a}}, v_h \rangle_{\Gamma_h} - \mu \int_{\Omega_h^{\mathfrak{C}}} \nabla \tilde{u}^{\mathrm{a}} \cdot \nabla v}_{\text{BEM error}}.
\end{aligned} \tag{4.7.10}$$

4.7.3 The interpolation error

The first part of the consistency error, the interpolation error, has already been estimated in [12].

Lemma 4.7.3. *The interpolation error can be estimated by, for any $v_h \in \mathcal{U}_h^*$ and v constructed as* (4.7.2)*,*

$$\begin{aligned}&\langle \delta\mathcal{E}_h^{\mathrm{ac}}(\Pi_h u^{\mathrm{a}}), v_h\rangle - \langle \delta\mathcal{E}_h^{\mathrm{ac}}(\tilde{u}^{\mathrm{a}}), v\rangle \\ &\quad \le c(M_2\|h\nabla^2\tilde{u}^{\mathrm{a}}\|_{L^2(\Omega_h\setminus\Omega^{\mathrm{a}})} + M_2\|\nabla^3\tilde{u}^{\mathrm{a}}\|_{L^2(\mathbb{R}^2\setminus\Omega^{\mathrm{a}})} + M_3\|\nabla^2\tilde{u}^{\mathrm{a}}\|^2_{L^4(\mathbb{R}^2\setminus\Omega^{\mathrm{a}})})\|\nabla v_h\|_{L^2}.\end{aligned} \tag{4.7.11}$$

Proof. We split the interpolation error into

$$\langle \delta\mathcal{E}_h^{\mathrm{ac}}(\Pi_h u^{\mathrm{a}}), v_h\rangle - \langle \delta\mathcal{E}_h^{\mathrm{ac}}(\tilde{u}^{\mathrm{a}}), v\rangle = \langle \delta\mathcal{E}_h^{\mathrm{ac}}(\Pi_h u^{\mathrm{a}}) - \delta\mathcal{E}_h^{\mathrm{ac}}(\tilde{u}^{\mathrm{a}}), v_h\rangle - \langle \delta\mathcal{E}_h^{\mathrm{ac}}(\tilde{u}^{\mathrm{a}}), v - v_h\rangle.$$

The first term can be bounded by a standard interpolation error estimate and the uniform boundedness of $\delta^2\mathcal{E}_h^{\mathrm{ac}}$,

$$\begin{aligned}\langle \delta\mathcal{E}_h^{\mathrm{ac}}(\Pi_h u^{\mathrm{a}}) - \delta\mathcal{E}_h^{\mathrm{ac}}(\tilde{u}^{\mathrm{a}}), v_h\rangle &\le \langle \delta^2\mathcal{E}_h^{\mathrm{ac}}(\theta)(\nabla\Pi_h u^{\mathrm{a}} - \nabla\tilde{u}^{\mathrm{a}}), v_h\rangle \\ &\le cM_2\|h\nabla^2\tilde{u}^{\mathrm{a}}\|_{L^2(\Omega_h^{\mathrm{c}})}\|\nabla v_h\|_{L^2(\Omega_h^{\mathrm{c}})}\end{aligned}$$

The bound for the second term follows from the exactly same argument as in the proof of [12, Theorem 3.2]. Since the interpolant v defined in (4.7.2) has property

$$v(x) - v_h(x) = 0, \quad \forall x \in \Gamma_h \cup \Omega^{\mathrm{a}} \cup \Omega^{\mathrm{i}}$$

we can integrate by part in Ω_h^{c} without obtaining boundary contributions. Let $Q := -\mathrm{div}\,[\partial_{\mathsf{F}} W(\nabla\tilde{u}^{\mathrm{a}})]$, then

$$\langle \delta\mathcal{E}_h^{\mathrm{ac}}(\tilde{u}^{\mathrm{a}}), v - v_h\rangle = \int_{\Omega_h^{\mathrm{c}}} Q\cdot(v_h - v)\,\mathrm{d}x = \int_{\Omega_h^{\mathrm{c}}} Q\cdot((v_h - v_1) - v_2)\,\mathrm{d}x.$$

Since v_2 is a piecewise-linear quasi-interpolant of $v_h - v_1$ as defined in [5], a direct consequence of Theorem 3.1 in [5] is that there exists $C > 0$ such that,

$$\langle \delta\mathcal{E}_h^{\mathrm{ac}}(\Pi_h u^{\mathrm{a}}) - \delta\mathcal{E}_h^{\mathrm{ac}}(\tilde{u}^{\mathrm{a}}), v_h\rangle \le C\|\nabla(v_h - v_1)\|_{L^2(\Omega_h^{\mathrm{c}})}\left(\sum_{\ell\in\mathcal{C}\cap\Omega_h^{\mathrm{c}}} d_\ell^2\int_{w_\ell}\phi_\ell^{\mathrm{PU}}|Q - \langle Q\rangle_\ell|^2\,\mathrm{d}x\right)^{1/2},$$

where $w_\ell := \mathrm{supp}(\phi_\ell)$, $\langle Q\rangle_\ell := 1/|w_\ell|\int_{w_\ell} Q(x)\,\mathrm{d}x$ and $d_\ell := \mathrm{diam}(w_\ell) = 1$. With the sharp Poincaré constant derived in [1], we obtain

$$\int_{w_\ell}\phi_\ell^{\mathrm{PU}}|Q - \langle Q\rangle_\ell|^2\,\mathrm{d}x \le \int_{w_\ell}|Q - \langle Q\rangle_\ell|^2\,\mathrm{d}x \le \tfrac{1}{4}d_\ell^2\|\nabla Q\|^2_{L^2(w_\ell)}.$$

On the other hand, v_1 is a standard quasi-interpolant of v_h in $\bigcup \mathcal{T}_h^c$, which implies that there exists $C' > 0$ such that

$$\|\nabla(v_h - v_1)\|_{L^2(\Omega_h^c)} \leq C' \|\nabla v_h\|_{L^2(\Omega_h^c)}.$$

Due to the fact that $d_\ell = 1$ and that each point in $\mathbb{R}^2 \setminus \Omega^a$ is covered by at most three w_ℓ, we have

$$\begin{aligned}
&\langle \delta\mathcal{E}_h^{ac}(\Pi_h u^a) - \delta\mathcal{E}_h^{ac}(\tilde{u}^a), v_h \rangle \\
\leq & C \max_\ell d_\ell^2 \|\nabla Q\|_{L^2(\Omega_h^c)} \|\nabla v_h\|_{L^2(\Omega_h^c)} \\
\leq & C \left(M_2 \|\nabla^3 \tilde{u}^a\|_{L^2(\Omega_h^c)} + M_3 \|\nabla^2 \tilde{u}^a\|_{L^4(\Omega_h^c)}^2 \right) \|\nabla v_h\|_{L^2(\Omega_h^c)},
\end{aligned}$$

where we used the following estimate, for some $c > 0$,

$$\begin{aligned}
\|\nabla Q\|_{L^2(\Omega_h)} &= \|\nabla \mathrm{div}[\partial_{\mathsf{F}} W(\nabla \tilde{u}^a)]\|_{L^2(\Omega_h^c)} \\
&= \|\nabla \left(\partial_{\mathsf{F}}^2 W(\nabla \tilde{u}^a) \nabla^2 \tilde{u}^a \right) \|_{L^2(\Omega_h^c)} \\
&= \left\| \partial_{\mathsf{F}}^2 W(\nabla \tilde{u}^a) \nabla^3 \tilde{u}^a + \partial_{\mathsf{F}}^3 W(\nabla \tilde{u}^a) \left(\nabla^2 \tilde{u}^a \right)^2 \right\|_{L^2(\Omega_h^c)} \\
&\leq c \left(M_2 \|\nabla^3 \tilde{u}^a\|_{L^2(\Omega_h^c)} + M_3 \|\nabla^2 \tilde{u}^a\|_{L^4(\Omega_h^c)}^2 \right),
\end{aligned}$$

employing the global bounds (4.2.3) and (4.2.4). □

4.7.4 The modelling error

Similar to §3.5.5, we rely on the following theorem from [44] of the pure modelling error estimate of G23 coupling method.

Theorem 4.7.4 (G23 modeling error). *For any $v \in \dot{\mathcal{U}}^{1,2}$ we have the G23 consistency error estimate*

$$\begin{aligned}
&\langle \delta\mathcal{E}^{ac}(u^a), v \rangle - \langle \delta\mathcal{E}^a(u^a), v \rangle \\
&\quad \leq c \left(M_2 \|\nabla^2 \tilde{u}^a\|_{L^2(\Omega^i)} + M_2 \|\nabla^3 \tilde{u}^a\|_{L^2(\Omega^c)} + M_3 \|\nabla^2 \tilde{u}^a\|_{L^4(\Omega^c)}^2 \right) \|\nabla v\|_{L^2(\mathbb{R}^2)}
\end{aligned} \tag{4.7.12}$$

Furthermore, the second term of the modelling error can be estimated as follows.

Lemma 4.7.5. *For any $v \in \dot{\mathcal{U}}^{1,2}$ we have*

$$\int_{\Omega_h^{\mathfrak{C}}} (\partial W(\nabla \tilde{u}) - \mu \nabla \tilde{u}) \cdot \nabla v \lesssim \|\nabla \tilde{u}^a\|_{L^4(\Omega_h^{\mathfrak{C}})}^2 \|\nabla v\|_{L^2(\Omega_h^{\mathfrak{C}})}.$$

Proof. This is a direct result from applying Taylor expansion,

$$\begin{aligned}\int_{\Omega_h^{\mathfrak{C}}}(\partial W(\nabla\tilde{u})-\mu\nabla\tilde{u})\cdot\nabla v &= \int_{\Omega_h^{\mathfrak{C}}}\left[\partial W(0)+\partial^2 W(0)\nabla\tilde{u}^{\mathrm{a}}+\frac{1}{2}\partial^3 W(\theta)(\nabla\tilde{u}^{\mathrm{a}})^2\right]\nabla v\\ &\quad-\int_{\Omega_h^{\mathfrak{C}}}\mu\nabla\tilde{u}^{\mathrm{a}}\nabla v\\ &\leq \frac{M_3}{2}\int_{\Omega_h^{\mathfrak{C}}}(\nabla\tilde{u}^{\mathrm{a}})^2\nabla v\\ &\lesssim \|\nabla\tilde{u}^{\mathrm{a}}\|^2_{L^4(\Omega_h^{\mathfrak{C}})}\|\nabla v\|_{L^2(\Omega_h^{\mathfrak{C}})},\end{aligned}$$

where we use the fact that $\partial W(0)=0$ and that $\partial^2 W(0)=\mu I$. □

Therefore the modelling error can be estimated by

$$\begin{aligned}&\langle\delta\mathcal{E}^{\mathrm{ac}}(\tilde{u}^{\mathrm{a}})-\delta\mathcal{E}^{\mathrm{a}}(\tilde{u}^{\mathrm{a}}),v\rangle-\int_{\Omega_h^{\mathfrak{C}}}(\partial W(\nabla\tilde{u}^{\mathrm{a}})-\mu\nabla\tilde{u}^{\mathrm{a}})\cdot\nabla v\\ &\lesssim\left(\|\nabla^2\tilde{u}^{\mathrm{a}}\|_{L^2(\Omega^{\mathrm{i}})}+\|\nabla^3\tilde{u}^{\mathrm{a}}\|_{L^2(\mathbb{R}^2\setminus\Omega^{\mathrm{a}})}+\|\nabla^2\tilde{u}^{\mathrm{a}}\|^2_{L^4(\mathbb{R}^2\setminus\Omega^{\mathrm{a}})}\right)\|\nabla v\|_{\mathbb{R}^2}\\ &\lesssim\left(\|\nabla^2\tilde{u}^{\mathrm{a}}\|_{L^2(\Omega^{\mathrm{i}})}+\|\nabla^3\tilde{u}^{\mathrm{a}}\|_{L^2(\mathbb{R}^2\setminus\Omega^{\mathrm{a}})}+\|\nabla^2\tilde{u}^{\mathrm{a}}\|^2_{L^4(\mathbb{R}^2\setminus\Omega^{\mathrm{a}})}\right)\|v_h\|_E,\end{aligned}\tag{4.7.13}$$

where we used the fact that $\|\nabla v\|_{L^2(\mathbb{R}^2)}\lesssim\|v_h\|_E$ from (4.7.4).

4.7.5 The BEM error

To complete the analysis of our numerical scheme it remains to estimate the BEM error contribution to the consistency error (4.7.10). Recall that we need to estimate

$$\langle g_h^{-1}\Pi_h u^{\mathrm{a}},v_h\rangle-\int_{\Omega_h^{\mathfrak{C}}}\nabla\tilde{u}^{\mathrm{a}}\cdot\nabla v,$$

where v is the interpolant defined in Section 4.7.1.1. Recall that v_h^E solves the exterior Laplace problem (4.7.1). Then we have

$$\int_{\Omega_h^{\mathfrak{C}}}\nabla\tilde{u}^{\mathrm{a}}\cdot\nabla v_h^E=\langle g^{-1}\tilde{u}_h^{\mathrm{a}},v_h\rangle_{\Gamma_h}.$$

Then the BEM error can be decomposed into

$$\begin{aligned}\langle g_h^{-1}\Pi_h u^{\mathrm{a}},v_h\rangle-\int_{\Omega_h^{\mathfrak{C}}}\nabla\tilde{u}^{\mathrm{a}}\cdot\nabla v &= \langle g_h^{-1}\Pi_h u^{\mathrm{a}},v_h\rangle-\langle g^{-1}\tilde{u}_h^{\mathrm{a}},v_h\rangle+\int_{\Omega_h^{\mathfrak{C}}}\nabla\tilde{u}^{\mathrm{a}}\cdot(\nabla v_h^E-\nabla v)\\ &= \langle g_h^{-1}(\Pi_h u^{\mathrm{a}}-\tilde{u}_h^{\mathrm{a}}),v_h\rangle+\langle(g_h^{-1}-g^{-1})w,v_h\rangle\\ &\quad+\langle g^{-1}(w-\tilde{u}_h^{\mathrm{a}}),v_h\rangle+\langle g_h^{-1}(\tilde{u}_h^{\mathrm{a}}-w),v_h\rangle\\ &\quad+\int_{\Omega_h^{\mathfrak{C}}}\nabla\tilde{u}^{\mathrm{a}}\cdot(\nabla v_h^E-\nabla v)\\ &=: A_1+A_2+A_3+A_4+A_5,\end{aligned}$$

where we use the fact that $v_h = v_h^E$ on Γ_h.

We will employ stability of g_h^{-1} and g^{-1}, as stated in Theorems 4.3.3 and 4.3.4. In addition, the estimate of A_1 relies on best approximation error bounds; A_2 is the standard BEM approximation error; A_3 and A_4 require the results on the auxiliary function w that we established in § 4.7.1.2; while estimating A_5 is analogous of the proof of Lemma 4.7.3.

4.7.5.1 Estimate of A_1

In this section we first discuss the best approximation error $\|\nabla \Pi_h u^{\mathrm{a}} - \nabla \tilde{u}^{\mathrm{a}}\|_{L^2(\Gamma_h)}$. We will exploit the theorems below, which are well established in the literature.

Theorem 4.7.6 (Interpolation). *Recall that the rescaled norms $H^{1/2}_{\Gamma_h}$ and $H^1_{\Gamma_h}$ are defined in* (4.3.11) *and* (4.3.12)*, respectively. Let $u \in H^1_{\Gamma_h}$ then we have*

$$\|u\|_{H^{1/2}_{\Gamma_h}} \leq \|u\|^{1/2}_{H^1_{\Gamma_h}} \|u\|^{1/2}_{H^0_{\Gamma_h}}.$$

Proof. Let $u_1(x) := u(Rx)$ and Γ_1 be the image of mapping $\Gamma_h \ni x \mapsto \frac{x}{R}$. Then, by definitions (4.3.11) and (4.3.12), we have

$$\begin{aligned}
\|u\|_{H^{1/2}_{\Gamma_h}} &= \|u_1\|_{H^{1/2}(\Gamma_1)}, \\
\|u\|_{H^1_{\Gamma_h}} &= \|u_1\|_{H^1(\Gamma_1)}, \quad \text{and} \\
\|u\|_{H^0_{\Gamma_h}} &= \|u_1\|_{H^0(\Gamma_1)}
\end{aligned}$$

The standard interpolation theorem (see, for example, Theorem 2.18 in [51]) states that

$$\|u_1\|_{H^{1/2}(\Gamma_1)} \leq \|u_1\|^{1/2}_{H^1(\Gamma_1)} \|u_1\|^{1/2}_{H^0(\Gamma_1)}.$$

Hence the result follows. □

Theorem 4.7.7. *Recall that Π_h was defined in Section 4.6.1 as the piecewise linear nodal interpolation operator. Then we have, for $v \in H^2(\Gamma_h)$,*

$$\begin{aligned}
\|v - \Pi_h v\|_{L^2(\Gamma_h)} &\leq c \|h^2 \nabla^2 v\|_{L^2(\Gamma_h)}, \quad \textit{and} \\
\|v - \Pi_h v\|_{H^1(\Gamma_h)} &\leq c \|h \nabla^2 v\|_{L^2(\Gamma_h)}.
\end{aligned}$$

Proof. This is a direct result of the Bramble-Hilbert Lemma. It is worth noting that in fact we only need the tangential part of $\nabla^2 v$ for this estimate. □

Thus, using also $\left[\frac{1}{2}\mathrm{diam}(\Gamma_h)\right] \approx N$, we can conclude that

$$\begin{aligned}
\|\Pi_h u^{\mathrm{a}} - \tilde{u}_h^{\mathrm{a}}\|_{H^{1/2}_{\Gamma_h}} &\leq \|\Pi_h u^{\mathrm{a}} - \tilde{u}_h^{\mathrm{a}}\|^{1/2}_{H^{1}_{\Gamma_h}} \|\Pi_h u^{\mathrm{a}} - \tilde{u}_h^{\mathrm{a}}\|^{1/2}_{H^{0}_{\Gamma_h}} \\
&\lesssim \left(N\|h\nabla^2 \tilde{u}_h^{\mathrm{a}}\|^2_{L^2(\Gamma_h)} + N^{-1}\|h^2\nabla^2\tilde{u}_h^{\mathrm{a}}\|^2_{L^2(\Gamma_h)}\right)^{1/4} \\
&\quad \cdot \left(N^{-1}\|h^2\nabla^2\tilde{u}_h^{\mathrm{a}}\|^2_{L^2(\Gamma_h)}\right)^{1/4} \\
&\lesssim \|h\nabla^2\tilde{u}_h^{\mathrm{a}}\|^{1/2}_{L^2(\Gamma_h)}\|h^2\nabla^2\tilde{u}_h^{\mathrm{a}}\|^{1/2}_{L^2(\Gamma_h)} + N^{-2}\|h^2\nabla^2\tilde{u}_h^{\mathrm{a}}\|_{L^2(\Gamma_h)} \\
&\lesssim \|h^{3/2}\nabla^2\tilde{u}_h^{\mathrm{a}}\|_{L^2(\Gamma_h)},
\end{aligned} \tag{4.7.14}$$

where, in the last line, we used the fact that $N^{-2}h \lesssim 1$ and that h is quasi-uniform on Γ_h.

By the stability estimate (4.3.15), we have

$$\|g_h^{-1}(\Pi_h u - \tilde{u}_h^{\mathrm{a}})\|_{H^{-1/2}(\Gamma_h)} \leq c\|\Pi_h u - \tilde{u}_h^{\mathrm{a}}\|_{H^{1/2}_{\Gamma_h}}.$$

Therefore we can estimate A_1 as follows

$$A_1 \leq C\|\Pi_h u^{\mathrm{a}} - \tilde{u}_h^{\mathrm{a}}\|_{H^{1/2}_{\Gamma_h}}\|v_h\|_{H^{1/2}_{\Gamma_h}} \lesssim \|h^{3/2}\nabla^2\tilde{u}^{\mathrm{a}}\|_{L^2(\Gamma_h)}\|v_h\|_{H^{1/2}_{\Gamma_h}}. \tag{4.7.15}$$

4.7.5.2 Estimate of A_2

Since w is the solution to the Laplace equation (4.7.5) with smooth boundary $\partial\mathcal{B}_R$, its conormal derivative $g^{-1}w$ on Γ_h is in $H^1(\Gamma_h)$. Hence we can apply Theorem 4.3.12 and then Lemma 4.3.11 to estimate

$$\begin{aligned}
A_2 &\leq \|(g_h^{-1} - g^{-1})w\|_{H^{-1/2}(\Gamma_h)}\|v_h\|_{H^{1/2}_{\Gamma_h}} \\
&\leq ch^{3/2}\|\nabla(g^{-1}w)\|_{L^2(\Gamma_h)}\|v_h\|_{H^{1/2}_{\Gamma_h}} \\
&\lesssim h^{3/2}\|\nabla^2 w\|_{L^2(\Gamma_h)}\|v_h\|_{H^{1/2}_{\Gamma_h}} \\
&\lesssim h^{3/2}N^{-5/2}\|v_h\|_{H^{1/2}_{\Gamma_h}},
\end{aligned} \tag{4.7.16}$$

where the last line results from (4.7.7) and the Trace Theorem (see, for example, [2]).

4.7.5.3 Estimates of A_3 and A_4

By the stability of g^{-1}, we have

$$A_3 \leq C_2\|\tilde{u}_h^{\mathrm{a}} - w\|_{H^{1/2}_{\Gamma_h}}\|v_h\|_{H^{1/2}_{\Gamma_h}}.$$

Since g^{-1} is positive-definite and bounded by Lemma 4.3.11, we can link $\|\cdot\|_{H^{1/2}_{\Gamma_h}}$ to $\|\nabla\cdot\|_{L^2(\Omega_h^{\complement})}$ through exterior Laplace problems.

Recall that $\tilde{u}_h^{\mathrm{a}} := \tilde{u}^{\mathrm{a}} - c_h \in H^{1/2}_*(\Gamma_h)$. Then by Theorem 4.3.9 the following exterior

Laplace problem has a unique solution

$$\begin{aligned} -\Delta y &= 0, \quad \text{in } \Omega_h^{\mathfrak{C}}, \\ y &= \tilde{u}_h^{\mathrm{a}}, \quad \text{on } \Gamma_h, \\ |y(x)| &= \mathcal{O}\left(\frac{1}{|x|}\right) \quad \text{as } |x| \to \infty. \end{aligned} \tag{4.7.17}$$

Then arguing exactly as in the proof of Lemma 4.7.1, we have

$$\|\nabla y - \nabla \tilde{u}^{\mathrm{a}}\|_{L^2(\Omega_h^{\mathfrak{C}})} \lesssim N^{-3}.$$

In addition, by the positive-definiteness of g^{-1} in Lemma 4.3.11 we have

$$C_1 \|\tilde{u}_h^{\mathrm{a}} - w\|^2_{H^{1/2}_{\Gamma_h}} \leq \langle g^{-1}(\tilde{u}_h^{\mathrm{a}} - w), (\tilde{u}_h^{\mathrm{a}} - w)\rangle = \int_{\Omega_h^{\mathfrak{C}}} |\nabla y - \nabla w|^2.$$

Therefore we have

$$\begin{aligned} A_3 &\lesssim \|\tilde{u}_h^{\mathrm{a}} - w\|_{H^{1/2}_{\Gamma_h}} \|v_h\|_{H^{1/2}_{\Gamma_h}} \\ &\lesssim \left(\|\nabla y - \nabla \tilde{u}_h^{\mathrm{a}}\|_{L^2(\Omega_h^{\mathfrak{C}})} + \|\nabla w - \nabla \tilde{u}_h^{\mathrm{a}}\|_{L^2(\Omega_h^{\mathfrak{C}})}\right) \|v_h\|_{H^{1/2}_{\Gamma_h}} \\ &\lesssim \left(N^{-3} + R^{-3}\right) \|v_h\|_{H^{1/2}_{\Gamma_h}} \\ &\lesssim N^{-3} \|v_h\|_{H^{1/2}_{\Gamma_h}}. \end{aligned} \tag{4.7.18}$$

For A_4, using the stability of g_h^{-1} in (4.3.15) and the same argument as for A_4, we have

$$A_4 \lesssim N^{-3} \|v_h\|_{H^{1/2}_{\Gamma_h}}. \tag{4.7.19}$$

4.7.5.4 Estimate of A_5

Now we consider

$$A_5 = \int_{\Omega_h^{\mathfrak{C}}} \nabla \tilde{u}^{\mathrm{a}} \cdot (\nabla v_h^E - \nabla v).$$

Recall that v is the quasi-interpolant of v_h^E defined in (4.7.2). Under the assumption **(B3)** we know that

$$v_h^E(x) - v(x) = 0 \quad \forall x \in \Gamma_h.$$

So we can use analogous argument to the proof of Lemma 4.7.3 to get

$$\begin{aligned} A_5 &\lesssim \|\nabla \mathrm{div}[\nabla \tilde{u}^{\mathrm{a}}]\|_{L^2(\Omega_h^{\mathfrak{C}})} \|\nabla v_h^E\|_{L^2(\Omega_h^{\mathfrak{C}})} \\ &\lesssim \|\nabla^3 \tilde{u}^{\mathrm{a}}\|_{L^2(\Omega_h^{\mathfrak{C}})} \|\nabla v_h^E\|_{L^2(\Omega_h^{\mathfrak{C}})}. \end{aligned}$$

By (4.7.3) we have

$$\|\nabla v_h^E\|_{L^2(\Omega_h^{\mathfrak{C}})} \lesssim \|v_h\|_{H^{1/2}_{\Gamma_h}}.$$

Therefore we have

$$A_5 \lesssim \|\nabla^3 \tilde{u}^{\mathrm{a}}\|_{L^2(\Omega_h^{\mathfrak{C}})} \|v_h\|_{H^{1/2}_{\Gamma_h}} \lesssim N^{-3} \|v_h\|_{H^{1/2}_{\Gamma_h}}. \tag{4.7.20}$$

Summarising all five components of the BEM error estimates (4.7.15), (4.7.16), (4.7.18), (4.7.19) and (4.7.20) we obtain

$$\text{BEM error} \lesssim \big(N^{-3} + \|h^{3/2}\nabla^2 \tilde{u}^{\mathrm{a}}\|_{L^2(\Gamma_h)}\big) \|v_h\|_{H^{1/2}_{\Gamma_h}}. \tag{4.7.21}$$

4.7.6 Proof of Theorem 4.4.4

Finally, recalling the decomposition in (4.7.10), we add the estimates for all three components (4.7.11), (4.7.13) and (4.7.21) together to get the following estimate. We have, for any $v_h \in \mathcal{U}_h^*$

$$\begin{aligned}
&\langle \delta \mathcal{E}_h^{\mathrm{tot}}(\Pi_h u^{\mathrm{a}}), v_h \rangle \\
\lesssim &(\|\nabla^2 \tilde{u}^{\mathrm{a}}\|_{L^2(\Omega^{\mathrm{i}})} + \|\nabla^3 \tilde{u}^{\mathrm{a}}\|_{L^2(\mathbb{R}^2 \setminus \Omega^{\mathrm{a}})} + \|\nabla^2 \tilde{u}^{\mathrm{a}}\|^2_{L^4(\mathbb{R}^2 \setminus \Omega^{\mathrm{a}})}) \|v_h\|_E \\
&\quad + \|h\nabla^2 \tilde{u}^{\mathrm{a}}\|_{L^2(\Omega_h^{\mathrm{c}})} \|\nabla v_h\|_{L^2(\Omega_h^{\mathrm{c}})} + N^{-3} \|\nabla v_h\|_{H^{1/2}_{\Gamma_h}} \\
&\quad + \|h^{3/2}\nabla^2 \tilde{u}^{\mathrm{a}}\|_{L^2(\Gamma_h)} \|v_h\|_{H^{1/2}_{\Gamma_h}}.
\end{aligned}$$

Therefore the result follows.

4.7.7 Proof of Theorem 4.4.5

We shall use the Inverse Function Theorem 4.6.1. To put this into the context of Theorem 4.6.1, let

$$\mathcal{G}_h(v) := \delta \mathcal{E}_h^{\mathrm{tot}}(v) - \delta f(v) \quad \text{and} \quad \bar{u}_h := \Pi_h u^{\mathrm{a}}.$$

Then Theorem 4.4.4 gives property (4.6.2) and Theorem 4.4.3 gives property (4.6.3). Then we can conclude that, for K, N sufficiently large, there exists $u_h \in \mathcal{U}_h^*$ such that

$$\mathcal{G}_h(u_h) = 0, \quad \text{and}$$

$$\begin{aligned}
\|u_h - \Pi_h u^{\mathrm{a}}\|_E \lesssim &\|\nabla^2 \tilde{u}^{\mathrm{a}}\|_{L^2(\Omega^{\mathrm{i}})} + \|\nabla^3 \tilde{u}^{\mathrm{a}}\|_{L^2(\mathbb{R}^2 \setminus \Omega^{\mathrm{a}})} + \|\nabla^2 \tilde{u}^{\mathrm{a}}\|^2_{L^4(\mathbb{R}^2 \setminus \Omega^{\mathrm{a}})} \\
&+ \|h\nabla^2 \tilde{u}^{\mathrm{a}}\|_{L^2(\Omega_h^{\mathrm{c}})} + \|h^{3/2}\nabla^2 \tilde{u}^{\mathrm{a}}\|_{L^2(\Gamma_h)} + N^{-3}.
\end{aligned}$$

Finally we add the best approximation error

$$\begin{aligned}\|\Pi_h u^{\mathrm{a}} - u_h\|_E^2 &= \|\nabla \Pi_h u^{\mathrm{a}} - \nabla u_h\|_{L^2(\Omega_h)}^2 + \|\Pi_h u^{\mathrm{a}} - u_h\|_{H_{\Gamma_h}^{1/2}}^2 \\ &\lesssim \|h\nabla^2 \tilde{u}^{\mathrm{a}}\|_{L^2(\Omega_h^{\mathrm{c}})}^2 + \|h^{3/2}\nabla^2 \tilde{u}^{\mathrm{a}}\|_{L^2(\Gamma_h)}^2,\end{aligned}$$

where the last term comes from (4.7.14). Thus the result follows.

Chapter 5

Summary of results

In Chapter 2 we outlined the general framework [33] for a/c coupling error analysis. The two core components of error analysis are consistency and stability estimates.

In Chapter 3 we obtained a sharp energy-norm error estimate for the G23 coupling method with P2-FEM discretisation of the continuum model. Most importantly we showed that increasing to $p > 2$ will not improve the rate of convergence, but increase the computational cost and algorithmic complexity. Numerically, we observe that the improvement of P2-GR23 over P1-GR23 is only modest at moderate number of degrees of freedoms, hence a P2-GR23 scheme would be primarily of interest if very high accuracy of the solution is required.

The techniques used in Chapter 3 can be transferred to other energy-based a/c coupling models, especially the construction of quasi-interpolants of test functions in §3.5.2 and the parameter optimization of computational schemes in §3.2.3.2.

In Chapter 4 we formulated a G23 coupling model with P1 finite elements in the continuum region and a linearised elasticity model in the far-field, which is approximated by P0 boundary elements. We obtained an energy-norm error estimate for this model and conclude that it is reasonable to entirely bypass the nonlinear elasticity model and couple the atomistic region directly to a linearised elasticity model. This is because, as discussed in §4.4.4, the linearisation error $\mathcal{O}(N^{-3})$ is significantly smaller than the coupling error $\mathcal{O}(K^{-5/2})$. Furthermore, using a large FEM region ($N \gg K$), the FEM error becomes strictly larger than the modelling error, which cannot be reduced by choice of computational parameters, whereas by choosing a small FEM region ($N \approx K$), both FEM and BEM errors are balanced with the modelling error. Hence removing the FEM region is beneficial both for reduction of computational complexity as well as for the error.

Chapter 6

Extensions and open problems

6.1 Energy error estimate

In Chapter 3, while our estimates for the error in energy-norm are sharp, our numerical results show the estimates for the energy errors are suboptimal. From Figure 3.8 and Figure 3.9, we can see that the numerical results indicate the energy error scales as

$$|E^h(\bar{u}_h) - E^{\rm a}(\bar{u}^{\rm a})| \lesssim K^{-5} \sim \mathcal{N}_h^{-5/2}.$$

However, by Theorem 3.2.4, our analysis only predicts $\mathcal{O}(K^{-7/2}) = \mathcal{O}(\mathcal{N}_h^{-7/4})$. We are unable, at present, to obtain an optimal energy error estimate. This appears to be an open problem throughout the literature on hybrid atomistic multi-scale schemes; see e.g. [18].

6.2 Stability in 2D/3D

In 1D, stability results are well-understood and there is a general construction of stable QNL-type schemes in the review paper [33]. However, in higher dimensions stability is still an open problem. As mentioned in §3.2.2, it is shown in [41] that there is a "universal" instability in 2D interfaces for QNL-type a/c couplings. Indeed, it is proven in [41] that, for a 2D many-body nearest-neighbour interaction coupled by the same GR-AC method as described in Chapter 3 and 4, but with a planar interface, the energy $\mathcal{E}^{\rm g23}$ is not stable but one can stabilise it. However, problems come in when the interface is more complex, e.g. if it has corners. The following argument extracted from [41] shows formally the instability and stabilisation method.

Suppose we have the same G23 coupling scheme as in §3.1, but with a planar interface. Let $H_0^{\rm a}, H_0^{\rm c}, H_0^{\rm g23}$ be the Hessians of the corresponding energies at the reference state, then we can write [41, Lemma 7.3], under simplifying conditions,

$$\langle H_0^{\rm g23} u, u\rangle = \langle H_0^{\rm a} u, u\rangle + c^{\rm g23}\langle K_0 u, u\rangle + \langle Su, u\rangle,$$

where $\langle K_0 u, u\rangle := \sum_{\ell\in\mathcal{I}} D_2 D_1 u(\ell) D_1(\ell)$, $\langle Su, u\rangle := \sum_{\ell\in\mathcal{I}} |D^2 u(\ell)|^2$ and c^{g23} is a constant determined by the interface structure. It is proven [41, Lemma 7.6] that there exists $c > 0$ such that,

$$\inf_{\|Du\|_{\ell^2}=1} \left\{ \langle K_0 u, u\rangle + \langle Su, u\rangle \right\} =: \lambda < -c.$$

Define $\gamma(H) = \inf_{\|Du\|_{\ell^2}=1} \langle Hu, u\rangle$. Hence, if the interface structure causes $c^{\mathrm{g23}} \neq 0$ (e.g. interface with corners) then we have [41, Theorem 7.7]

$$\gamma(H_0^{\mathrm{a}}) = 0 \implies \gamma(H_0^{\mathrm{g23}}) < 0$$

which indicates instability. Therefore a stabilised energy is defined as

$$\mathcal{E}^{\mathrm{stab}}(u) := \mathcal{E}^{\mathrm{g23}}(u) + \kappa \langle Su, u\rangle.$$

It shown in [41, Theorem 7.9] that there exist constants $C_1, C_2 > 0$ and κ such that

$$-\frac{C_1}{(\kappa+1)^2} < \lambda < -\frac{C_2}{(\kappa+1)^2}. \tag{6.2.1}$$

This leads to [41, Corollary 7.1] which states, under the appropriate technical conditions, that

$$\gamma(H_0^{\mathrm{a}}) - \frac{C_1}{\kappa} < \gamma(H_0^{stab}) < \gamma(H_0^{\mathrm{a}}) - \frac{C_2}{\kappa}.$$

Hence we can choose appropriate κ by adjusting the interface structure to ensure that $\gamma(H_0^{stab}) > 0$. Unfortunately this may cause larger consistency error for the stabilised energy. Moreover, since the proof of (6.2.1) relies on Fourier analysis, this stabilisation method has not yet been generalised to domain with corners. Therefore future investigation is needed regarding stability of 2D/3D couplings.

6.3 BEM in higher dimensions

In Chapter 4, a concept of using BEM to approximate the elasticity model is proposed. However the current error analysis only applies for displacement maps $u : \mathbb{R}^2 \to \mathbb{R}$, since the elasticity linearization is characterized by homogeneous Laplace problems, whereas displacements mapped to 2D or 3D require more complexity. The theory of BEM for general elliptic systems in 2D and 3D has been discussed in [8] and [23]. Thus it is possible to explore the employment of BEM in A/C coupling in higher dimensions. For example, in [20] a method is presented to compute the lattice Green's function for a planar interface with arbitrary atomic interactions suited for the study of line defect/interface interactions. However this approach does not consider the ghost-forces or the stability of coupling atomistic interactions with lattice Green's functions without any "buffer" region. A more comprehensive study on this topic has yet to come.

6.4 BEM and A/C for other defects

Let us now consider a "point-defect" where $D^j u(x) \sim |x|^{1-p-j}$ for a general p. If $p > 1$ (2D) and $p > 1.5$ (3D) then this is still a finite-energy configuration. It is artificial (it does not correspond to a real defect) but it helps us to think about the consequences for more long-range defects such as dislocation and charged defects. How does the error estimate change now? Is there a critical p below which the FEM region is beneficial? What happens as $p \to 1$ (dislocations and charged defects)?

6.5 Numerical investigation of A/C coupling with BEM

A thorough numerical investigation of A/C coupling using the boundary element method should be undertaken to verify our results from Chapter 4. The efficiency gain due to removing the finite element regions is offset by the numerical cost of the boundary element method. The structure of the system matrix of the boundary element method is quite different from the sparse structure of finite element discretizations, and the cost for solving these systems can be non-negligible. For the 2D displacement problem studied here we only need to solve a problem on a curve. And since we can choose $N \approx K$, the length of this curve is not too large. Therefore the size of the BEM problem will still be small enough to use dense direct solvers and more sophisticated strategies based, for example, on an H-matrix structure will not be required. But to really be able to meaningfully compare the A/C coupling using FEM and the method using BEM, a careful choice of the quantities to compare against is crucial. Simply choosing the degrees of freedom, as discussed in Chapter 3, is not a reliable indicator for the computational complexity of both problems. Comparing the run time directly requires careful tuning of the solver process, e.g., the choice of preconditioning.

6.6 Extension to transitions state theory

A natural extension from modeling static states with zero temperature is to consider a thermal process taking account of kinetic energy. This leads us to transition state (TST) theory for chemical reaction kinetics, e.g. [22]. There has been interest in using TST in various defects models in recent years, see [53], [35] and [21] for examples. TST calculates the rate of slow thermal processes. In particular, we are concerned with the TST rate at which a solid-state system residing in the metastable region crosses over into an adjacent metastable region. This simplified point of view is particularly useful at "low" temperature (or room temperature for many applications).

6.6.1 A saddle-point problem

We shall formally discuss the formulation of a saddle-point problem related to TST. Consider the case when two strong local minima A and B are connected via an index-1 saddle

point. Consider a system of N particles in d dimensions at a fixed temperature T. Let $\mathbf{q} \in \mathbb{R}^{dN}$ and $\mathbf{p} \in \mathbb{R}^{dN}$ denote the position and momentum vectors of the particles respectively. The total energy, or Hamiltonian, of the system is given by

$$\mathcal{H}(\mathbf{q}, \mathbf{p}) = \mathcal{V}(\mathbf{q}) + \mathcal{K}(\mathbf{p}).$$

Then the TST rate is defined to be the equilibrium flux across the dividing surface Γ_{AB}:

$$\begin{aligned} R^{TST}_{A\to B} :&= \frac{1}{2}\frac{\int\int_{\Gamma_{AB}} |\mathbf{p}\cdot\mathbf{n}| e^{-\beta\mathcal{H}(\mathbf{q},\mathbf{p})} dS d\mathbf{p}}{\int\int_{\Omega_A} e^{-\beta\mathcal{H}(\mathbf{q},\mathbf{p})} d\mathbf{q} d\mathbf{p}} \\ &= \frac{1}{2}\sqrt{\frac{2}{\pi\beta m}}\frac{\int_{\Gamma_{AB}} e^{-\beta\mathcal{V}_s(\mathbf{q})} dS}{\int_{\Omega_A} e^{-\beta\mathcal{V}(\mathbf{q})} d\mathbf{q}}, \end{aligned} \tag{6.6.1}$$

where $\beta := (k_B T)^{-1}$, k_B is the Boltzmann's constant, m is the mass of each atom, and $\mathbf{n}$ is the normal vector of Γ_{AB} towards B.

The partition function integrals in (6.6.1) cannot be carried out for general potentials due to potentially complex dividing surface. The harmonic transition state (HTST) rate is therefore introduced as a good approximation for solid-state kinetics at low temperature. It has two addition assumptions:

1. The kinetic bottleneck is an energy barrier.
2. The potential $\mathcal{V}$ can be locally extended to 2nd order.

Hence we can Taylor expand $\mathcal{V}(\mathbf{q})$ around the minimum $\mathbf{q}_m$ and $\mathcal{V}_s(\mathbf{q})$ around the saddle point $\mathbf{q}_s$, giving

$$\begin{aligned} \mathcal{V}(\mathbf{q}) &\approx \mathcal{V}(\mathbf{q}_m) + \frac{1}{2}(\mathbf{q}-\mathbf{q}_m)\cdot\mathbf{H}_m(\mathbf{q}-\mathbf{q}_m), \\ \mathcal{V}_s(\mathbf{q}) &\approx \mathcal{V}(\mathbf{q}_s) + \frac{1}{2}(\mathbf{q}-\mathbf{q}_s)\cdot\mathbf{H}_s(\mathbf{q}-\mathbf{q}_s), \end{aligned} \tag{6.6.2}$$

where $\mathbf{H}_m$ and $\mathbf{H}_s$ are the Hessian matrices of $\mathcal{V}$ at the minimum and saddle respectively.

Let λ^m_j and λ^s_j, $1 \le j \le dN$ denote the eigenvalues of $\mathbf{H}_m$ and $\mathbf{H}_s$ respectively. We assume that $\mathbf{q_s}$ is an index-1 saddle. Then we can write $\lambda^s_1 < 0 < \lambda^s_2 < \lambda^s_3, ..., \lambda^s_{dN}$. The harmonic approximation to (6.6.1) reads

$$R^{HTST}_{A\to B} = \underbrace{\frac{1}{2}\sqrt{\frac{2}{\pi\beta m}}\left(\frac{\prod_{j=1}^{dN}\lambda^m_j}{\prod_{j=2}^{dN}\lambda^s_j}\right)^{1/2}}_{\text{The frequency of attempts to transistion}} \underbrace{\exp(-\beta(\mathcal{V}_s - \mathcal{V}_m))}_{\text{Probability that attempts success}}. \tag{6.6.3}$$

Thus we are interested in the energy difference $\mathcal{V}_s - \mathcal{V}_m$.

6.6.2 An attempt to formulate the minimum-saddle problem when $N \to \infty$

In order to assess the accuracy of simulations, we need to formulate a problem that compares the computational results on a finite domain with the "real" solution on a large scale, i.e. when $N \to \infty$.

Let us consider an infinite lattice. $\exists \bar{q}^m, \bar{q}^s$, eigenvalue $\lambda < 0$ and associated eigenvector $\bar{v}$ such that, for all φ

$$\begin{aligned}
&\delta\mathcal{V}(\bar{q}^m) = 0, \quad \delta\mathcal{V}(\bar{q}^s) = 0, \\
&\langle \delta^2\mathcal{V}(\bar{q}^m)\varphi, \varphi\rangle \geq C_o\|\nabla\varphi\|_{L^2}^2, \quad \text{(strongly stable minimum)} \\
&\delta^2\mathcal{V}(\bar{q}^s)\bar{v} = \lambda\bar{v}, \qquad (6.6.4) \\
&\langle \delta^2\mathcal{V}(\bar{q}^s)\varphi, \varphi\rangle \geq C\|\nabla\varphi\|_{L^2}^2, \qquad \forall\varphi \perp_{\ell^2} \bar{v}. \qquad (6.6.5)
\end{aligned}$$

(6.6.4) and (6.6.5) are the strong index-1 saddle condition. This is the natural definition of the minimum-saddle problem.

6.6.3 A Galerkin approximation

Let $\dot{W}^{1,2}(\Lambda, \mathbb{R}^d)$ be the discrete Soblev space equipped with $\|\nabla\cdot\|_{L^2}$ (identified with linear interpolants). Define a finite subspace

$$W_R := \{q \in \dot{W}^{1,2} : q = 0 \text{ in } \Lambda \setminus \mathcal{B}_R\}.$$

In the present, we can find $\bar{q}_R^m, \bar{q}_R^s$, eigenvalue $\mu_R < 0$ and associated eigenvector $\bar{w}_R$ such that

$$\begin{aligned}
&\delta\mathcal{V}(\bar{q}_R^m) = 0, \quad \delta\mathcal{V}(\bar{q}_R^s) = 0, \\
&\langle \delta^2\mathcal{V}(\bar{q}_R^m)\varphi_R, \varphi_R\rangle \geq C_o\|\nabla\varphi_R\|_{L^2}^2, \\
&\langle \delta^2\mathcal{V}(\bar{q}_R^s)\bar{w}_R, \varphi_R\rangle = \mu_R\langle\nabla\bar{w}_R, \nabla\varphi_R\rangle, \\
&\langle \delta^2\mathcal{V}(\bar{q}_R^s)\varphi, \varphi\rangle \geq C\|\nabla\varphi\|_{L^2}^2, \qquad \forall\varphi \perp_{H^1} \bar{w}_R.
\end{aligned} \qquad (6.6.6)$$

However, even if we found such $\bar{q}_R^s$,, μ_R and $\bar{w}_R$, sending $R \to \infty$ still does not give (6.6.4) and (6.6.5), since the eigenmodes are not in the same space. Observe that (6.6.4) implies $\bar{v} \in \ell^2$ whereas the Galerkin minimum $\bar{w}_R$ satisfying (6.6.6) is in the subspace $\dot{W}^{1,2}$ with the seminorn $\|\nabla\cdot\|_{L^2}$. At the moment, we can only prove convergence to the limit problem if we replace the condition (6.6.4) with

$$\langle \delta^2\mathcal{V}(\bar{q}^s)\bar{v}, \varphi\rangle = \lambda\langle\nabla\bar{v}, \nabla\varphi\rangle, \qquad \forall\varphi \in \dot{\mathcal{U}}^{1,2}.$$

6.6.4 Problems to tackle

First of all, we need to obtain a well-defined formulation for $N \to \infty$ that allows a rigorous error analysis for numerical schemes.

Secondly, let us assume we can prove convergence of the approximation. Write $\Delta\mathcal{V} := \mathcal{V}_s - \mathcal{V}_m$, $\Delta\mathcal{V}_R := \mathcal{V}_s^R - \mathcal{V}_m^R$. We know that

$$|\mathcal{V}_s - V_s^R| \lesssim R^{-d},$$
$$|\mathcal{V}_m - V_m^R| \lesssim R^{-d}.$$

Then we have

$$|\Delta\mathcal{V} - \Delta V^R| \leq |\mathcal{V}_s - V_s^R| + |\mathcal{V}_m - V_m^R| \lesssim R^{-d}.$$

The problem we would like to explore is that whether this convergence rate can be improved due to cancellation effects.

Bibliography

[1] G. Acosta and R. G. Duran. An optimal Poincaré inequality in L1 for convex domains. *Proc. AMS 132(1)*, 195-202, 2003.

[2] R. A. Adam. *Sobolev Spaces.* Academic Press, New York, London, 1975.

[3] O. Axelsson. *Iterative Solution Methods.* Cambridge University Press, 1996.

[4] M. Born and K. Huang. *Dynamical Theory of Crystal Lattices.* Oxford University Press, 1954.

[5] C. Carstensen. Quasi-interpolation and a posteriori error analysis in finite element methods. *M2AN Math. Model. Numer. Anal.*, 33:1187–1202, 1999.

[6] A.-L. Cauchy. De la pression ou tension dans un systéme de points matériels. in oeuvres complétes d'Augustin Cauchy, 1882.

[7] M. Costabel. Principles of boundary element methods. *Computer Physics Reports*, 6, 1987.

[8] M. Costabel. Boundary integral operators on Lipschitz domains: elementary results. *SIAM J. Math. Anal.*, 19(3), 1988.

[9] W. A. Curtin and R. M. Miller. Atomistic/continuum coupling in compu- tational materials science. *Model. Simul. Mater. Sci.*, 11:R33R68, 2003.

[10] M. S. Daw and M. I. Baskes. Embedded-Atom Method: Derivation and Application to Impurities, Surfaces, and other Defects in Metals. *Physical Review B*, 20, 1984.

[11] M. S. Daw, S. M. Foiles, and M. I. Baskes. The embedded-atom method: a review of theory and application. *Materials Science Reports*, 9, 1993.

[12] A. Dedner, H. Wu, and C. Ortner. Analysis of patch-test consistent atomistic-to-continuum coupling with higher-order finite elements. *ArXiv e-prints:1607.05936, to appear in ESAIM: M2AN*, 2016.

[13] M. Dobson, M. Luskin, and C. Ortner. Accuracy of quasicontinuum approximations near instabilities. *J. Mech. Phys. Solids*, 58(10):1741–1757, 2010.

[14] M. Dobson, M. Luskin, and C. Ortner. Sharp stability estimates for the force-based quasicontinuum approximation of homogeneous tensile deformation. *Multiscale Model. Simul.*, 8(3):782–802, 2010.

[15] M. Dobson, M. Luskin, and C. Ortner. Stability, instability, and error of the force-based quasicontinuum approximation. *Arch. Ration. Mech. Anal.*, 197(1):179–202, 2010.

[16] W. E, J. Lu, and J. Z. Yang. Uniform accuracy of the quasicontinuum method. *Phys. Rev. B*, 74(21):214115, 2006.

[17] W. E and P. Ming. Analysis of the local quasicontinuum method. In *Frontiers and prospects of contemporary applied mathematics*, volume 6 of *Ser. Contemp. Appl. Math. CAM*, pages 18–32. Higher Ed. Press, Beijing, 2005.

[18] V. Ehrlacher, C. Ortner, and A. V. Shapeev. Analysis of boundary conditions for crystal defect atomistic simulations. *Arch. Ration. Mech. Anal.*, 222, 2016.

[19] H. Fischmeister, H. Exner, M.-H. Poech, S. Kohlhoff, P. Gumbsch, S. Schmauder, L. S. Sigi, and R. Spiegler. Modelling fracture processes in metals and composite materials. *Z. Metallkde*, 80:839–846, 1989.

[20] M. Ghazisaeidi and D. R. Trinkle. Lattice green's function for crystals containing a planar interface. *Phys. Rev. B*, 82:064115, 2010.

[21] S. Hara and J. Li. Adaptive strain-boost hyperdynamics simulations of stress-driven atomic processes. *Phys. Rev. B*, 82:184114, 2010.

[22] N. E. Henriksen and F. Y. Hansen. *Theories of Molecular Reaction Dynamics*. Oxford University Press, 2008.

[23] G. C. Hsiao and W. L. Wendland. *Boundary element methods: foundation and error analysis. In Encyclopedia of Computational Mechanics*. Edited by Erwin Stein, Ren'e de Borst and Thomas J. R. Hughes, John Wiley & Sons, Ltd., 2004.

[24] T. Hudson and C. Ortner. On the stability of Bravais lattices and their Cauchy–Born approximations. *ESAIM:M2AN*, 46:81–110, 2012.

[25] J. E. Jones. On the Determination of Molecular Fields. III. From Crystal Measurements and Kinetic Theory Data. *Proc. Roy. Soc. London A.*, 106:709–718, 1924.

[26] H. Kanzaki. Point defects in face-centred cubic lattice I: Distortion around defects. *J. Phys. Chem. Solids*, 2:24–36, 1957.

[27] S. Kohlhoff and S. Schmauder. A new method for coupled elastic-atomistic modelling. In V. Vitek and D. J. Srolovitz, editors, *Atomistic Simulation of Materials: Beyond Pair Potentials*, pages 411–418. Plenum Press, New York, 1989.

[28] B. Van Koten and M. Luskin. Analysis of energy-based blended quasicon- tinuum approximations. *SIAM J. Numer. Anal.*, 49:21822209, 2011.

[29] X. Li. Boundary condition for molecular dynamics models of solids: A variational formulation based on lattice green's functions. *preprint*, 2009.

[30] X. H. Li, C. Ortner, A. Shapeev, and B. Van Koten. Analysis of blended atomistic/continuum hybrid methods. *Numer. Math.*, 134, 2016.

[31] W. K Liu, E. G. Karpov, and H. S. Park. *Nano Mechanics and Materials: Theory, Multiscale Methods and Applications*. John Wiley & Sons, Ltd., 2006.

[32] J. Lu and P. Ming. Stability of a force-based hybrid method in three dimensions with sharp interface. *arxiv:1212.3643*, 2012.

[33] M. Luskin and C. Ortner. Atomstic-to-continuum coupling. *Acta Numerica*, 22:397 – 508, 2013.

[34] M. Luskin, C. Ortner, and B. Van Koten. Formulation and optimization of the energy-based blended quasicontinuum method. *Comput. Methods Appl. Mech. Engrg.*, 253, 2013.

[35] J. K. Mason, A. C. Lund, and C. A. Schuh. Determining the activation energy and volume for the onset of plasticity during nanoindentation. *Phys. Rev. B*, 73:054102, 2006.

[36] R. E. Miller and E. B. Tadmor. The Quasicontinuum Method: Overview, Applications and Current Directions. *Journal of Computer-Aided Materials Design*, 9:203–239, 2003.

[37] M. Mullins and M. Dokainish. Simulation of the (0 0 1) plane crack in α-iron employing a new boundary scheme. *Phil. Map. A*, 46:771–787, 1982.

[38] M. Ortiz, R. Phillips, and E. B. Tadmor. Quasicontinuum analysis of defects in solids. *Philosophical Magazine A*, 73(6):1529–1563, 1996.

[39] C. Ortner. The role of the patch test in 2D atomistic-to-continuum coupling methods. *ESAIM Math. Model. Numer. Anal.*, 46, 2012.

[40] C. Ortner and A. Shapeev. Interpolation of lattice functions and applications to atomistic/continuum multiscale methods, 2012. ArXiv e-prints, 1204.3705.

[41] C. Ortner, A. Shapeev, and L. Zhang. (In-)Stability and stabilisation of QNL-type atomistic-to-continuum coupling methods, 2014.

[42] C. Ortner and E. Süli. A note on linear elliptic systems on $\mathbb{R}^d$. *ArXiv e-prints*, 1202.3970, 2012.

[43] C. Ortner and F. Theil. Justification of the Cauchy–Born approximation of elastodynamics. *Arch. Ration. Mech. Anal.*, 207, 2013.

[44] C. Ortner and L. Zhang. Construction and sharp consistency estimates for atomistic/continuum coupling methods with general interfaces: a 2D model problem. *SIAM J. Numer. Anal.*, 50, 2012.

[45] C. Ortner and L. Zhang. Atomistic/continuum blending with ghost force correction. *SIAM J. Sci. Comput.*, 38, 2016.

[46] Christoph Ortner. A priori and a posteriori analysis of the quasinonlocal quasicontinuum method in 1D. *Math. Comp.*, 80(275):1265–1285, 2011.

[47] C. Schwab. *p- and hp- finite element methods: theory and applications in solid and fluid mechanics*. Oxford Universiy Press, Oxford, 1998.

[48] V. B. Shenoy, R. Miller, E. B. Tadmor, D. Rodney, R. Phillips, and M. Ortiz. An adaptive finite element approach to atomic-scale mechanics–the quasicontinuum method. *J. Mech. Phys. Solids*, 47(3):611–642, 1999.

[49] T. Shimokawa, J. J. Mortensen, J. Schiotz, and K. W. Jacobsen. Matching conditions in the quasicontinuum method: Removal of the error introduced at the interface between the coarse-grained and fully atomistic region. *Phys. Rev. B*, 69(21):214104, 2004.

[50] J. E. Sinclair. Improved atomistic model of a bcc dislocation core. *Journal of Applied Physics*, 42:5321, 1971.

[51] O. Steinbach. *Numerical Approximation Methods for Elliptic Boundary Value Problems: Finite and Boundary Elements*. Springer New York, 2008.

[52] B. Van Koten, X. H. Li, M. Luskin, and C. Ortner. A computational and theoretical investigation of the accuracy of quasicontinuum methods. *Numerical Analysis of Multiscale Problems. Springer Lecture Notes in Computational Science and Engineering*, 83, 2012.

[53] C. R. Weinberger, A. T. Jennings, K . Kang, and J. R. Greer. Atomistic simulations and continuum modeling of dislocation nucleation and strength in gold nanowires. *J. Mech. Phys. Solids*, 60, 2012.

[54] C. Woodward and S. Rao. Flexible ab initio boundary conditions: Simulating isolated dislocations in bcc Mo and Ta. *Phys. Rev. Lett.*, 88:216402, 2002.

[55] S. P. Xiao and T. Belytschko. A bridging domain method for coupling continua with molecular dynamics. *Comput. Methods Appl. Mech. Engrg.*, 193(17-20):1645–1669, 2004.